THE UNIVERSITY
of EDINBURGH

This thesis has been submitted in fulfilment of the requirements for a postgraduate degree (e.g. PhD, MPhil, DClinPsychol) at the University of Edinburgh. Please note the following terms and conditions of use:

This work is protected by copyright and other intellectual property rights, which are retained by the thesis author, unless otherwise stated.

A copy can be downloaded for personal non-commercial research or study, without prior permission or charge.

This thesis cannot be reproduced or quoted extensively from without first obtaining permission in writing from the author.

The content must not be changed in any way or sold commercially in any format or medium without the formal permission of the author.

When referring to this work, full bibliographic details including the author, title, awarding institution and date of the thesis must be given.

Computed tomography imaging of the heart

by Dr Michelle Claire Williams

Supervisors : Professor D. E. Newby, Dr G. McKillop, Dr N. Uren

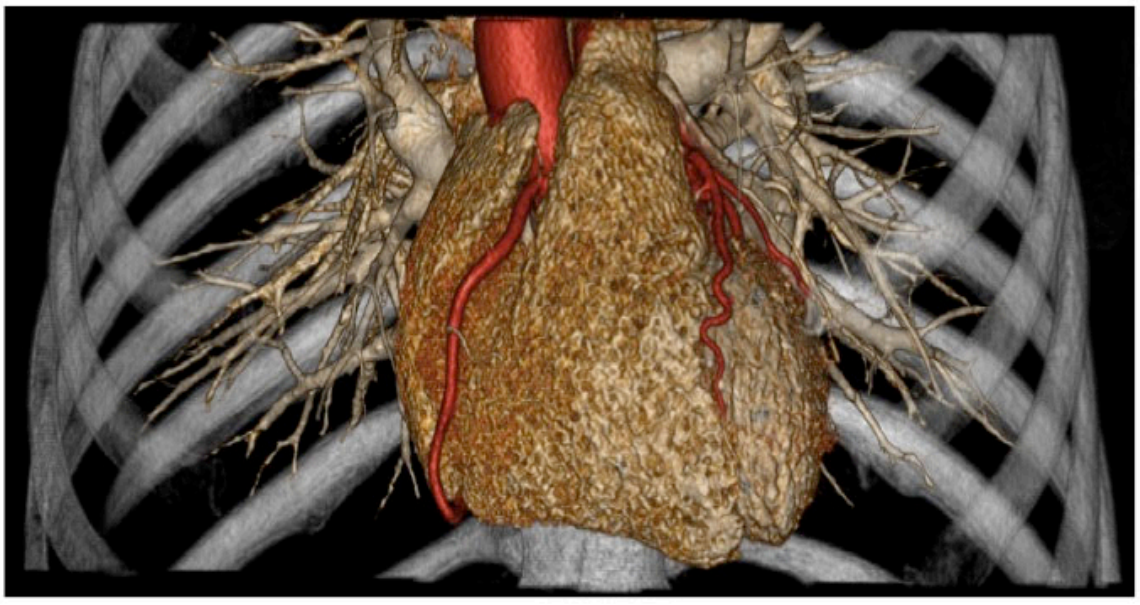

Doctor of Philosophy
The University of Edinburgh
2015

Abstract

Computed tomography imaging has revolutionised modern medicine and we can now study the body in greater detail than ever before. Cardiac computed tomography has the potential to provide information not just on coronary anatomy, but also on myocardial function, perfusion and viability. This thesis addresses the optimisation and validation of computed tomography imaging of the heart using a wide volume 320-multidetector scanner.

Computed tomography coronary angiography now has diagnostic accuracy comparable to invasive coronary angiography. However, radiation dose remains an important concern. It is therefore important to minimise computed tomography radiation dose while maintaining image quality. I was able to demonstrate that iterative reconstruction and patient tailored imaging techniques led to a 39% reduction in radiation dose in computed tomography coronary angiography, while maintaining subjective and objective assessments of image quality. In addition, I demonstrated that diagnostic images can be obtained in 99% of unselected patients presenting with suspected coronary artery disease when using single heart-beat 320-multidetector computed tomography coronary angiography.

Computed tomography myocardial perfusion imaging can provide additional and complementary information as compared to computed tomography coronary angiography that can aid diagnosis and management. I established both quantitative

and qualitative assessment of computed tomography myocardial perfusion imaging and validated it against both a clinical "gold-standard", fractional flow reserve during invasive coronary angiography, and a physiological "gold-standard", positron emission tomography with oxygen-15 labelled water. Finally, I was able to show that techniques to reduce radiation dose can also be applied to computed tomography myocardial perfusion imaging, leading to a 60% reduction in radiation dose, while maintaining image quality.

In my thesis, I have established that comprehensive cardiac angiographic and perfusion imaging can be performed with wide volume computed tomography in a broad generalizable population of patients with relatively low radiation exposure. These techniques provide both structural and functional assessments from a single imaging modality that are valid and readily applicable to the clinic in the assessment and management of patients with suspected coronary artery disease.

Lay Summary of Thesis

THE UNIVERSITY of EDINBURGH

The lay summary is a brief summary intended to facilitate knowledge transfer and enhance accessibility, therefore the language used should be non-technical and suitable for a general audience. (See the Degree Regulations and Programmes of Study, General Postgraduate Degree Programme Regulations. These regulations are available via: http://www.drps.ed.ac.uk/.)

Name of student:	Dr Michelle Claire Williams	UUN	S9900581
University email:			
Degree sought:	Doctorate	No. of words in the main text of thesis:	43180
Title of thesis:	Computed tomography imaging of the heart		

Insert the lay summary text here - the space will expand as you type.

Heart disease is a major source of ill health and an important cause of death throughout the world. In order to treat heart disease appropriately we need accurate methods to identify heart disease and to assess its severity. In addition, these diagnostic tests need to be easy to perform, quick to undergo, and as safe as possible.

This thesis assesses the use of computed tomography scans to evaluate the heart. Computed tomography uses x-rays to build up a three dimensional picture of the inside of the body. In this thesis computed tomography is used to assess the blood vessels that supply nutrients to the heart, and also the blood flow to the heart muscle itself.

Using the latest technologies, a protocol for computed tomography imaging of the heart was developed. This is capable of comprehensively assessing the heart's structure and function in less than thirty minutes with good image quality.

In addition, computed tomography imaging of the heart was compared to commonly used methods to assess the heart, such as invasive coronary angiography, and new and exciting methods that are in development, such as oxygen-15 water positron emission tomography. This showed that computed tomography could accurately assess both the blood vessels to the heart and the heart muscle itself.

This work establishes that computed tomography imaging can be used to study the heart in great detail and that it has excellent accuracy as compared to other imaging modalities.

Document control

Related policies/regulations: www.docs.sasg.ed.ac.uk/AcademicServices/Regulations/PGR_AssessmentRegulations.pdf	
If you require this document in an alternative format please email Academic.Services@ed.ac.uk or telephone 0131 650 2138.	Date last reviewed: 15.05.15

K:\AAPS\D-AcademicAdministration\02-CodesOfPractice,Guidelines&Regulations\24-MainReferencesCopiesPolicies\01-Current\Assessment BOE SCC & Feedback\Forms\ThesisLaySummary

Contents

Abbreviations

^{o}C	*degrees centigrade*
BMI	*body mass index*
CAD	*coronary artery disease*
CT	*computed tomography*
CTCA	*computed tomography coronary angiography*
CTP	*computed tomography myocardial perfusion imaging*
ECG	*electrocardiogram*
FFR	*fractional flow reserve*
HU	*Hounsfield Units*
ICA	*invasive coronary angiography*
kV	*kilovoltage*
LAD	*left anterior descending artery*
LAO	*left anterior oblique*
LCX	*left circumflex artery*
mA	*milliampere*
mGy	*milliGray*
mL	*millilitre*
MRI	*magnetic resonance imaging*
mSv	*millisievert*
NPV	*negative predictive value*
^{15}*O-Water*	*oxygen-15 labelled water*

PET	*positron emission tomography*
PPV	*positive predictive value*
RAO	*right anterior oblique*
RCA	*right coronary artery*
SPECT	*single positron emission tomography*

Tables

Figures

Figure 5.2: An example of images obtained in Group 1 showing a perfusion defect identified during adenosine stress in septum on short axis images (B, yellow arrow). This was fully reversible and rest images were normal (A). This helped to confirm that the indeterminate lesion identified on CTCA in the LAD stent (C) was functionally significant.

Figure 5.3: An example of the images obtained in Group 2 showing a perfusion defect identified during adenosine stress in the basal inferior and infero-septal segments on the short axis images (A, arrows) and the overlaid transmyocardial perfusion ratio plots (B, hypo-perfused area purple/pink). The CTCA image shows a significant stenosis in right coronary artery (C, arrow).

Figure 5.4: Radiation dose reduction in computed tomography imaging for (A) rest, (B) stress, (C) the total protocol.

Figure 6.1: Computed tomography coronary angiography curved planar reformations and vessel cross sections showing lesions with different stenosis severity (none, <10%; mild, 10-49%; moderate, 50-70%; severe, >70%).

Figure 6.2: Bland-Altman plots for intra and inter observer variability for the assessment of total Agatston score (dotted lines represent the limits of agreement).

Figure 6.3: Bland-Altman plots for intra and inter observer variability for the assessment of total Agatston score for patients with a calcium score < 1000 (one outlier was excluded from the inter observer variability assessment, dotted lines represent the limits of agreement.).

Figure 6.4: Computed tomography coronary angiography curved planar reconstruction of the left anterior descending artery showing calcified and non-calcified plaque. The location of this plaque, which spans the origin of the first diagonal vessel, can cause differences in segmental classification between observers.

Figure 6.5: Computed tomography coronary angiography images of a heavily calcified left anterior descending artery. The "blooming" artefact from such heavily calcified plaque can lead to differences in observer classification of stenosis severity.

Figure 7.1: Images from a 69-year old female patient who underwent comprehensive cardiac computed tomography imaging and invasive coronary angiography. Images (A) and (B) show short axis views of the left ventricle during adenosine stress showing hypo-enhancement in the territory of the left anterior descending artery (LAD, yellow arrows) and left circumflex artery (LCX, grey arrows). Stenoses were identified in LAD, first diagonal and LCX arteries and confirmed by invasive coronary angiography (C, D, E). Transmyocardial perfusion ratio during rest (F) and adenosine stress (G) are shown in "bull's-eye plots" with normal areas shown in yellow/orange and abnormal areas are highlighted in purple/blue. The transmyocardial perfusion ratio during adenosine stress is superimposed on short axis views of the left ventricle in image (B). Stress imaging identified reversible defects in LAD and LCX territories (A, B). Functional assessment identified a mild antero-septal wall motion abnormality. Delayed enhancement was not identified on CT or subsequent MRI imaging.

Figure 8.1: Bland-Altman plots of intra- and inter-observer variability in the assessment of global myocardial blood flow by oxygen-15 water positron emission tomography at baseline and during hyperaemia. (Dotted lines show limits of agreement)

Figure 8.2: Myocardial blood flow in all segments at rest and during adenosine stress.

Figure 8.3: The quantitative assessment of myocardial blood flow by oxygen-15 labelled water positron emission tomography as compared to computed tomography coronary angiography (CTCA) and myocardial perfusion (CTP) and invasive coronary angiography (ICA) with fractional flow reserve (FFR). (A) and (B) show baseline and hyperaemic myocardial blood flow in obstructive and non-obstructive

vessels as defined by ICA/FFR. (C) and (D) show baseline and hyperaemic myocardial blood flow in obstructive and non-obstructive vessels as defined by CTCA/CTP. (E) and (F) show the correlation between myocardial blood flow corrected for rate pressure product and CT contrast enhancement at rest and during hyperaemia respectively.

Figure 8.4: Baseline (A) and hyperaemic (B) myocardial blood flow assessed by oxygen-15 labelled water positron emission tomography in normal, non-obstructive and obstructive vessels as defined by computed tomography coronary angiography and myocardial perfusion.

Figure 8.5: Computed tomography myocardial contrast enhancement at rest and during adenosine stress computed tomography imaging.

Figure 8.6: This 74-year old non-smoker with hypertension, hypercholesterolemia and atypical chest pain underwent multimodality assessment of his cardiac anatomy and physiology. (A) shows short axis basal, mid and apical images of the left ventricle at rest and during hyperaemia along with three dimensional representations of the transmyocardial perfusion ratio and coronary anatomy. Hypoattenutation is seen in right coronary artery (RCA) and left anterior descending (LAD) artery during hyperaemia. There is also mild hypoattenuation in the RCA territory on rest imaging. (B) shows the corresponding oxygen-15 labelled water PET images which identified the same perfusion abnormalities in terms of the absolute myocardial blood flow (mL/g/min). (C) shows the corresponding images from ICA which identified an occluded LAD and severe stenosis of the RCA with FFR <0.80.

Declaration

.

I declare that:

(a) that the thesis has been composed by the candidate, and

(b) either that the work is the candidate's own, or, if the candidate has been a member of a research group, that the candidate has made a substantial contribution to the work, such contribution being clearly indicated, and

(c) that the work has not been submitted for any other degree or professional qualification.

Dr Michelle Williams

January 17, 2016

Chapter One: Introduction

Extracts of this chapter are published in:

Williams MC, Reid J, McKillop G, Weir N, van Beek EJR, Uren, NG, Newby DE. Cardiac and coronary CT comprehensive imaging approach in the assessment of coronary heart disease. Heart. 2012: 98(7); 512-2.

Summary

Coronary artery disease remains a major cause of morbidity and mortality throughout the world. Computed tomography imaging of the heart can assess cardiac anatomy, function, perfusion and viability in one rapid diagnostic test. Validation of computed tomography imaging as compared to "gold standard" invasive and non-invasive techniques will establish the diagnostic accuracy of computed tomography myocardial perfusion imaging. Optimisation of this technique, including methods to reduce radiation dose and improve image quality, are essential in order to develop clinically useful comprehensive computed tomography imaging of the heart.

Introduction

Cardiovascular disease remains the remains the commonest cause of global mortality. [1] In the United Kingdom coronary heart disease accounts for 18% of all deaths among men and 12% of all deaths among women. [2] Cardiovascular disease is the leading cause of death in Europe, responsible for 4.1 million deaths per year. [3] In addition cardiovascular disease is a significant contributor to morbidity in Europe. [3] Chest pain is responsible for up to 40% of emergency hospital admissions [4] and 1% of all primary care consultations. [5] Thus methods to accurately diagnose coronary artery disease are essential.

Patients presenting to cardiology clinics undergo a series of investigations in order to establish the diagnosis of coronary artery disease and to identify risk factors,

complications and treatment options. This is necessitated by the fact that many of the available modalities have limited sensitivity and specificity, as well as an inability to assess simultaneously both structure and function. This often leaves the clinician needing to reaffirm earlier test findings and undertaking multiple complementary tests that may ultimately lead to invasive coronary angiography as a prelude to potential coronary revascularisation. Thus there is a clinical need for diagnostic imaging techniques that are capable of assessing anatomy, function, perfusion and viability in a rapid diagnostic test and at a low radiation dose.

Invasive coronary angiography

The current "gold standard" method to assess the presence and severity of coronary artery disease is invasive coronary angiography (ICA). This catheter angiography technique was developed by the pioneering work of Werner Forssmann in 1929 and later in 1941 by Andre F. Cournard and Dickinson W. Richards. [6] Invasive coronary angiography is now the mainstay for the diagnosis of coronary artery disease, and in 2009 over 1 million diagnostic cardiac catheterisations were performed in the US. [7] However, as the term suggests, this is an invasive technique. Complications of invasive coronary angiography include myocardial infarction, stroke, arrhythmia, vascular complications and contrast reactions. [8] In addition, there are some patients for whom invasive coronary angiography cannot be performed for technical reasons, such as patients with a high body mass index or with complex coronary anatomy. Thus there is a requirement for non-invasive techniques to identify and stratify coronary artery disease.

Invasive coronary angiography is currently the only method in routine practice where coronary revascularisation can be performed at the same time, such as the implantation of coronary artery stents. However, a significant proportion of invasive coronary angiograms are performed in patients with normal coronary arteries. Previous studies have shown that up to forty per cent of patients undergoing invasive coronary angiography have normal coronary arteries. [9,10] Thus superior diagnostic techniques are required to identify patients who would benefit from revascularisation prior to invasive coronary angiography.

Invasive coronary angiography assesses the coronary lumen, but we know that coronary artery disease is a complex disease involving a process of healing and remodelling of the coronary arteries. [11] Evidence from histology and imaging studies shows that coronary artery plaques are complex eccentric structures. [12] The assessment of the functional significance of a coronary stenosis using invasive coronary angiography alone is based on the evaluation of multiple two dimensional views. Defining significant coronary artery disease based on the per cent stenosis from visual assessment of invasive coronary angiography is particularly limited in patients with diffuse disease, extensive coronary artery remodelling or endothelial dysfunction. [13] Thus the diagnosis of coronary artery disease has advanced beyond the mere assessment of luminal stenosis.

Invasive coronary angiography is limited as a “gold standard” comparator for studies of cardiac CT. Invasive coronary angiography assesses only the lumen of the coronary arteries where as CT can assess the coronary artery lumen, coronary artery

wall, atherosclerotic plaque composition and surrounding structures. Using invasive coronary angiography as the "gold standard" can therefor make CT coronary angiography appear to overestimate disease severity. It also ignores additional benefits of CT coronary angiography such as the identification of potentially vulnerable plaques. Therefor, new or combined "gold standards" are required to comprehensively assess cardiac CT.

Fractional flow reserve

Invasive physiological testing during coronary angiography can provide additional functional information to aid the selection of lesions that would benefit from revascularisation. [14] Fractional flow reserve (FFR) measured during invasive coronary angiography can provide additional information regarding the hemodynamic significance of a suspected coronary artery lesion that can be used to guide management decisions.

Fractional flow reserve is calculated during invasive coronary angiography using measurements of pressure during maximal hyperaemia. The fractional flow reserve is the ratio of the mean distal coronary artery pressure to the mean aortic pressure during maximal hyperaemia. [15] The measurement of fractional flow reserve assumes that there is a linear relationship between pressure and flow when coronary auto-regulation is abolished during hyperaemia. [16] The assessment of fractional flow reserve during invasive coronary angiography is considered to be the gold

standard method of assessing the clinical significance of an individual coronary artery stenosis.

Fractional flow reserve can be used to define the threshold for revascularisation. A cut-off of <0.80 can be used to select patients for revascularisation and is associated with improved prognosis. [17-21] In addition, revascularisation guided by fractional flow reserve is cost effective when compared to medical therapy, invasive coronary angiography driven revascularisation or strategies guided by additional non-invasive imaging. [22-24] Selecting patients for revascularisation using fractional flow reserve is associated with reduced adverse cardiovascular events, lower rates of revascularisation, shorter hospital stays and lower net costs. [18]

There are a number of limitations to the use of fractional flow reserve. Firstly, this is an invasive technique that necessitates the passage of additional pressure catheters during invasive coronary angiography. The measurements do not take into account the effect of cardiac contraction or heart rate on the pressure/flow relationship. [16] In addition, variations in micro-vascular resistance can influence the accuracy of fractional flow reserve measurements. [16] The choice of threshold value to define an abnormal fractional flow reserve is also important. A fractional flow reserve of less than 0.75 is almost always associated with ischaemia and a fractional flow reserve of above 0.8 is almost always associated with no inducible ischaemia. [25] However, between these two values there is a degree of uncertainty. The choice of threshold for fractional flow reserve will therefor have an important implication for studies that use this as a “gold standard” assessment. Finally, fractional flow reserve

measurements may be inaccurate when there are multiple or complex stenoses in the same vessel, left main stem disease or recent myocardial infarction. [26] Therefore, alternative non-invasive techniques are required to assess the functional significance of coronary artery disease.

Computed tomography

In his Nobel prize acceptance speech in 1979, Sir Godfrey Hounsfield recognised future cardiac uses of his new computed tomography technology when he said, [27]

> *"A further promising field may be the detection of the coronary arteries. It may be possible to detect these under special conditions of scanning."*

These remarkably insightful words preceded the era of computed tomography cardiac imaging. Hounsfield even included in his Nobel lecture a picture of the chest, synchronised to the cardiac cycle, where the left ventricle myocardium could be clearly identified.

Over the past twenty years computed tomography has revolutionised diagnostic imaging and has transformed all aspects of health care. Today an estimated 70 million computed tomography scans are performed annually in the United States of America [28] and 4 million computed tomography scans are performed annually in the United Kingdom. [29,30] From the 1990s onwards, concerted attempts were

made to image the heart using computed tomography. Initial images were limited by motion artefact and low spatial and temporal resolutions. However, advances such as slip-ring technology, multidetector arrays and software developments means that it is now possible to image the heart in a fraction of a heartbeat. [31]

Computed tomography coronary angiography (CTCA) uses iodinated contrast to assess the coronary arteries. In addition to providing information on the coronary lumen and coronary artery stenoses, it can also identify characteristics of atherosclerotic plaques. More recently cardiac CT has also been used to gain additional functional information, such as with CT myocardial perfusion imaging or CT derived fractional flow estimates (CT FFR). CT myocardial perfusion imaging involves the assessment of myocardial contrast attenuation during rest and stress in order to identify perfusion defects. CT FFR uses computational fluid dynamic modelling based on coronary anatomy from resting CTCA in order to calculate fractional flow reserve. These new techniques have the potential to further improve the diagnostic accuracy of CTCA.

CTCA has an excellent diagnostic accuracy compared to invasive coronary angiography. In particular, the high negative predictive value means that computed tomography coronary angiography is especially useful to rule out coronary artery disease in low risk patients. However, the presence of artefacts such as motion artefact and calcium blooming artefact continue to limit the diagnostic accuracy of computed tomography coronary angiography in high-risk patients.

Diagnostic accuracy

For many patients, the standard initial investigation to diagnose angina due to coronary heart disease is the exercise electrocardiogram. However, this has poor discriminatory accuracy for the detection of coronary heart disease and has recently been criticised in national guidelines. [32] Other investigations such as exercise tolerance tests, cardiac radio-nucleotide imaging and stress echocardiography have similarly low accuracy (Table 1.1). A limitation of these other non-invasive tests is that they assess relative markers of coronary artery disease rather than visualising the coronary lumen itself. More recently magnetic resonance imaging has shown some promise in assessing the coronary arteries, but this technique remains time consuming and technically challenging. [33] Thus computed tomography coronary angiography is the only non-invasive method routinely used to visualise the coronary arteries.

Computed tomography coronary angiography now has a diagnostic accuracy comparable to invasive coronary angiography in populations with a low prevalence of coronary artery disease. [34] Pooled analysis of over 800 patients indicates sensitivity of 89% (95% confidence interval, 87-90%) and specificity of 96% (95% confidence interval, 96-97%) for 64-multidetector computed tomography in comparison with invasive coronary angiography. [34] However, the accuracy of computed tomography coronary angiography is more modest when assessing populations with a higher prevalence of coronary artery disease. [35] The major strength of computed tomography coronary angiography is the negative predictive value and thus the ability to exclude coronary artery disease.

Table 1.1: Diagnostic accuracy of investigations for the detection of coronary heart disease. Data from NICE 2010 document. [32]

Diagnostic test	Sensitivity (%)	Specificity (%)
Exercise electrocardiogram	61	70
Stress Echocardiography	79	87
Single photon emission computed tomography	88	73
Computed tomography coronary angiography	96 to 99	88 to 97

Coronary artery plaque composition

Computed tomography coronary angiography provides important additional information about the coronary artery wall that goes beyond the 'luminal' information provided by conventional angiography. The latter cannot reliably document plaque burden without the use of intravascular ultrasound, whereas computed tomography coronary angiography can provide detailed information regarding mural atherosclerotic plaque burden and subtype (Figure 1.1). In addition to detecting calcified plaque, computed tomography coronary angiography can also detect non-calcified atherosclerotic plaque and attenuation measurements may allow subtypes of non-calcified plaque to be differentiated. [36-38] However, the overlap in plaque density between subtypes makes the differentiation of potentially vulnerable plaques difficult with computed tomography alone. [39] The presence of larger plaque volume, lower attenuation density, higher remodelling index and 'spotty' calcifications are associated with culprit lesions and can potentially be used in scoring systems to identify vulnerable plaques. [37,38,40]

Figure 1.1: Computed tomography coronary angiography curved planar reconstruction (A) and invasive coronary angiography (B) images of the left anterior descending coronary artery. Blooming artefact is apparent in the calcified plaque and this does not correspond to a significant stenosis on the invasive coronary angiogram image.

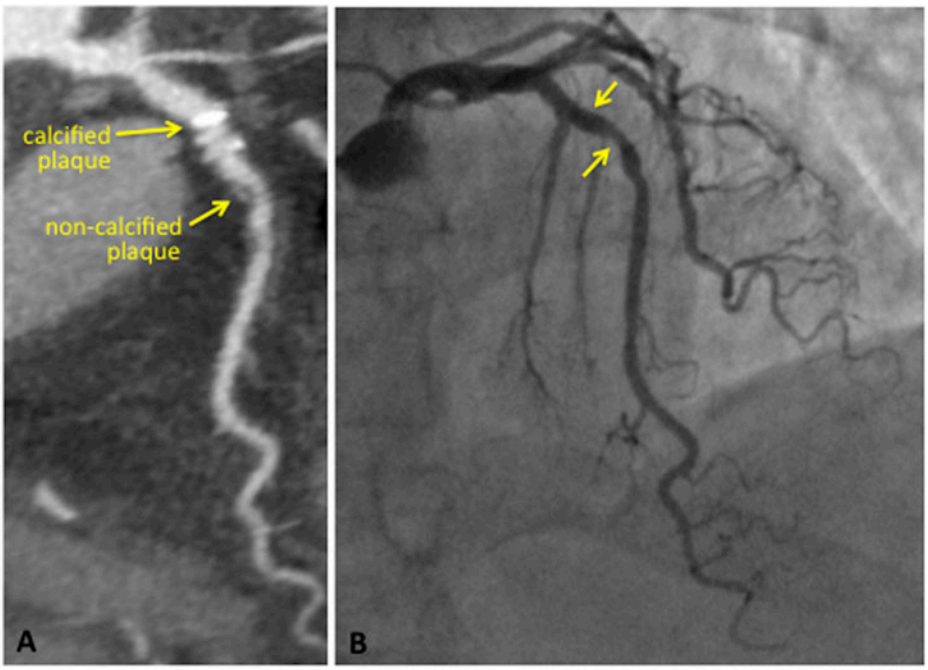

Calcified plaque and "blooming" artefacts

The presence of heavily calcified vessels or dense objects such as coronary artery stents can reduce the diagnostic accuracy of computed tomography coronary angiography. Computed tomography coronary angiography systematically overestimates the significance of calcified plaques [40] and thus a 50% stenosis on computed tomography coronary angiography may be a poor predictor of reversible ischaemia. [41] High attenuation materials such as calcium or stents appear larger ("blooming" artefact) because limited spatial and point spread resolution causes spill

over into adjacent lower intensity voxels. This partial volume averaging and interpolation means that high attenuation structures are incorporated into the adjacent lower attenuation voxels. Further advances in computed tomography technology to reduce these artefacts include improved detector resolution, reconstruction algorithms and improved mathematical models. [42] Dual energy computed tomography was first conceived in 1976 [43,44] and has more recently been applied clinically. The acquisition of two images at different tube voltages allows the separation of materials based on differences in attenuation and may enable more accurate quantification of calcified plaque with reduced "blooming" artefact. [45] Spectral computed tomography using energy-dependent photon counting can further classify materials and improves visualisation of calcified plaques and stents in phantom studies. [46] The combination of spectral computed tomography and contrast agents such as gold, gadolinium or bismuth may enable more detailed imaging of atherosclerotic plaque in the future. [47] However, at present blooming artefact is a limitation of computed tomography coronary angiography when used alone in patients at high risk of coronary artery disease or with a heavy burden of calcification.

Image quality

Optimal image quality is important to maximise diagnostic accuracy in computed tomography coronary angiography. A variety of factors can influence image quality including heart rate, heart rate variability, body mass index, coronary calcification, and the presence of breathing artefacts. [48-50] In the CORE64 study, image quality was associated with ethnicity, body mass index, heart rate and breathing artefacts,

but not with coronary artery calcium score. [51] Motion artefacts, particularly in the mid portion of the right coronary artery, can limit the diagnostic accuracy of computed tomography coronary angiography due to under or overestimation of the presence of coronary artery disease. Heart rate reduction with rate limiting medications such as beta-blockers and the selection of prospective or retrospective protocols is thus important to optimise image quality. New methods to improve image quality include iterative reconstruction algorithms that aim to reduce image noise. However, optimal image quality must be balanced against the risks of radiation exposure.

Computed tomography image generation

In order to transform the x-ray projection data acquired during CT into images for viewing an image reconstruction algorithm is required. These can be divided into two main categories, analytical reconstruction and iterative reconstruction. Analytical methods use one reconstruction where as iterative reconstructions use multiple repetitions in order to converge on a solution. Iterative reconstruction was used in early CT scanners and is widely used in nuclear medicine. [52] However, the high computational requirements of iterative reconstruction meant that until recently filtered back projection was more widely used.

Filtered back projection is an analytical reconstruction method that uses a combination of multiple back-projections with a ramp filter. Back projection involves the “smearing” of the acquired projection data across the image at the angle at which it was acquired. Multiple back projections are required to build up a CT

image. The ramp filter adjusts for the fact that the resulting image will have overlapping projections and reduces blurring. However, it also increases image noise so subsequent filters (also known as kernels) are also required. [53] These additional software filters are used to produce images that are targeted towards the assessment of a particular tissue, such as lung or soft tissue.

The starting point for an iterative reconstruction algorithm can be either an empty data set or an initial estimate from known information such as a filtered back projection reconstruction or standard volume. All iterative reconstruction algorithms have three key steps. Firstly a forward projection is produced from the initial estimate in order to create artificial raw data. Secondly a comparison is made between the real measured data and the artificial raw data in order to calculate a correction term. The correction term is then back projected onto the initial estimate. These steps are repeated either for a fixed number of repetitions or until a predefined criteria in the image are met. [52,53]

There are a variety of different iterative reconstruction methods. Algebraic methods are the most straightforward and involve non-statistical modelling of acquisition geometry. Statistical methods incorporate photon-counting statistics, using an assumed Poisson distribution, and work in either the raw data domain, image domain or during the iterative reconstruction process. Although statistical methods are technically a form of modelling, the term “model based” is reserved for methods that go beyond modelling the detected photons as a Poisson distribution. Geometric modelling considers the acquisition system as a three-dimensional object and models

the focal spot of the x-ray tube or detectors. Physical modelling incorporates models of photon interactions within the object. Prior object information modelling ("knowledge based modelling") corrects for unrealistic situations based on known information. [52,53]

Unfortunately all iterative reconstruction algorithms in current clinical use are "black box" systems. Some of the names of the algorithms contain hints of their actions (Table 1.2) and some information is available in the marketing material from the manufactures. However, insufficient information is provided to ascertain the details of how these algorithms work. In addition, iterative (or other) reconstruction algorithms are not comparable between manufacturers.

Table 1.2: Commercial iterative and model based reconstruction algorithms

Name	Manufacturer
Adaptive statistical iterative reconstruction, ASIR	GE
Veo (Model based iterative reconstruction)	GE
Image reconstruction in image space, IRIS	Siemens
Sinogram affirmed iterative reconstruction, SAFIRE	Siemens
Advanced Modelled Iterative Reconstruction, ADMIRE	Siemens
iDose (Hybrid iterative reconstruction)	Philips
Iterative Model Reconstruction, IMR	Philips
Adaptive iterative dose reconstruction, AIDR	Toshiba
Adaptive iterative dose reconstruction three dimensional, AIDR3D	Toshiba
Forward projected model-based Iterative Reconstruction SoluTion (FIRST)	Toshiba

All stages of the reconstruction process have the ability to impact the final CT image quality. This includes the choice of reconstruction algorithm, filter and post

processing techniques such as “windowing”. Iterative reconstruction algorithms can reduce image noise compared to filtered back projection algorithms from the same manufacturer. This can enable the use of a lower tube current or tube voltage in order to produce an image with a similar level of image noise. However, image noise is only one aspect of image quality. Early iterative reconstruction algorithms were often described as having a “plastic” or “pixelated” texture as compared to previous filtered back projection algorithms. These changes in image appearance have the potential to impact diagnostic accuracy, particularly in small structures such as atherosclerotic plaques. Changes in CT image generation may also lead to changes in the Hounsfield units of a material. This may lead to difficulties in quantitative tasks such as measuring calcium scores [54], attenuation density of atherosclerotic plaques and quantification of myocardial perfusion. [55] More recent model based reconstruction algorithms can provide further reductions in image noise. In addition, the incorporation of additional factors that simulate the image acquisition geometry may lead to more accurate solutions, at the cost of higher computational power or increased time to produce reconstructions. However, the implementation of any reconstruction algorithm must be assessed carefully in order to ascertain any potential impact on diagnosis.

There are now a large number of papers assessing the effect of iterative or model based reconstructions in phantom, animal and human studies. The ideal study would perform repeated imaging in individual patients in order to directly assess the effect of each reconstruction parameter. However, due to concerns regarding radiation dose this is not possible. The research in this thesis represents early work on the use of

iterative reconstruction in cardiac CT and therefor was performed prior a number of more recent papers. A recent meta-analysis identified that iterative reconstruction algorithms improved or maintain image noise and subjective image quality in reduced radiation dose cardiac CT studies as compared to standard radiation dose studies reconstructed with filtered back projection. [56] However, further work is required to assess the effect of cardiac CT reconstructions on diagnosis.

Radiation dose

The most important risk of computed tomography is the potential for radiation-induced carcinogenesis. In the US, it has been estimated that between 0.4 and 2% of all cancers are due to radiation exposure during computed tomography imaging. [57] The lifetime risk of developing cancer from computed tomography imaging is greater for women and young people. [58] When attempting to quantify risk, a radiation dose of between 1 and 10 mSv has an approximate lifetime risk of fatal cancer of 1 in 10,000, which can be described as "very low".[59] However, estimates of cancer risk are derived from data from atomic bomb survivors and radiation workers. Thus they may not reflect the true biological risk of the repeated small radiation exposures due to medical imaging. [57]

The radiation dose from computed tomography coronary angiography is rapidly decreasing. The radiation dose of computed tomography imaging in the CORE64 study published in 2009 was 14 mSv for men and 15 mSv for women. [35] However, it is now possible to perform computed tomography coronary angiography at a radiation dose of below 1 mSv. [60] However, limitations such as heart rate, body

mass index and anatomy means that such low radiation doses are not always possible. Techniques to minimise radiation dose include using individualised protocols, optimal heart rate reduction, postero-anterior acquisition of scout images, minimising the detector range and optimised electrocardiogram gating. Thus it is important to minimise radiation dose while optimising image quality in computed tomography coronary angiography.

Computed tomography myocardial perfusion imaging

Myocardial perfusion can be assessed using a variety of techniques including magnetic resonance imaging (MRI) or nuclear myocardial perfusion imaging with single photon emission tomography (SPECT) or positron emission tomography (PET). In addition, fractional flow reserve and stress echocardiography provide surrogate methods to assess myocardial perfusion. These techniques use visualisation or quantification methods in order to identify haemodynamically significant coronary artery stenoses. The assessment of myocardial perfusion imaging has been shown to have prognostic implications for predicting the risk of cardiovascular events, alone or additive to invasive coronary angiography assessment. [61-63] The additional information provided by myocardial perfusion assessment can also be used to guide management decisions.

Computed tomography myocardial perfusion imaging is based on differences in the passage of iodinated contrast material through normal and ischaemic or infarcted myocardium. [64] Images obtained at rest and during pharmacological stress are

assessed for areas of relative hypo-enhancement. Two image acquisition methods have emerged for the assessment of computed tomography myocardial perfusion imaging. The "snap shot" technique acquires one, or a small number, of images at maximal hyperaemia and contrast enhancement. The "dynamic" technique acquires multiple images over several heartbeats in order to visualise the wash-in and wash-out of contrast material, similar to magnetic resonance myocardial perfusion imaging. Dynamic computed tomography myocardial perfusion is an exciting technique that is currently limited by radiation dose and the incomplete coverage of the myocardium. However, as techniques to reduce radiation dose in cardiac imaging progress, this may have promising applications in the future. This thesis concentrates on the validation of the "snap shot" technique for myocardial perfusion imaging.

The potential for myocardial perfusion imaging using multidetector computed tomography was first established in animals [64] and small studies of humans. [65-68] The sensitivity of computed tomography myocardial perfusion ranges from 79 to 97% and specificity from 72 to 98% depending on the scanner type, reference standard, and whether analysis is per-patient, segment or territory. [69] In the multicentre CORE320 study, which compared computed tomography myocardial perfusion imaging to invasive coronary angiography and SPECT myocardial perfusion imaging, they identified sensitivity, specificity, positive and negative predictive values for the detection of greater than or equal to 50% stenosis of 80%, 74%, 65% and 86% respectively. [70] In addition, computed tomography myocardial perfusion imaging has been found to be additive to computed tomography coronary angiography in the identification of coronary artery disease. [70]

Computed tomography has a higher spatial resolution than PET or SPECT and therefore it has the ability to identify the transmural extent of myocardial perfusion abnormalities. [66] SPECT and PET imaging are also limited by radiation dose from the administration of radioactive material and attenuation artefacts that may be misinterpreted as perfusion defects. [71] Myocardial ischaemia is initially apparent in the subendocardium [72] and non-transmural ischaemia can be detected by magnetic resonance and computed tomography imaging. Computed tomography can detect smaller areas of ischaemia than other modalities and so can potentially identify perfusion defects earlier in the ischaemia cascade. [73] This can also aid in the assessment of patients with three-vessel coronary artery disease, which may be underestimated by methods with lower spatial resolutions.

Quantitative assessment of perfusion defects can be performed using computed tomography imaging. The transmurality of a perfusion defect can be assessed either visually or quantitatively with the transmyocardial perfusion ratio (TPR). TPR attempts to identify subendocardial perfusion defects by dividing the subendocardial attenuation density by subepicardial attenuation density. This is inversely related to percentage diameter stenosis on quantitative coronary angiography. [74,75] The mean TPR in patients without obstructive coronary artery disease is 1.12 ± 0.13 and an abnormal TPR is less than 0.99. [76,77] However, the normal left ventricular myocardium is a complex organ that is heterogeneous in cell type, function, energy requirements and perfusion. Microsphere studies in animals have identified spatial blood flow heterogeneity throughout the myocardium and spatial heterogeneity of

myocardial blood flow has been identified in humans using positron emission tomography. Thus the identification of perfusion defects becomes difficult when "normal" tissue is itself heterogeneous.

The presence of artefacts may also limit the assessment of myocardial perfusion by computed tomography. Beam hardening artefacts occur when x-rays pass through a dense object and low energy photons are preferentially absorbed, thus locally increasing the x-ray beam mean energy and causing a false apparent reduction in the attenuation in adjacent areas. Dense objects in the field of view include vertebrae, sternum, ribs and the contrast filled left ventricle and aorta. Beam hardening artefacts may be mistaken for perfusion defects [78] and are particularly common in the basal inferior wall. [67] Advances in iterative reconstruction and beam hardening correction algorithms can reduce the effect of these artefacts on the assessment of myocardial perfusion. [78]

Comprehensive cardiac imaging with computed tomography

One of the main advantages of computed tomography imaging is the ability to assess anatomy, function, perfusion and viability in one rapid diagnostic test (Figure 1.2). This reduces the number of investigations that the patient must undergo in order to inform their diagnosis. In addition to information on anatomy, the presence of coronary artery stenoses and myocardial perfusion defects, this protocol can also assess ventricular function and myocardial viability.

Figure 1.2: Comprehensive cardiac assessment using computed tomography.

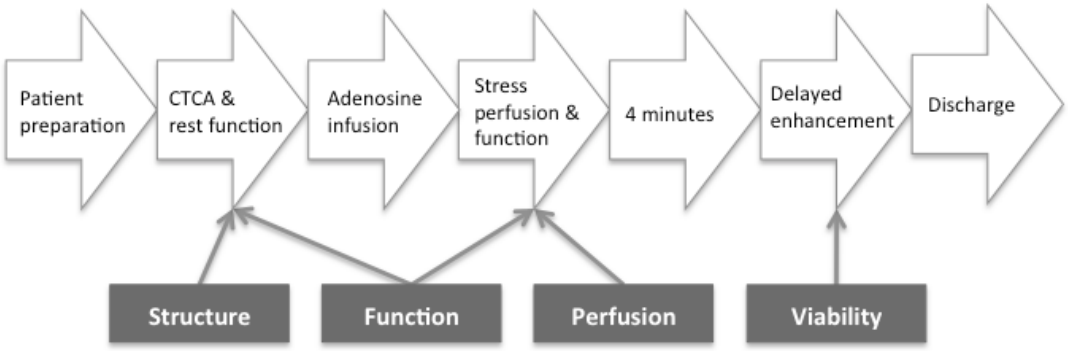

Ventricular function

Left ventricular volumes and function are independent predictors of morbidity and mortality. [79] Cardiac magnetic resonance is the gold standard for the assessment of left ventricular function. [80] The acquisition of computed tomography images at end-systole and end-diastole allow the calculation of left ventricular volumes and the reconstruction of images across the cardiac cycle enables the assessment of regional wall motion abnormalities. (Figure 1.3) There is good agreement between computed

tomography measurements and magnetic resonance and echocardiographic assessments. [81] In addition, the functional information acquired during stress computed tomography perfusion can increase the diagnostic accuracy of cardiac computed tomography imaging. [82]

Figure 1.3: Computed tomography assessment of cardiac function showing (A) end diastolic and (B) end systolic images from a patient with an infero-lateral regional wall motion abnormality.

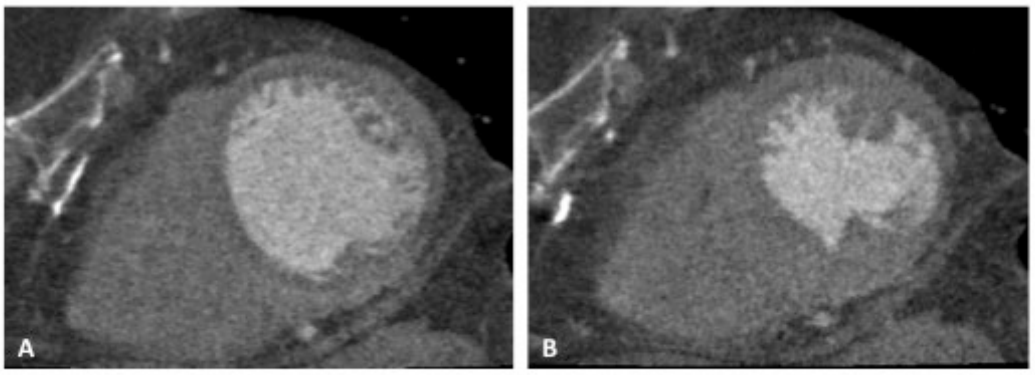

Myocardial viability

Normal myocytes are densely packed but in the setting of infarction the loss of membrane integrity allows an increased tissue concentration of contrast. [83] This can be identified as hyper-enhancement on delayed imaging (Figure 1.4). Cardiac magnetic resonance imaging is the gold standard for the assessment of myocardial viability and the presence of late gadolinium enhancement predicts functional recovery after revascularisation and is related to prognosis. [80] However, it is also possible to assess delayed hyper-enhancement on computed tomography imaging in

animals [84] and in humans. [85-88] There is a strong relationship between the extent of a perfusion defect and late enhancement and myocardial functional recovery. [89] However, the optimal scan timing, scan order, tube voltage and current, contrast volume and post processing techniques are yet to be determined. [83]

Figure 1.4: Myocardial late enhancement identified by computed tomography (A) and subsequent magnetic resonance imaging (B).

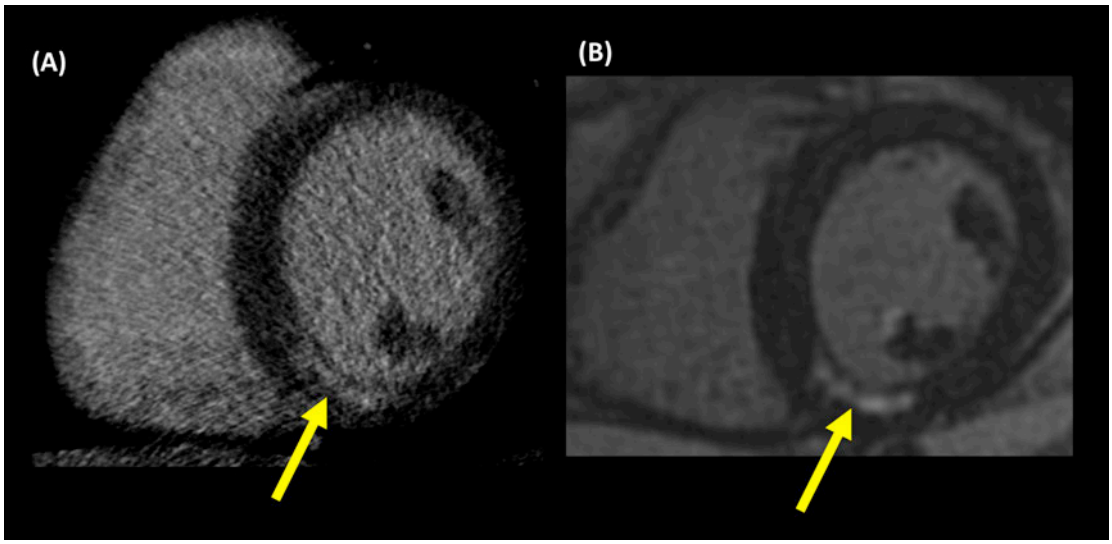

Oxygen-15 labelled water positron emission tomography

Most currently used methods to assess myocardial perfusion evaluate "relative" perfusion defects by comparing abnormal areas to normal areas in the same patient. This has the disadvantage that for patients with severe three-vessel disease the abnormal areas may not be identified. In addition, the current clinical “gold standard” of fractional flow reserve may under or overestimated stenosis severity. Thus a superior "gold standard" method to assess myocardial perfusion and the haemodynamic significance of coronary artery stenosis is required.

Measurement of absolute myocardial perfusion can be performed using oxygen-15 labelled water positron emission tomography (PET). Oxygen-15 labelled water is a freely diffusible metabolically inert tracer with a high extraction fraction that is independent of flow rate. [90-92] This makes it the ideal "gold standard" for the assessment of myocardial blood flow. In addition, this technique can assess absolute rather than relative myocardial blood flow.

Myocardial blood flow measurements from oxygen-15 labelled water PET have been validated against in vivo radiolabelled microspheres in animal models. [93-99] In addition, human studies have established the accuracy of this technique compared to invasive coronary angiography, fractional flow reserve, SPECT, magnetic resonance imaging and computed tomography coronary angiography. [100-107] Previous studies have identified good inter-observer and intra-observer variability for the assessment of myocardial blood flow by oxygen-15 labelled water PET and there is

low variation between repeat scans and scanners or image analysis software. [108-110]

Thus oxygen-15 labelled water PET is the ideal physiological "gold standard" for the evaluation of techniques assessing myocardial perfusion.

Aims and Hypotheses

In this thesis I aim to develop a comprehensive technique for the assessment of coronary artery disease using 320-multidetector computed tomography imaging. In addition, I aim to optimise the technique in order to produce diagnostic quality images at the lowest possible radiation dose. I hypothesise that 320-multidetetor computed tomography will provide an accurate non-invasive method for assessing the presence, severity and physiological consequence of coronary artery disease in a single examination and at an acceptable level of radiation exposure.

Chapter 2 discusses the methods used in this thesis including computed tomography coronary angiography, computed tomography myocardial perfusion, invasive coronary angiography, fractional flow reserve and oxygen-15 labelled water positron emission tomography.

Optimisation of computed tomography coronary angiography is essential in order to obtain diagnostic quality images at the lowest possible radiation dose. I hypothesise that the application of radiation dose reduction techniques such as iterative

reconstruction algorithms and individualised automatic tube current selection will reduce radiation dose whilst maintaining image quality in computed tomography coronary angiography (Chapter 3).

Computed tomography coronary angiography with a 320-multidetector scanner can be performed using single or multi-segment reconstructions. I hypothesise that single segment reconstructions can provide diagnostic image quality in the majority of unselected patients (Chapter 4). In addition, Chapter 4 will assess the factors that affect image quality in single heartbeat computed tomography coronary angiography using a 320-multidetetor scanner.

The techniques used to reduce radiation dose in computed tomography coronary angiography can also be applied to computed tomography myocardial perfusion imaging. I hypothesise that iterative reconstruction will also reduce radiation dose in computed tomography myocardial perfusion imaging, whilst maintaining image quality (Chapter 5).

Observer variability is an important factor for all diagnostic imaging techniques. I hypothesise that good inter and intra observer variability will be identified for computed tomography coronary angiography (Chapter 6), computed tomography myocardial perfusion imaging (Chapter 7) and oxygen-15 labelled water positron emission tomography (Chapter 8). This will provide additional evidence to support the clinical use of these techniques. In addition I hypothesise that the reduction in stair-step and other artefacts in 320-multidetector computed tomography coronary

angiography will lead to an increase in the number of diagnostic segments as compared to 64-multidetector computed tomography coronary angiography.

The combination of computed tomography coronary angiography and computed tomography myocardial perfusion (CTCA/CTP) imaging will be compared to two "gold standard" methods of assessing coronary artery disease. I hypothesise that CTCA/CTP will have good diagnostic accuracy as compared to the clinical gold standard of invasive coronary angiography and fractional flow reserve (Chapter 7). In addition, I hypothesise that the quantitative assessment of CT myocardial attenuation density during hyperaemia will correlate with the physiological gold standard of absolute myocardial blood flow assessed by oxygen-15 labelled water positron emission tomography (Chapter 8).

Conclusion

The ideal diagnostic test for coronary artery disease would combine information on cardiac and coronary anatomy, cardiac function, myocardial perfusion and myocardial viability in one rapid non-invasive diagnostic test. Advances in computed tomography imaging means that it has the potential to provide such comprehensive cardiovascular assessment.

At the Clinical Research Imaging Centre in Edinburgh the 320-multidetector computed tomography scanner (Aquilion ONE, Toshiba Medical Systems) is capable

of wide volume imaging of the heart. This thesis discusses the optimisation of computed tomography coronary angiography and computed tomography myocardial perfusion imaging using this computed tomography scanner. In addition, computed tomography myocardial perfusion imaging is validated against clinical and physiological "gold standard" assessments, namely fractional flow reserve during invasive coronary angiography and oxygen-15 labelled water PET.

Chapter Two: Methods

Extracts of this chapter are published in:

Williams MC, Weir NW, Mirsadraee S, et al. Image quality with single heart beat 320 multidetector computed tomography coronary angiography. Journal of Computer Assisted Tomography 2014: 38 (3); 444-450.

Williams MC, Weir NW, Mirsadraee S, et al. Iterative reconstruction and individualized automatic tube current selection reduce radiation dose while maintaining image quality in 320-multidetector computed tomography coronary angiography. Clinical Radiology 2013: 2013: 68(11); e570-7.

Summary

This thesis applies a number of state of the art technologies to assess the heart including computed tomography, invasive coronary angiography, fractional flow reserve and oxygen-15 labelled water positron emission tomography. This chapter discusses the methods used to perform and analyse these investigations.

Study conduct

All studies were conducted in accordance with the Declaration of Helsinki and local research ethics committee approval was obtained. In addition, for studies involving PET imaging, ARSAC (Administration of Radioactive Substances Advisory Committee) approval was obtained.

Comprehensive computed tomography cardiac imaging

Patient preparation

Adequate patient preparation is essential in order to perform good quality computed tomography imaging. Patients were assessed in a calm environment in order to minimise anxiety and evaluate their heart rate. Patients undergoing myocardial perfusion imaging were asked to refrain from caffeine for 12 hours. Heart rate and blood pressure were measured and intravenous access was obtained.

Rate limiting medication

Prior to computed tomography, patients with a heart rate greater than 60 /min received rate limiting medication. Intravenous metoprolol was administered up to a maximum dose of 50 mg, in order to obtain a target heart rate of below 60 /min. If beta-blockade was contraindicated then oral and/or intravenous verapamil was considered (80 mg oral and 2.5 to 5 mg intravenous), but was used infrequently.

Sublingual glyceryl trinitrate

Sublingual glyceryl trinitrate dilates the coronary arteries and can lead to improved visualisation of distal coronary artery segments. [111] We assessed images before and after the introduction of sublingual glyceryl trinitrate (Chapter 4) to our computed tomography coronary angiography protocol. Subsequently sublingual glyceryl trinitrate (300 μg) was administered prior to rest imaging for all patients.

Computed tomography

Computed tomography imaging was performed using a 320-multidetector scanner (Aquilion ONE, Toshiba Medical Systems, Japan) at the Clinical Research Imaging Centre in Edinburgh.

Coronary artery calcium score

Non-contrast imaging was performed to assess coronary artery calcification. This was performed after the acquisition of scout images and before contrast enhanced imaging. Imaging was performed using a tube voltage of 120 kV, tube current based

on body mass index and scan range from 2 cm below the carina to the base of the heart using volume sizes of 160, 140, 128, 120, 100 or 80 mm.

Computed tomography coronary angiography

Computed tomography coronary angiography was performed using prospective, electrocardiogram-gated contrast-enhanced imaging. Either single (half) or multi-segment imaging was used and the rotation time was 0.35ms. Detector coverage was selected based on scout images or non-contrast imaging to cover from 2 cm below the carina to the base of the heart with volume sizes of 160, 140, 128, 120, 100 or 80 mm. A tri-phasic injection of intravenous contrast agent (Iomeron400, Bracco, Italy) was administered based on body mass index (<30 kg/m^2, 50 mL; >30 kg/m^2, 60 mL, >40 kg/m^2, 70 mL). Window of acquisition was selected based on heart rate. For patients with a heart rate below 65 /min, images were acquired with an acquisition window of 70 to 80% of the interval between two consecutive QRS complexes. For patients with a heart rate above 65 /min the acquisition window was widened to 30 to 80% of the interval between two consecutive QRS complexes.

For patients undergoing only computed tomography coronary angiography, automatic bolus triggering was used to start the scan when the attenuation reached 140 HU in the left ventricle. For patients undergoing rest and stress imaging, a threshold of 300 HU in the descending aorta and manual triggering was used.

Computed tomography myocardial perfusion

Pharmacological stress was induced using an adenosine infusion (140 μg/kg/min). Stress imaging was performed at least 10 min after rest imaging and after at least 4 min of adenosine. The same tube voltage, tube current and contrast protocol was used as for rest imaging. However, tube current modulation was used to obtain data over a single heartbeat in order to obtain additional functional imaging. In order to minimise radiation dose the scan range was reduced to cover only the left ventricle.

Late enhancement imaging

A further low dose non-contrast computed tomography image was obtained at 3 to 4 minutes after the last injection of contrast in order to assess myocardial late enhancement. This was performed with a tube voltage of 80 or 100 kV depending on body mass index. Tube current was selected based on body mass index. A targeted acquisition at 75% of the interval between two consecutive QRS complexes was used in order to minimise radiation dose.

Image reconstruction

Images were reconstructed using half-segment or multi-segment reconstruction. Images were reconstructed with an automatically selected best phase and a 10-ms window either side of this. If artefacts were apparent on these initial images then additional reconstructions were produced at intervals of 5% across the period scanned.

Images for the assessment of coronary calcification were reconstructed with 3mm non-overlapping slices with the FC02 reconstruction kernel (smooth kernel, Toshiba

Medical Systems). Images for cardiac assessment were reconstructed with a slice thickness of 0.5 mm and an increment of 0.25 mm with the FC05 reconstruction kernel (smooth kernel, Toshiba Medical Systems). Images for the assessment of rest or stress myocardial perfusion were reconstructed with the FC03 reconstruction kernel (smooth kernel, Toshiba Medical Systems) that contains additional beam hardening correction. [78]

Images were reconstructed with either the standard filtered back projection reconstruction algorithm (QDS+, Boost) or iterative reconstruction (AIDR, or AIDR3D) as detailed in each chapter.

Radiation dose

The dose length product displayed on the scanner console after imaging was recorded. This was converted to millisieverts (mSv) using the commonly used conversion factor of 0.014 mSv/mGy.cm and an scanner specific conversion factor of 0.029 mSv/mGy.cm calculated using the method described by Huda *et al*. [59]

Image analysis

Images were analysed on a dedicated post-processing workstation (Vitrea fX, Vital Images, Minnetonka, USA). Images were assessed by two trained observers, and differences were agreed by consensus. Assessment of imaging was performed blinded to results of other modalities.

Coronary artery calcium score was assessed using the Agatston calcium scoring method. [112] Coronary artery calcium scoring was performed using dedicated software (VScore, Vital Images or Siemens console software). Coronary artery calcification was defined as an area in the course of a coronary artery that had attenuation threshold of ≥120 Hounsfield units (HU) and was ≥1 mm^2. On each axial slice the area of calcification that met this requirement was measured and then multiplied by a weighting factor dependent on the peak attenuation within the region. These weighted areas were summed to produce the total Agatston coronary artery calcium score.

Assessment of coronary artery stenosis was performed using a 15-segment model. [113,114] Luminal cross-sectional area was classified as normal (<10%), mild (10-49%), moderate (50-70%) and severe (≥70%).

Assessment of computed tomography myocardial perfusion was performed using the 17-segment model. [115] Segmental data were consolidated into 3 territories for per-vessel perfusion analysis. [115] Obstructive coronary artery disease was defined as stenosis >50% with corresponding hypoperfusion on computed tomography myocardial perfusion imaging. Images were assessed in the short axis starting with a window width of 200 and level of 100, minimum intensity projection and thick slices. [116] Viewing parameters were manually adjusted as required.

Quantitative assessment of computed tomography myocardial attenuation density was performed on short-axis images of the left ventricle. The apex was excluded

from quantitative analysis. Automatically applied myocardial contours were edited manually as required. Attenuation density was measured in each myocardial segment for the endocardium, mid-wall, epicardium and full thickness. The transmyocardial perfusion ratio was calculated as the ratio of segmental subendocardial attenuation divided by mean subepicardial attenuation of the short-axis slice. [66] Computed tomography attenuation density corrected for rate pressure product was calculated from heart rate and blood pressure during imaging.

Invasive coronary angiography and fractional flow reserve

Invasive coronary angiography was performed via the radial approach under systemic heparinisation as per standard practice. Standard angiographic views of the left (right anterior oblique (RAO), RAO caudal, left anterior oblique (LAO) caudal, LAO cranial) and right coronary arteries (RAO, LAO and LAO cranial) were performed as required.

Fractional flow reserve was assessed for major coronary epicardial vessels with a stenosis >50%, where technically possible. Pharmacological stress was induced using an infusion of adenosine (140 μg/kg/min). A 0.014-inch pressure sensor angioplasty guide wire (Radi Medial Systems, Sweden) was inserted through a guiding catheter into the target artery. The sensor wire's pressure signal was matched to the aortic (guide catheter) pressure and then the catheter was advanced across the lesion to be assessed. The mean pressure distal to the stenosis was measured at maximal hyperaemia. Fractional flow reserve was defined as the ratio between distal

coronary pressure and aortic pressure measured simultaneously at maximal hyperaemia. To assess serial lesions or diffuse coronary artery disease, the pressure wire was pulled back steadily from distal to proximal vessel to record the pressure pullback curve. [21]

Obstructive coronary artery disease was defined as luminal stenosis ≥70% on invasive coronary angiography and/or fractional flow reserve <0.80. [21]

Oxygen-15 labelled water positron emission tomography

Oxygen-15 labelled water production

Oxygen-15 was produced using an on site cyclotron (PETtrace 8, GE Healthcare) using a nitrogen target and deuteron reaction (14N(d,n)15O). This produces $^{15}O_2$ gas that is piped from the cyclotron to the scanner room.

Oxygen-15 labelled water was produced using a radio-water generator (Hydex Oy, Finland). The $^{15}O_2$ and H_2 gasses are processed into water vapour in an oven at 700^{o}C. Using a diffusion membrane the radioactive water vapour is trapped into sterile saline solution in order to continuously produce the oxygen-15 labelled water tracer ($H_2{}^{15}O$). [117]

Positron emission tomography/Computed tomography

PET/CT imaging was performed using a hybrid scanner (64-multidetector Biograph mCT, Siemens Medical Systems, Erlangen, Germany).

Attenuation correction CT was performed using 100 kV and 40 mAs either before rest imaging or before rest and stress imaging.

Rest imaging was performed using a target of 500 MBq of oxygen-15 labelled water (bolus over 15 s, followed by 2 min saline flush). Dynamic acquisition was performed over 5 min (14x5, 3x10, 3x20 and 4x30 s). After suitable decay (approximately 10 min), stress imaging was performed. This was started 2 min after commencing an adenosine infusion, with a further 500 MBq oxygen-15 labelled water. Dynamic acquisition was performed, as for rest imaging, during the infusion of adenosine. Dynamic emission images were reconstructed using the UltraHD algorithm (Siemens Medical Systems, Germany; zoom 2, matrix 128x128, voxel size 3.18x3.18x3 mm).

Image analysis

PET images were analysed using dedicated software (Carimas 2.4, Finland) using a single tissue compartment model with correction for perfusable tissue fraction and spill-over. [118] Images were reoriented into short-axis and myocardial contours were defined on digital subtraction images automatically, with manual adjustment. Myocardial blood flow was analysed for the entire left ventricle. Segmental data was consolidated into 3 territories for per-vessel analysis. [115] Coronary vasodilator reserve was defined as the ratio of peak hyperaemic to resting myocardial blood flow. [119] Total coronary resistance was calculated as mean arterial pressure divided by myocardial blood flow at baseline and hyperaemia. [119] Myocardial

blood flow corrected for rate pressure product was calculated from heart rate and blood pressure during imaging.

Statistical analysis

Statistical analysis was performed using PASWStatistics (Version 18 for Mac OS X, IBM) and Graphpad Prism (Version 6 for Mac).

Normally distributed continuous variables are presented as mean and 95% confidence intervals. Non-normally distributed data are presented with median and interquartile range. Categorical variables are presented as frequencies and percentage.

Statistical significance was assessed using analysis of variance, Student's t-test, Mann-Whitney U test, Dunnett's t-test or Pearson's chi-squared test as appropriate. Correlations between normally distributed variables were assessed using the Pearson or Spearman correlation coefficients.

Sensitivity, specificity, positive predictive value (PPV) and negative predictive value (NPV) were calculated on a per-vessel, per-segment and per-patient basis. Receiver operator characteristic curves were constructed to assess diagnostic accuracy and area under the curve and optimal cut off values assessed.

Inter and intra-observer variability were assessed using Kappa statistics and Bland-Altman plots. A Kappa statistics of less than 0.2 indicated poor agreement, 0.21 to 0.4 fair agreement, 0.41 to 0.6 moderate agreement, 0.61 to 0.8 good agreement and 0.81 to 1 excellent agreement.

A statistically significant difference was defined as a two-sided P value <0.05.

Chapter Three: Computed tomography coronary angiography radiation dose reduction

Extracts of this chapter are published in:

Williams MC, Weir NW, Mirsadraee S, et al. Iterative reconstruction and individualized automatic tube current selection reduce radiation dose while maintaining image quality in 320-multidetector computed tomography coronary angiography. Clinical Radiology 2013: 2013: 68(11); e570-7.

Abstract

Introduction

The effect of two iterative reconstruction algorithms (AIDR and AIDR3D) and individualised automatic tube current selection on radiation dose and image quality in computed tomography coronary angiography (CTCA) was assessed.

Methods

In a single centre cohort study, 942 patients underwent electrocardiogram-gated CTCA using a 320-multidetector scanner. Images from Group 1 (n=228) were reconstructed with a filtered back projection algorithm (QDS+). Iterative reconstruction was used for Group 2 (AIDR, n=379) and Group 3 (AIDR3D, n=335). Tube current was selected based on BMI for Groups 1 and 2 and selected automatically based on scout image attenuation for Group 3. Subjective image quality was graded on a four-point scale (1 excellent, 4 non-diagnostic).

Results

There were no differences in age (P=0.975), body mass index (P=0.435) or heart rate (P=0.746) between groups. Image quality improved with iterative reconstruction and automatic tube current selection (1.3 (95% confidence intervals: 1.2, 1.4), 1.2 (1.1, 1.2) and 1.1 (1.0, 1.2) respectively; P <0.001) and radiation dose decreased (274 (260, 290), 242 (230, 253) and 168 (156, 180) mGy.cm respectively, P <0.001).

Conclusion

The application of the latest iterative reconstruction algorithm and individualised automatic tube current selection can substantially reduce radiation dose whilst improving image quality in CTCA.

Introduction

A variety of strategies to reduce radiation exposure in computed tomography coronary angiography have been developed including prospective electrocardiogram gating, tube current modulation, tube voltage reduction, minimised scan range and heart rate reduction. [120,121] Patient tailored imaging is important to avoid under or over exposure that can lead to grainy images or an unnecessarily high radiation dose. Patient tailored imaging based on body mass index is widely used in computed tomography coronary angiography. [122,123] However, body mass index is not necessarily an accurate guide to thoracic attenuation due to the wide variation in body habitus and fat distribution. Alternative methods proposed to select exposure settings include measurement of chest dimensions [124], chest tissue composition [125], scout image attenuation [126], pre-contrast attenuation [127] and the use of automatic exposure control. [128]

Advances in computed tomography technology have led to the development of iterative reconstruction techniques that have the potential to reduce radiation dose while maintaining image quality. Iterative reconstruction techniques were applied in early computed tomography scanners and have been widely used in nuclear medicine techniques, such as positron emission tomography. However, the high computational demands and consequent long reconstruction times of previous iterative reconstruction algorithms meant that filtered back projection became more widely used in computed tomography. Adaptive Iterative Dose Reduction (AIDR, Toshiba Medical Systems, Japan) reduces image noise in phantom studies [129] and

maintains image quality in reduced dose computed tomography coronary angiography. [130]

The combination of iterative reconstruction technology and individualised automatic tube current selection has the potential to reduce radiation dose whilst maintaining image quality. In this study, we assessed the effect of applying iterative reconstruction and software that automatically selects tube current based on scout image attenuation, on radiation and image quality in computed tomography coronary angiography.

Methods

Study design

In a single centre retrospective cohort study, we assessed the images of 942 consecutive patients who underwent clinically indicated computed tomography coronary angiography using a 320-multidetector scanner (Aquilion ONE, Toshiba Medical Systems, Japan). The local ethics committee waived the requirement for gaining informed consent, as this was part of clinical service development. Exclusion criteria for computed tomography were documented severe allergy to iodinated contrast medium, impaired renal function (estimated glomerular filtration rate <30 mL/min), pregnancy or a weight exceeding the maximum tolerance of the scanner bed (250 kg).

Patients were divided into three groups based on the reconstruction algorithm and method of tube current selection. Images from Group 1 (n=228) were reconstructed with a filtered back projection reconstruction algorithm (QDS+). Iterative reconstruction was applied in Group 2 (AIDR, n=379) and Group 3 (AIDR3D, n=335). Tube current was selected based on body mass index for Group 1 and 2 but was selected automatically based on scout image attenuation for Group 3.

Computed tomography

Computed tomography coronary angiography was performed as described in Chapter 2. For patients with a heart rate below 65 /min, images were acquired with an acquisition window of 70 to 80% of the interval between two consecutive QRS complexes. For patients with a heart rate above 65 /min the acquisition window was widened to 30 to 80%. Tube voltage was selected based on body mass index. For Group 1 and 2, a tube voltage of 100 kV was used for patients with a body mass index <27 kg/m^2, 120 kV for 27-38 kg/m^2, and 135 kV >38 kg/m^2. For Group 2, a tube voltage of 100 kV was used for patients with a body mass index ≤30 kg/m^2 and 120 kV for patients >30 kg/m^2. Tube current was selected based on body mass index for Group 1 and Group 2 (Table 3.1). For Group 3 individualised, automated tube current selection based on scout image attenuation was applied (SUREexposure, Toshiba Medical Systems, Japan). The predetermined level of image noise was set at a standard deviation of 45 (slice thickness 0.5 mm, reconstruction kernel filter FC05 (smooth kernel, Toshiba Medical Systems)). For Groups 1 and 2, imaging was triggered when a threshold of 180 Hounsfield units was reached in the left ventricle. A more rapid triggering mechanism was available along with the software used in

Group 3 where bolus triggering could occur during inspiration with a reduced delay. Therefor, in Group 3 the scan was triggered with a threshold of 340 Hounsfield units in the left ventricle in order to obtain equivalent contrast in the coronary arteries compared to Group 1 and Group 2.

Table 3.1: The selection of exposure settings for computed tomography coronary angiography for Group 1, Group 2 and Group 3.

Body Mass Index (kg/m^2)	Group 1 (QDS+)		Group 2 (AIDR)		Group 3 (AIDR 3D and SUREexposure)	
	Tube voltage (kV)	Tube current (mA)	Tube voltage (kV)	Tube current (mA)	Tube voltage (kV)	Tube current (mA)
<20	100	400 to 450	100	320 to 360	100	Automatic selection based on scout image attenuation
20-26		450 to 580		360 to 460		
27-30	120	510 to 530	120	410 to 420	120	
31-38		560 to 570		450 to 460		
39-40	135	480 to 500		480 to 500		
>40		500	135	500		

Image reconstruction

All images were reconstructed with a slice thickness of 0.5 mm and an increment of 0.25 mm. Images from Group 1 were reconstructed using the standard filtered back projection algorithm (Quantum Denoising Software, QDS+) and a reconstruction kernel filter optimised for cardiac imaging (FC03 (smooth kernel, Toshiba Medical Systems)). Images from Group 2 were reconstructed using an iterative reconstruction algorithm (Adaptive iterative dose reduction, AIDR) and the same reconstruction

kernel filter (FC03 (smooth kernel, Toshiba Medical Systems)). Images from Group 3 were reconstructed using a new iterative reconstruction algorithm (AIDR3D) with the standard level of blending. This produced visually softer images as compared to QDS+ or AIDR algorithms and thus a slightly sharper reconstruction kernel filter (FC05 (smooth kernel, Toshiba Medical Systems)) was used to obtain images that were subjectively assessed as similar between the three groups.

Image analysis

Images were analysed on a dedicated post-processing workstation (Vitrea fX, Vital Images, Minnetonka, USA) and were assessed by two trained observers. Image quality was assessed on a four-point Likert scale (1 excellent; 2 mild reduction in image quality; 3 moderate reduction in image quality; 4 severe reduction in image quality).

Image noise was assessed with regions of interest placed in the ascending aorta at the level of the left main stem, the proximal interventricular septum and in the liver. Image noise was determined as the standard deviations of the Hounsfield units within the region of interest. Contrast-to-noise ratio was calculated as the attenuation value in the aorta minus the attenuation value in the liver divided by the image noise in the aorta. Contrast-to-myocardium ratio was calculated as the attenuation value in the aorta minus the attenuation value in the interventricular septum divided by the image noise in the aorta.

Statistical analysis

Statistical analysis was performed as described in Chapter 2. Statistical significance was assessed using analysis of variance, Dunnett's t-test or Pearson's Chi-squared test as appropriate.

Results

The images of 942 patients were assessed (Group 1, n=228; Group 2, n=379; Group 3, n=335). There were no differences in age, heart rate or body mass index between groups (Table 3.2). There was a small increase in the number of males imaged in Groups 2 and 3. There was a small reduction in z-axis volume size and an increase in 30-80% acquisition windows between Group 1 and Groups 2 and 3. (Table 3.3) There was no difference in the volume of contrast used between groups.

Table 3.2: Demographic details for Chapter 3.

	Group 1 (QDS+)	**Group 2 (AIDR)**	**Group 3 (AIDR3D and SUREexposure)**	***P***
N	228	379	335	-
Age (years)	58 (56, 59)	58 (57, 59)	58 (57, 59)	0.975
Male	89 (39%)	182 (48%)	181 (54%)	0.002
Body mass index (kg/m^2)	29 (28, 30)	30 (29, 30)	29 (29, 30)	0.453
Heart rate (beats per min)	60 (58, 61)	60 (59, 61)	59 (58, 60)	0.746

(Mean (95% confidence interval) or number (percentage))

Table 3.3: Computed tomography coronary angiography imaging parameters for Group 1, Group 2 and Group3.

		Group 1 (QDS+)	Group 2 (AIDR)	Group 3 (AIDR3D and SUREexposure)	*P*
Scan range (mm)		133 (131, 134)	130 (129, 131)	128 (127, 129)	0.003
Acquisition window (30-80% / 70-80%)		33/195	80/299	76/259	0.046
Contrast (mL)		55 (54, 56)	56 (55, 56)	55 (54, 56)	0.561
Tube voltage (kV)	100	34.2%	31.1%	57.3%	<0.001
	120	57.5%	59.6%	42.7%	<0.001
	135	8.3%	9.2%	0%	<0.001
Tube current (mA)	100 kV	538 (530, 547)	432 (425, 440)	334 (313, 355)	<0.001
	120 kV	538 (533, 543)	431 (428, 434)	426 (404, 448)	<0.001

(Mean (95% confidence interval) or percentage)

There was an increase in the use of the lower tube voltage in Group 3 (P <0.001) and a reduction in tube current between Group 1 and both Groups 2 (P <0.001) and 3 (P <0.001; Table 3.3). The use of scout image-based selection of tube current led to the use of a much wider range of tube currents in Group 3 (Figures 3.1).

Compared to filtered back projection (QDS+) reconstructions, the application of iterative reconstructions led to an improvement in subjective image quality (P <0.001; Table 3.4). There was no statistically significant difference in subjective image quality obtained between the two iterative reconstruction algorithms (P

=0.861). Figures 3.2, 3.3 and 3.4 show examples of sub-millisievert images from patients in Group 3 with normal coronary arteries, and those with moderate and severe coronary artery disease. Figure 3.5 shows coronary artery images from all three groups from patients with the same body mass index and gender.

For Group 3, the attenuation density was higher in the aorta and lower in the liver (Table 3.4). However there was no difference in attenuation density measured in the interventricular septum. There was an apparent small but not statistically significant reduction in noise between Group 1 and Group 2 in the liver and interventricular septum. There was an increase in noise in the aorta and interventricular septum in Group 3. There was no difference in contrast-to-noise or contrast-to-myocardium between the three groups.

Figure 3.1: Box plots showing the reduction in mean tube current for scans performed at (A) 100 kV and (B) 120 kV. Box plot with circles denoting outliers.

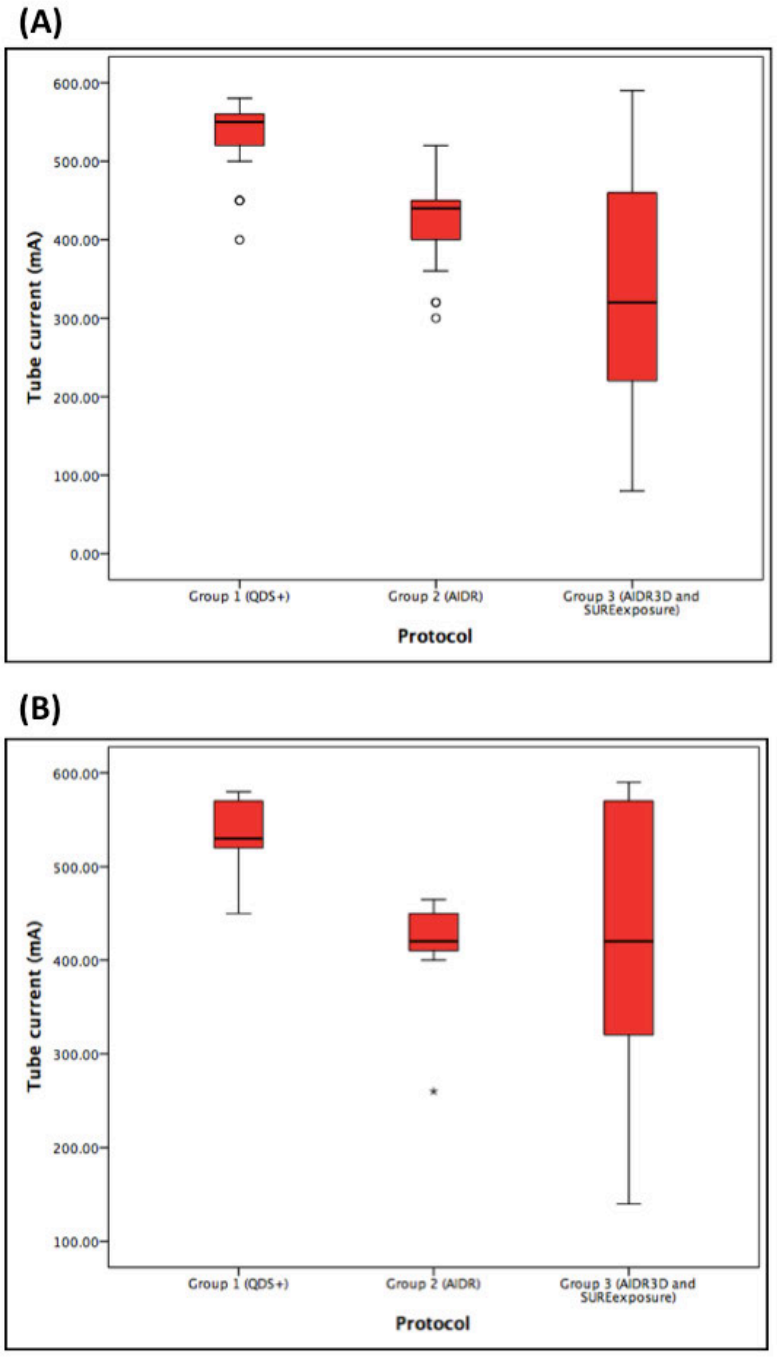

Table 3.4: The effect of reconstruction on image quality and radiation dose.

	Group 1 (QDS+)	**Group 2 (AIDR)**	**Group 3 (AIDR3D and SUREexposure)**	**P**
Subjective image quality	1.3 (1.2, 1.4)	1.2 (1.1, 1.2) *	1.1 (1.0-1.2) *	<0.001
Aorta attenuation (HU)	430 (416, 443)	426 (417, 434)	508 (495, 520) * §	<0.001
Liver attenuation (HU)	65 (62, 68)	61 (59, 63) *	59 (58, 61) * §	<0.001
IVS attenuation (HU)	89 (86, 92)	84 (83, 86) *	87 (85, 89)	0.007
Image noise aorta (HU)	32 (31, 33)	31 (30, 32)	41 (40, 41) * §	<0.001
Image noise liver (HU)	39 (38, 41)	37 (36, 38) *	39 (39, 40) §	0.001
Image noise IVS (HU)	34 (33, 36)	31 (31, 32) *	37 (36, 37) * §	<0.001
Contrast-to-noise ratio	12 (12, 13)	12 (12, 13)	11 (11, 12) § *	0.005
Contrast-to-myocardium ratio	11 (11, 12)	11 (11, 12)	11 (10, 11) §	0.008
DLP (mGy.cm)	274 (260, 290)	242 * (230, 253)	168 * § (156, 180)	<0.001

*(Mean (95% confidence interval), IVS, intraventricular septum; DLP, dose length product; Hounsfield unit, HU; * P<0.05 compared to Group 1; § P<0.05 compared to Group 2)*

Figure 3.2: Images from a Group 3 patient with normal coronary arteries showing (A) 3D image of the heart, (B) LAD and (C) RCA. The female patient had a BMI of 20 kg/m^2 and a radiation dose of 0.54 mSv (k=0.014).

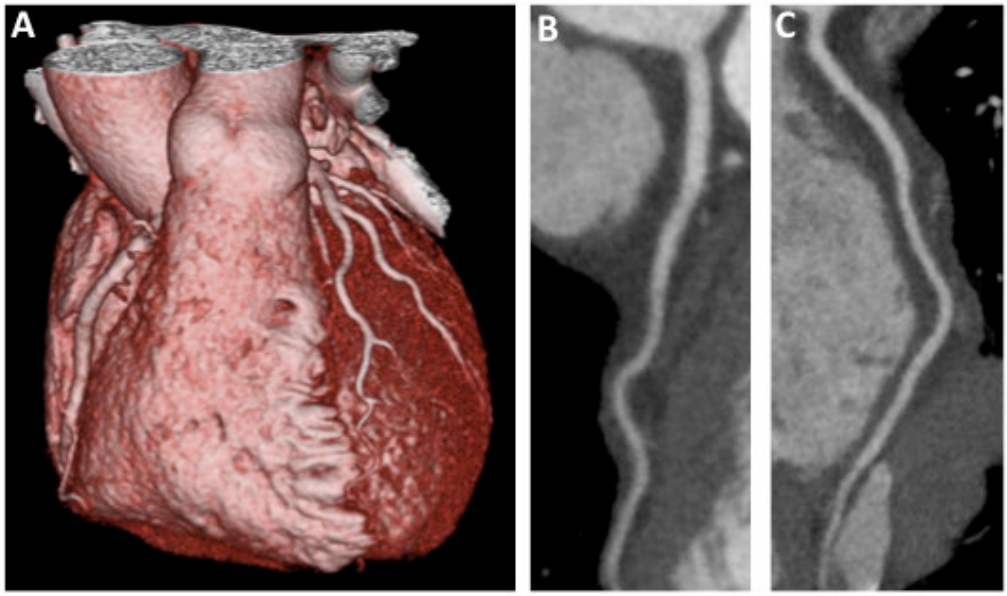

Figure 3.3: Images from a Group 3 patient with moderate coronary artery disease showing (A) 3D image of the heart, (B) eccentric calcified plaque in the LAD, (C) normal LCX and (D) mixed calcified and non-calcified plaque in the RCA. The male patient had a BMI of 18 and a radiation dose of 0.66 mSv (k=0.014).

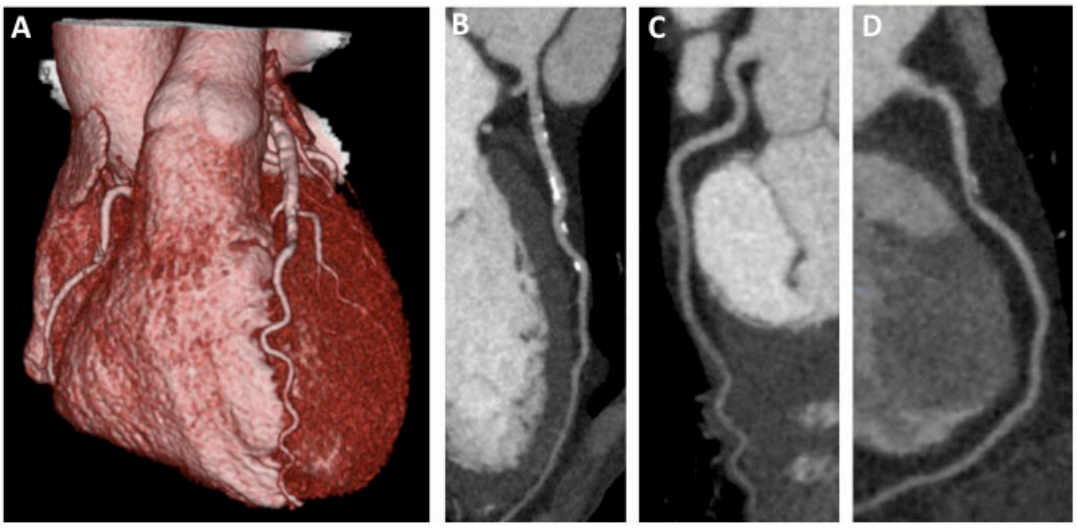

Figure 3.4: Images from a Group 3 patient with severe three-vessel coronary artery disease. There was a severe stenosis of the RCA (yellow arrows) identified on the 3D image of the heart (A), curved planar reformation (B), invasive coronary angiography (C) and cross sectional images of the coronary artery (D) with areas of non-calcified plaque and both macro and micro calcifications. There were significant stenoses (white arrows) in the LAD (E) and LCX (F) that corresponded to images obtained by invasive coronary angiography (G). The male patient had a BMI of 23 kg/m^2 and a radiation dose of 0.86 mSv (k=0.014).

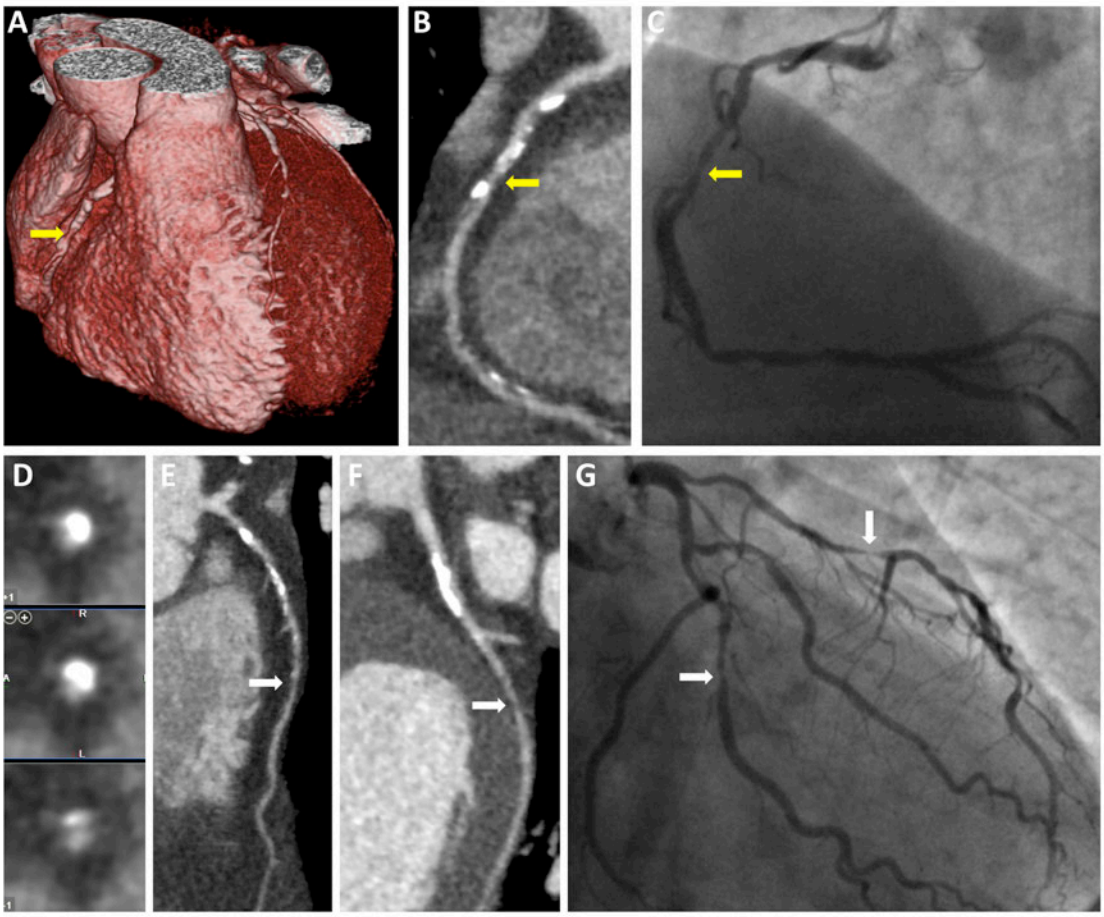

Figure 3.5: Example images from three patients with stenoses in their proximal LAD. The patients had the same body mass index (27 kg/m^2) and gender (male), and were from Group 1 (A), Group 2 (B) or Group 3 (C).

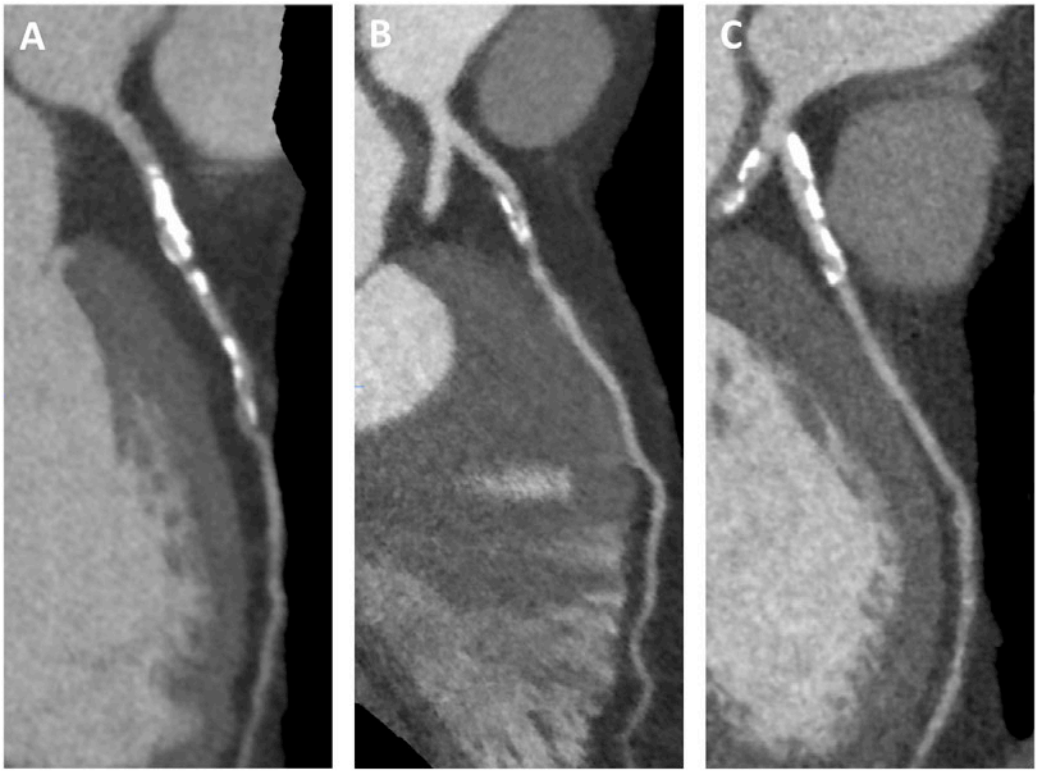

There was a reduction in radiation dose with the application of AIDR and AIDR3D protocols compared to the standard imaging protocol (P=0.001 and P<0.001 respectively; Table 3.4, Figure 3.6). Using the 0.014 mSv/mGy.cm conversion factor, this equates to radiation exposures of 3.84 (3.64, 4.06) mSv for Group 1, 3.39 (3.22, 3.54) mSv for Group 2 and 2.35 (2.18, 2.52) mSv for Group 3. Using the 0.028 mSv/mGy.cm conversion factor, this equates to radiation exposures of 7.67 (7.28, 8.12) mSv for Group 1, 6.78 (6.44, 7.08) mSv for Group 2 and 4.7 (4.37, 5.04) mSv for Group 3.

Figure 3.6: Box plots showing the reduction in radiation dose in Groups 1, 2 and 3.

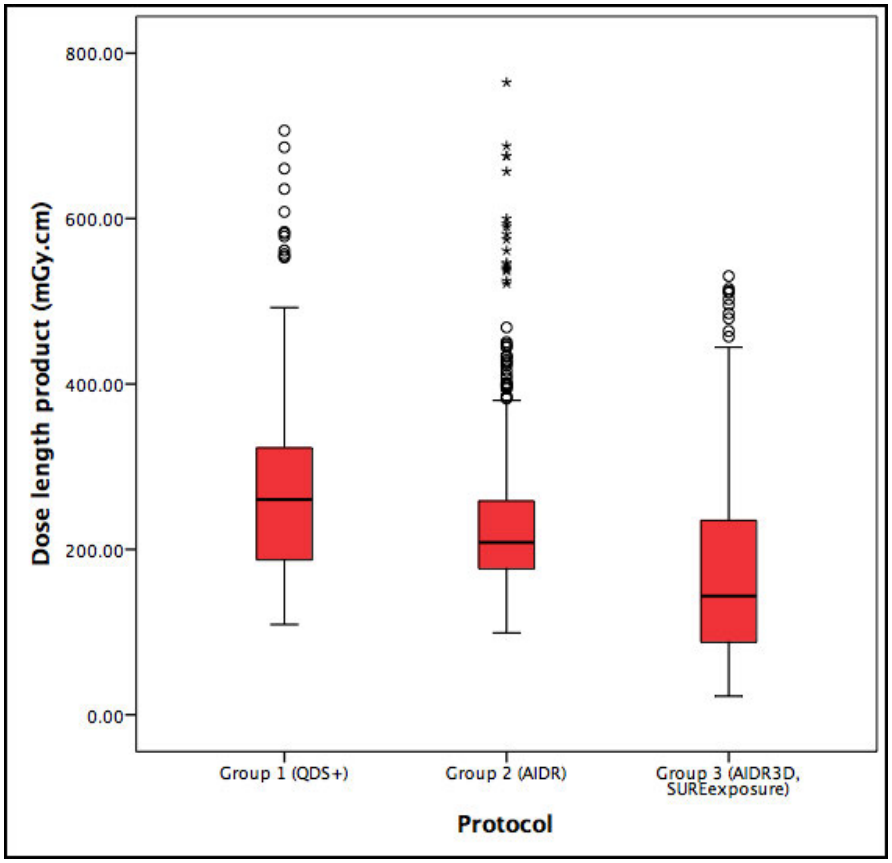

In addition, we performed a post-hoc analysis of 200 patients from each group matched for body mass index, gender and acquisition window (Table 3.5). The results were similar with a reduction in radiation dose (261 (246, 276) mGy.cm versus 211 (199, 223) mGy.cm versus 141 (129, 153) mGy.cm, $P<0.001$), improvement in subjective image quality (1.3 (1.2, 1.4) versus 1.1 (1.1, 1.2) versus 1.1 (1.1, 1.2), $P<0.001$) and no difference in contrast-to-noise ratio between groups (12 (12, 13) for all groups, $P=0.747$).

Thus compared to the standard imaging protocol, the application of AIDR and AIDR3D protocols led to a 12% and 39% reduction in radiation dose respectively.

Table 3.5: Post-hoc analysis of 200 patents from each group matched for gender, body mass index and acquisition window.

		Group 1 (QDS+)	Group 2 (AIDR)	Group 3 (AIDR3D and SUREexposure)	*P*
N		200	200	200	-
Male		44.5%	44.5%	44.5%	<0.001
Age (years)		58 (56, 59)	57 (56, 59)	59 (57, 60)	0.565
Heart rate (/min)		59 (58, 61)	59 (57, 60)	58 (57, 59)	0.479
Body mass index (kg/m^2)		28 (27, 29)	28 (28, 29)	28 (27, 29)	0.912
Acquisition window (30-80% versus 70-80%)		28 / 172	28 / 172	28 / 172	<0.001
Scan range (mm)		128	128	128	<0.001
Contrast (mL)		55 (54, 56)	54 (53, 54)	53 (52, 54)	0.064
Tube voltage (kV)	100	39%	43%	69%	<0.001
	120	58%	53%	31%	
	135	3%	4%	0%	
Tube current (mA)	100 kV	538 (530, 547)	447 (441, 453)	331 (307, 355)	<0.001
	120 kV	536 (531, 541)	426 (421, 430)	397 (362, 431)	<0.001
Subjective image quality		1.3 (1.2, 1.4)	1.1 (1.1, 1.2) *	1.1 (1.1, 1.2) *	<0.001
Aorta attenuation (HU)		430 (415, 443)	423 (411, 436)	533 (517, 549) * §	<0.001
Liver attenuation (HU)		65 (62, 67)	62 (60, 64)	60 (58, 62) *	0.01
IVS attenuation (HU)		88 (85, 92)	85 (83, 88)	88 (85, 90)	0.23
Image noise aorta (HU)		31 (30, 32)	31 (30, 32)	40 (39, 41) * §	<0.001
Image noise liver (HU)		39 (38, 41)	38 (37, 40)	39 (38, 40)	0.534
Image noise IVS (HU)		34 (32, 35)	32 (31, 33) *	37 (36, 38) * §	<0.001
Contrast-to-noise ratio		12 (12, 13)	12 (12, 13)	12 (12, 13)	0.747
Contrast-to-myocardium ratio		12 (11, 12)	12 (11, 12)	11 (11, 12)	0.823
DLP (mGy.cm)		261 (246, 276)	211 (199, 223) *	141 (129, 153) * §	<0.001

*(Mean (95% confidence interval) or percentage (%); IVS, intraventricular septum; DLP, dose length product; HU, Hounsfield units; * P<0.05 compared to Group 1; § P<0.05 compared to Group 2)*

Discussion

This study has shown that the application of iterative reconstruction and automated selection of tube current based on the attenuation density of scout images can reduce radiation dose whilst maintaining image quality in computed tomography coronary angiography. Reduction in radiation dose is important for computed tomography coronary angiography if this technique is going to be widely used in the clinic. This is particularly important as the patients with low to intermediate risk of coronary artery disease, in whom computed tomography coronary angiography is potentially most beneficial, are often young and female, and therefore at the greatest risk from radiation exposure.

Iterative reconstruction algorithms have been shown to reduce image noise in computed tomography coronary angiography. Tatsugami *et al* showed that reconstructing images using AIDR reduced image noise and contrast-to-noise ratio compared to the same data reconstructed with a filtered back projection algorithm. [131] Similar results have been reported with other iterative reconstruction algorithms. [132,133] This decrease in image noise provides the potential to reduce tube current and voltage, and thus radiation dose, in computed tomography coronary angiography. In a study of 70 patients, the application of AIDR, smaller scan ranges, and 100 kV tube voltage as part of a low-dose protocol led to an 80% reduction in radiation dose. [130] In the present study, we observed a more modest reduction in radiation dose but this reflected the fact that we had already implemented smaller scan ranges and 100 kV tube voltage where appropriate. Studies of other iterative

reconstruction algorithms have identified radiation dose reductions of between 50 and 63%. [123,134,135] In a study of 243 patients imaged using the Adaptive Statistical Iterative Reconstruction (ASIR, GE Health Care) algorithm compared to 331 patients using filtered back projection, there was a 27% reduction in radiation dose when adjusted for scan settings. [136] Similar to our study, the reduction in radiation dose was due to the ability to reduce tube voltage and tube current. Although the lowest tube voltage used in our study was 100 kV, the use of iterative reconstruction in combination with lower tube voltages such as 80 kV could further reduce radiation dose. [137]

The application of AIDR in this study led to a reduction in image noise and maintenance of the contrast-to-noise ratio. However, the use of a different triggering mechanism and a different reconstruction kernel, in addition to the use of AIDR3D and SUREexposure, led to an increase in aorta contrast attenuation and image noise. Despite this, there was a small increase in subjective image quality in AIDR and AIDR3D groups. Iterative reconstruction algorithms may have effects in addition to alterations in image noise as they have been shown to reduce the blooming artefact from calcified plaque [138] and other dense structures, such as coronary artery stents [139] and mechanical prosthetic heart valves. [140] This has potential implications for the quantification of myocardial perfusion imaging.

We used both body mass index and scout image attenuation to tailor images to the individual patient. Using scout image attenuation to select tube current led to a larger range of more appropriate tube currents being used for individual patients. The use of

chest tissue attenuation to select exposure settings reduces radiation dose in computed tomography coronary angiography [126,127] and coronary artery calcium scoring. [141] These previous studies used manual measurements and calculations whereas the automated method applied in this study was rapid and easy to use. Patient tailored imaging is important in order to follow the ALARA (As Low As Reasonably Achievable) principle. This is particularly important for young women who are at the greatest life-time risk of developing cancer. [142] Patient tailored imaging also enables the maintenance of more consistent image quality: an important consideration since image quality is associated with diagnostic accuracy. [51]

This is an observational cohort study as the nature of the software changes between reconstruction algorithms precluded a randomised study. Differences in software may have contributed to the results of the study out with the effect of iterative reconstruction. For example, scanner software Versions 4.4, 4.5 or 4.6 were applied for Group 1, Version 4.6 for Group 2 and Version 4.7 for Group 3. These data were collected over a prolonged period of time and thus changes in referral patterns led to a difference in gender frequencies between the groups. Men tend to have larger coronary arteries and better image quality on computed tomography coronary angiography. [51] Thus we cannot exclude that some of the observed benefit in image quality may be attributable to this. The difference in the scan range between groups may also have contributed to the results. However, in the post-hoc analysis the results were similar and there was no difference in scan range.

We did not assess diagnostic accuracy in comparison to invasive coronary angiography. The iterative reconstruction algorithm produces smoother images and thus there is the possibility that the degree of stenosis could be misinterpreted, particularly in smaller vessels, heavily calcified vessels or coronary artery stents. In addition, the use of lower tube voltages such as 80 kV may not produce images that are diagnostically similar to 100 or 120 kV. In striving to reduce radiation dose, it is important that we do not compromise image quality and diagnostic accuracy. Evidence of harm from radiation exposure at these levels is extrapolated and remains controversial. In addition, iterative reconstruction should not be applied as an alternative to good practice in applying optimised protocols.

A further limitation is that image quality was assessed on a per-patient rather than a per-segment level. We felt it was more clinically relevant to assess image quality on a per-patient level, as this will most directly influence future investigations or treatments. It was not possible to blind observers to the reconstruction technique as, although reconstruction kernel filters were chosen to produce similar results, it is possible to differentiate between the images based on subtle differences.

Computed tomography coronary angiography is an increasing source of population radiation exposure and this can be dramatically reduced by the application of patient tailored imaging protocols and iterative reconstruction. The application of these techniques can minimise the potential harm from radiation exposure in computed tomography coronary angiography imaging. These approaches can now be routinely used in clinical practice. In addition, this work sets a precedent for further work with

iterative reconstruction and patient tailored imaging in computed tomography myocardial perfusion imaging.

Chapter Four: Computed tomography coronary angiography image quality

Extracts of this chapter are published in:

Williams MC, Weir NW, Mirsadraee S, et al. Image quality with single heart beat 320 multidetector computed tomography coronary angiography. Journal of Computer Assisted Tomography 2014: 38 (3); 444-450.

Abstract

Introduction

This chapter establishes the feasibility of single heartbeat imaging with 320-multidetector computed tomography coronary angiography, and assesses the variables that affect image quality.

Methods

Consecutive patients (n=249, 38% male) underwent contrast enhanced prospective electrocardiogram-gated single heartbeat computed tomography coronary angiography. Tube current and voltage were selected based on body mass index and acquisition window was selected based on heart rate. Images were assessed by two trained observers and image quality was graded on a 4-point scale (1, excellent; 4, poor).

Results

The mean heart rate was 60 /min (95% confidence interval 59, 62), body mass index 29 kg/m^2 (28, 30), age 58 years (56, 59) and dose-length product 283 mGy.cm (266, 301). During scanning, 133 (51%) received sublingual glyceryl trinitrate (GTN), 9 (4%) had ectopic beats, and 12 (5%) had atrial fibrillation. Diagnostic image quality was obtained in 99%, with mean image quality 1.4 (1.3, 1.5). Age, gender, atrial fibrillation, ectopics, diabetes mellitus (12%) and the presence of obstructive coronary disease were not related to image quality. A lower heart rate and GTN were associated with improved image quality ($P \leq 0.001$).

Conclusion

Optimal image quality in single heartbeat 320-multidetector computed tomography coronary angiography is achievable at low radiation doses in 99% of unselected patients. Image quality is further improved by lower heart rate and sublingual GTN.

Introduction

Computed tomography coronary angiography is now widely applied in the diagnosis of coronary artery disease. [35] It has a diagnostic accuracy similar to invasive coronary angiography, and in particular has a high negative predictive value. [143] The diagnostic accuracy of computed tomography coronary angiography can be affected by image quality [51] and, despite advances in low dose computed tomography coronary angiography, radiation exposure remains an important concern. It is therefore important that imaging protocols are optimised to obtain diagnostic images at the lowest possible radiation dose.

Wide-volume computed tomography with 160 mm detector coverage is capable of covering the whole heart in a single rotation. This eliminates stair-step reconstruction artefacts that are often present when using a smaller detector coverage. It can also reduce the effect of artefacts due to inconsistent breath holding, arrhythmias and variable heart rates. Images can be reconstructed from one heartbeat (half-segment reconstruction) or the temporal resolution can be increased by combining images from multiple heartbeats (multi-segment reconstruction). However, multi-segment reconstruction increases radiation dose and may decrease image quality due to beat-to-beat differences in the position of the coronary arteries. [144] For patients with heart rates above 65 /min or irregular heartbeats, multi-segment reconstruction and a widened acquisition window continues to be used even with 320-multidetector computed tomography scanners. [145]

It has been established that image quality in 64-multidetector computed tomography coronary angiography can be affected by heart rate, heart rate variability, body mass index, calcification and the presence of co-morbidities. [48-50,146-150] In multi-segment 320-multidetector computed tomography, heart rate is also reported to affect image quality and radiation dose, but not diagnostic accuracy. [145]

This study assesses the feasibility of half-segment reconstruction for all patients, irrespective of heart rate, and establishes the patient and imaging characteristics that influence image quality.

Methods

Study population

In this retrospective single centre cohort study we assessed the images of 249 unselected consecutive patients referred for clinically indicated computed tomography coronary angiography were assessed. Exclusion criteria for computed tomography were documented severe allergy to iodinated contrast medium, impairment in renal function (estimated glomerular filtration rate <30 mL/min), pregnancy or a weight exceeding the maximum tolerance of the scanner bed (250 kg).

Computed tomography

Computed tomography coronary angiography was performed using a 320-multidetector scanner (Aquilion ONE, Toshiba Medical Systems). Prospective, contrast enhanced, electrocardiogram-gated computed tomography was performed using 350 ms gantry rotation time and 320 x 0.5 mm detector configuration.

The smallest possible detector coverage (160, 140, 128, 120, 100 or 80 mm) was selected based on the scout images. The tube voltage, tube current and volume of iodinated contrast agent were selected based on body mass index (Table 4.1). A tri-phasic injection of intravenous contrast agent (Iomeron400, Bracco, Italy) was administered and image acquisition was triggered when a region of interest in the left ventricle reached a peak of 180 Hounsfield units.

Table 4.1: Imaging protocol for Chapter 4.

Body Mass Index (kg/m^2)	**Tube voltage (kV)**	**Tube current (mA)**	**Iodinated contrast volume (mL)**
<20	100	400 to 450	50
20-26	100	450 to 580	50
27-30	120	510 to 530	50
31-38	120	560 to 570	60
39-40	135	480 to 500	60
>40	135	500	70

For patients with a heart rate <65 /min, images were acquired from a single heartbeat with a with an acquisition window of 70 to 80% of the interval between two consecutive R waves (R-R interval). For patients with a heart rate >65 /min images were acquired again from a single heartbeat, but the acquisition window was increased to 30 to 80% of the R-R interval. This protocol was also used for patients with frequent ectopic beats (>3 ectopic beats in the 5 min prior to computed tomography), atrial fibrillation or a variable heart rate. The heart rate at the time of computed tomography was calculated from the time interval between two consecutive R waves.

We assessed images before and after the introduction of sublingual glyceryl trinitrate to our computed tomography coronary angiography protocol. After its introduction, sublingual glyceryl trinitrate (300 μg) was administered to all patients.

Image reconstruction

Images were reconstructed using half-segment reconstruction for all patients using a filtered back projection reconstruction algorithm (QDS+, Boost) and a reconstruction kernel optimised for coronary artery assessment (FC03 (smooth kernel, Toshiba Medical Systems)), as described in Chapter 2.

Image assessment

Images were transferred to a dedicated post-processing workstation for analysis (Vitrea fX 6.0, Vital Images). Images were assessed by two independent trained observers blinded to protocol type and patient characteristics. Image quality was

assessed on a four-point Likert scale (1 excellent; 2 mild reduction in image quality; 3 moderate reduction in image quality; 4 severe reduction in image quality). This involved a combined subjective assessment of image noise, contrast enhancement, coronary motion and visibility of small diameter vessels. Obstructive coronary artery disease was defined as the presence of one or more luminal stenosis >70% in one or more major epicardial vessels.

Statistical analysis

Radiation dose between groups with different heart rates was assessed using analysis of variance and Dunnett's t-test against the lowest heart rate category. The effect of patient characteristics on image quality was evaluated by multivariate regression analysis.

Results

Images from 249 unselected consecutive patients were assessed (Table 4.2). The mean body mass index was 29 kg/m^2 (95% confidence interval 28 to 30, range 17 to 56) and the mean age was 58 years (95% confidence interval 56 to 59). Computed tomography identified obstructive coronary artery disease in 70 patients (27%), 89 patients (45%) had non-obstructive coronary artery disease and 100 patients (39%) had normal coronary arteries.

Table 4.2: Demographic and scan details for Chapter 4.

Parameter	**Patients**
n	249
Age	58 (56, 59)
Gender (Male/Female)	38%/62%
Body mass index (kg/m^2)	29 (28, 30)
Diabetes	30 (12%)
Atrial fibrillation	12 (5%)
Ectopic beats	9 (4%)
Taking oral beta-blockers	64 (25%)
Rate limiting medication	180 (72%)
Glyceryl trinitrate	133 (51%)
Heart rate	60 (59, 62)
Narrow phase window (70-80%)	215 (86%)
Widened phase window (30-80%)	34 (13%)
Obstructive coronary artery disease	70 (27%)
Non-obstructive coronary artery disease	89 (45%)
Normal coronary arteries	100 (39%)

(Mean (95% confidence interval) or number (percentage))

At the time of the computed tomography scan, 64 patients (25%) were taking oral beta-blockers as part of their normal medical treatment. Additional rate limiting medication was administered to 180 patients (72%) prior to imaging. Sublingual glyceryl trinintrate was administered to 133 patients (51%). The mean heart rate at the time of computed tomography was 60 /min (95% confidence intervals 59 to 62, range 35 to 135). Ectopic beats occurred in 9 patients (4%) and 12 patients (5%) patients had atrial fibrillation. There was no difference in heart rates between the group that received and did not receive glyceryl trinitrate (60 (95% confidence interval 58 to 62) versus 60 (95% confidence interval 58 to 63), *P*=0.745). The mean dose of metoprolol administered in the group given glyceryl trinitrate was slightly higher (14.6 mg (95% confidence interval 12.2 to 17.1) versus 19.8 mg (95% confidence interval 16.0 to 23.5), *P*=0.023).

A half-segment reconstruction was used for all patients. The acquisition window was widened to 30 to 80 per cent of the R-R interval for 34 patients (13%). The mean temporal location for the reconstruction with the best image quality was at 76 per cent of the R-R interval (95% confidence interval, 71 to 82 per cent). End-diastolic phase reconstructions had the best image quality for 243 patients (94%) and end-systolic phase reconstructions had the best image quality for 16 patients (6%). Patients where the end-diastolic phase reconstruction had the best image quality had a slower heart rate than those where end-systolic phase reconstructions had the best image quality (59 (58 to 61) versus 74 (67 to 81), *P*=0.001).

Diagnostic image quality was obtained in 257 scans (99.2%). The mean image quality score was 1.4 (95% confidence interval, 1.3 to 1.5). For patients with a body mass index of 30 kg/m^2 or above (n = 111) diagnostic image quality was obtained in 109 scans (98%) and excellent image quality was obtained in 78 scans (70%) (Figure 4.1). For patients with a heart rate above 65 /min (n = 58) diagnostic image quality was obtained in 98% (57 scans) and excellent image quality was obtained in 36% (21 scans). All patients with arrhythmia (atrial fibrillation or ectopic beats, n = 20) had scans with diagnostic image quality and 70% (14 scans) had excellent image quality.

Figure 4.1: The effect of heart rate, body mass index (BMI) and arrhythmia on the proportion of computed tomography coronary angiograms with diagnostic image quality.

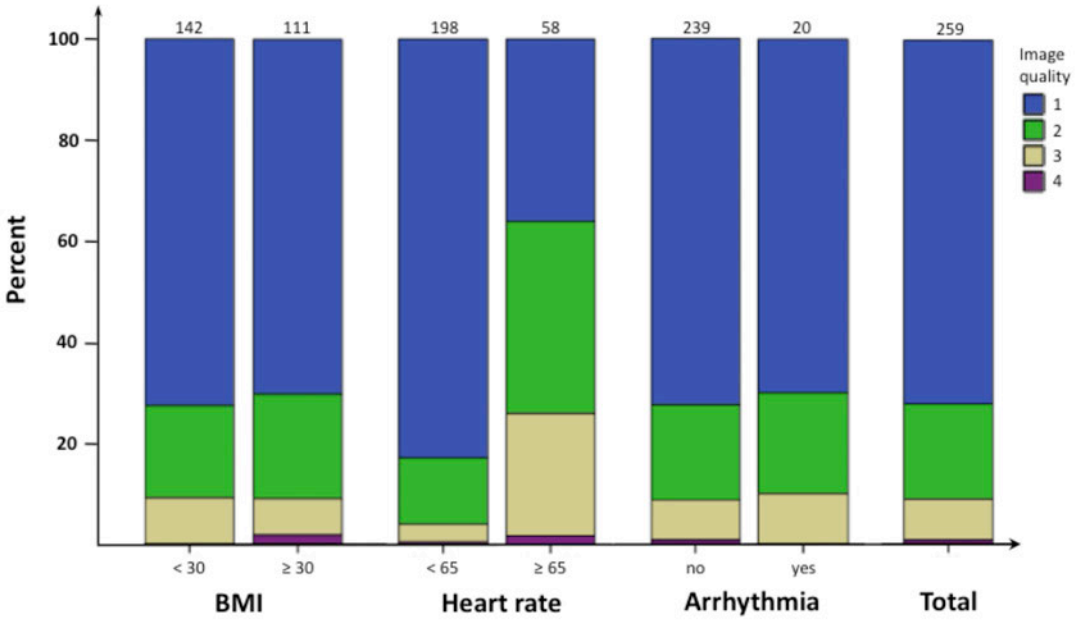

There were weak correlations between image quality and body mass index (r=0.016, *P*=0.046; Figure 4.2, Table 4.3), heart rate (r=0.187, *P*<0.001) (Figure 4.3, Table 4.4) and the use of glyceryl trinitrate (r=0.029, *P*=0.007). Image quality did not correlate with age, gender, diabetes mellitus, or the presence of obstructive coronary artery disease, atrial fibrillation or ectopic beats. In multivariate regression analysis, the only variables to affect image quality were heart rate (beta=0.439, *P*<0.001) and the use of glyceryl trinitrate (beta=-0.199, *P*=0.001).

The mean dose-length product was 283 mGy.cm (95% confidence interval, 266 to 301). Using the conservative 0.014 mSv/mGy.cm conversion factor, this equates to a radiation dose of 3.96 mSv and using the 0.028 mSv/mGy.cm conversion factor this equates to 7.92 mSv. Patients with a heart rate <60 /min had a mean dose-length product of 259 mGy.cm (95% confidence interval, 243 to 276). An increase in heart rate led to an increase in radiation dose (Figure 4.4), to a mean of 377 mGy.cm (286 to 268) for patients with a heart rate of >80 /min (*P*<0.001; Table 4). A higher radiation dose was also associated with a BMI above 30 (DLP 231 (95% confidence interval, 213 to 248) versus 353 (95% confidence interval, 330 to 377), *P* <0.001; Figure 4.5) and the presence of arrhythmia (DLP 275 (95% confidence interval, 259 to 290) versus 384 (95% confidence interval, 301 to 467), *P*=0.013).

Table 4.3: Effect of body mass index on radiation dose and image quality in half-segment 320-multidetector computed tomography coronary angiography.

BMI (kg/m^2)	Dose length product (mGy.cm)		Image quality	
		P		***P***
18.5-24.99	175 (151, 199)		1.45 (1.23, 1.66)	
25-29.99	259 (237, 281)	<0.001	1.32 (1.20, 1.45)	0.694
30-34.99	314 (292, 337)	<0.001	1.31 (1.15, 1.48)	0.687
35-39.99	405 (341, 468)	<0.001	1.43 (1.21, 1.65)	1.00
>40	431 (367, 494)	<0.001	1.75 (1.25, 2.25)	0.341

(Mean (95% confidence interval))

Figure 4.2: The effect of body mass index (BMI) on image quality in half-segment 320-multidetector computed tomography coronary angiography.

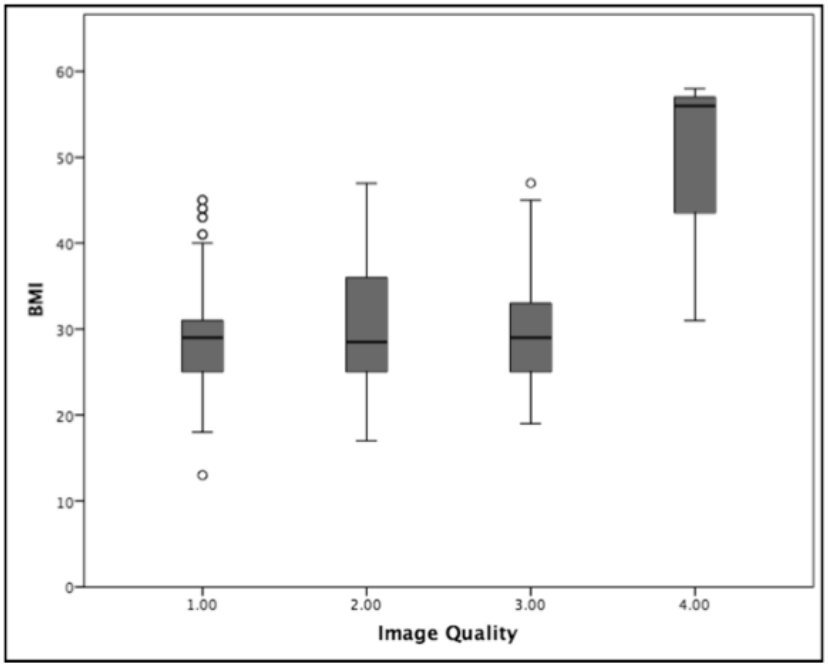

Table 4.4: Effect of heart rate on radiation dose and image quality in half-segment 320-multidetector computed tomography coronary angiography

Heart rate	Dose length product (mGy.cm)		Image quality	
		P		***P***
<60	259 (243, 276)		1.18 (1.10, 1.25)	
60-70	291 (259, 323)	0.094	1.53 (1.35, 1.71)	<0.001
70-80	275 (273, 478)	0.003	1.85 (1.36, 2.33)	<0.001
>80	377 (287, 468)	<0.001	2.12 (1.68, 2, 56)	<0.001

(Mean (95% confidence interval))

Figure 4.3: The effect of heart rate on image quality in half-segment 320-multidetector computed tomography coronary angiography.

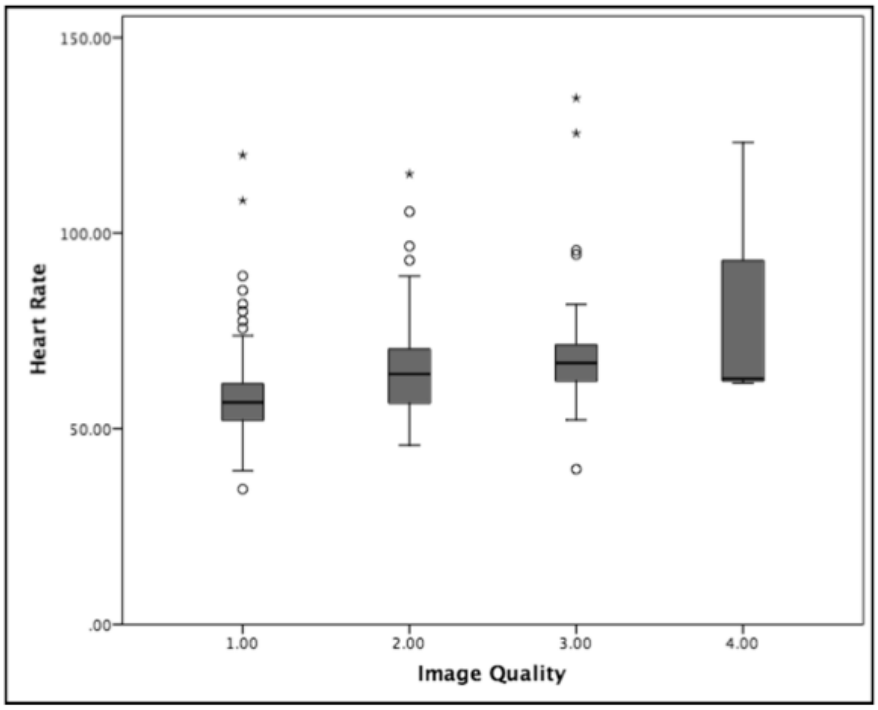

Figure 4.4: The effect of heart rate on radiation dose in half-segment 320-multidetector computed tomography coronary angiography.

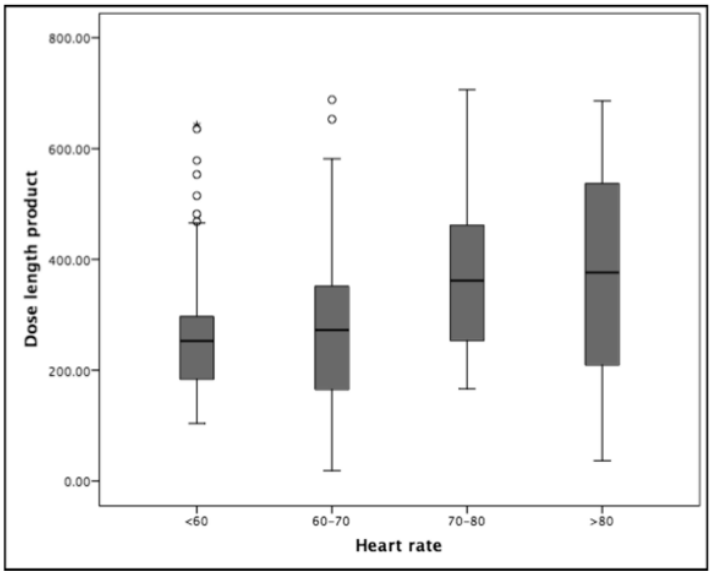

Figure 4.5: The effect of body mass index on radiation dose in half-segment 320-multidetector computed tomography coronary angiography.

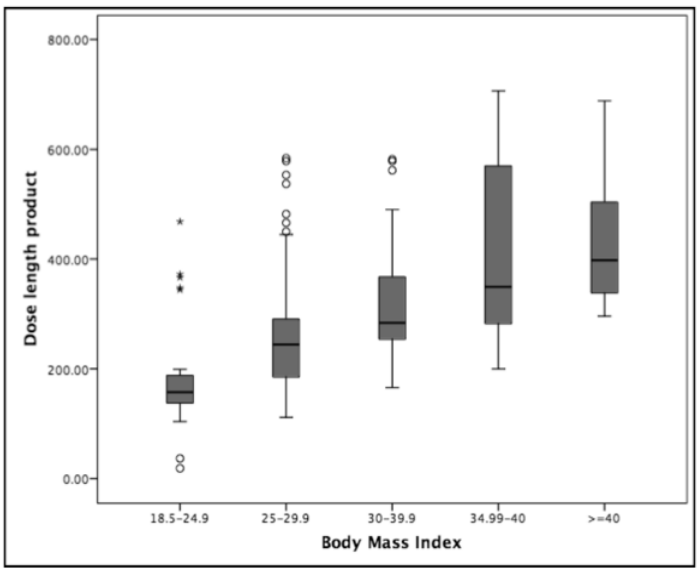

Discussion

We have demonstrated that single-beat half-segment reconstruction can be used in all unselected patients referred for computed tomography coronary angiography with 99% of studies being of diagnostic image quality despite including patients with a high body mass index and significant arrhythmia. We have also reaffirmed the need for heart rate reduction and the use of sublingual glyceryl trinitrate to optimise image quality.

In 64-multidetector computed tomography coronary angiography, image quality has been associated with heart rate, heart rate variability, body mass index, coronary calcification, ethnicity and the presence of breathing artefacts. [48-50,146-150] In the acute setting, co-morbidities such as diabetes and hypertension were also reported to influence image quality. [150] The selection of prospective or retrospective protocols is an important determinant of image quality, particularly with faster heart rates or arrhythmias. In dual-source computed tomography coronary angiography heart rate and heart rate variable also influence image quality. [151,152] The diagnostic accuracy of computed tomography coronary angiography can be influenced by image quality. In the CORE64 study, image quality was associated with ethnicity, BMI, heart rate and breathing artefacts, but not with coronary artery calcium score. [143] Neither the coronary artery calcium score nor age translated into reduced diagnostic accuracy at the vessel level. [143] In 320-multidetector computed tomography, diagnostic accuracy was not altered by heart rate or heart rate variability. [145]

The advantage of 320-multidetector computed tomography coronary angiography is that the heart can be imaged in one volume, thus eliminating stair-step reconstruction artefacts. Previous studies of 320-multidetector computed tomography have shown that heart rate, but not heart rate variability, influenced image quality. [145] Using 320-multidetector computed tomography and multi-segment reconstruction above a heart rate of 65 /min, diagnostic image quality was obtained in 99.7% of segments in a study of 94 patients, [145] in 96.66% of segments in a study of 174 patients [153], in 96.8% of segments in a study of 37 patients with atrial fibrillation [154] and in 96% of segments in a study of 24 patients with atrial fibrillation. [155] Thus our results of a 99% per-patient diagnostic accuracy with single segment reconstruction compares favourably to these previous studies. Reduced diagnostic accuracy in these previous studies was found in segments with the most motion, such as the right coronary artery. [145] However, in coronary arteries where there is a high degree of motion, half-segment reconstruction has an improved image quality compared to multi-segment reconstructions. [144]

A major advantage of half-segment reconstruction is the potential reduction in radiation dose. In a study of 94 patients where half-segment reconstruction was used below a heart rate of 70 /min and multi-segment reconstruction above a heart rate of 70 /min, the mean effective radiation dose (k=0.029) was 14.8±9.8 mSv. [145] For patients with a heart rate of above 70 /min, this rose to 20.7±5.9 mSv and for patients with a heart rate of above 80 /min this rose to 23.7±5.4 mSv. Even allowing for the difference in conversion factor between the two studies, the radiation

exposure using half-segment reconstruction is lower than multi-segment reconstruction. Radiation dose remains a major health care concern thus it is important to maintain diagnostic image quality whilst minimising radiation dose. Further advances in computed tomography including the use of iterative reconstruction algorithms promise to reduce radiation dose further, and it will be important to assess the effect of this on image quality and diagnostic accuracy.

Sublingual nitrates in patients undergoing 64-multidetector computed tomography improves image quality through the dilation of peripheral vessels and improvement in the intraluminal contrast. [111] This dilation enables more septal branches to be visualised [156] and increases the diameter of proximal vessels. [157] In a study of 76 patients undergoing 16-multidetector computed tomography coronary angiography, sublingual nitrates improved the diagnostic accuracy. [158] Our study is the first to show that the use of glyceryl trinitrate is associated with improved image quality in 320-multidetector computed tomography.

In the present study, we did not assess diagnostic accuracy in comparison to invasive coronary angiography. In addition this is a cohort observational study rather than a randomised study. A further limitation of this study is that image quality was assessed on a per-patient rather than a per-segment level. Quality indices may vary by segment, however, we felt it was more clinically relevant to assess quality per-patient as this will most directly influence future investigations or treatment.

This study has established the use of half-segment reconstruction in all patients undergoing wide volume computed tomography coronary angiography irrespective of heart rate, ectopic beats and the presence of atrial fibrillation. A widened window of acquisition can be used to improve image quality in patients with a heart rate >65 /min. In addition we have established that the use of glyceryl trinitrate improves image quality in 320-multidetector computed tomography coronary angiography.

Chapter Five: Radiation dose reduction in computed tomography myocardial perfusion imaging

Abstract

Introduction

This chapter assesses the application of iterative reconstruction and patient tailored imaging on radiation dose in computed tomography (CT) myocardial perfusion imaging. (CTP)

Methods

Participants underwent rest CT coronary angiography and adenosine stress CTP using a 320-multidetector scanner (Aquilion ONE, Toshiba). Group 1 underwent imaging with a standard protocol. Radiation dose reduction techniques used in Group 2 included iterative reconstruction (AIDR3D), tube current adjustment based scout attenuation and half-segment reconstruction. Dose length product (DLP) and image noise were recorded. Subjective image quality was assessed (from 1 (excellent) to 4 (uninterpretable)) and summed for the 17 myocardial segments.

Results

There was no difference in gender, body mass index, heart rate at rest or stress, or z-axis collimation at rest or stress between patients in Group 1 (n=28) and those in Group 2 (n=28). There was a reduction in tube current (467 (449,485) versus 318 (245,392) mA, $P<0.001$), and tube voltage (100% versus 33% at 120 kV, $P<0.001$) in Group 2. DLP was lower in Group 2 during rest (224 (210,238) versus 141 (109,173) mGy.cm, $P<0.001$) and stress imaging (604 (486,722) versus 232

(177,286) mGy.cm, P <0.001). There was no difference in subjective image quality between groups.

Conclusion

Iterative reconstruction and patient tailored imaging led to a 60% reduction in radiation dose in CT myocardial perfusion imaging, while maintaining image quality.

Introduction

Computed tomography myocardial perfusion imaging is now an established diagnostic technique for the assessment of coronary artery disease.[70] The additional information provided by computed tomography myocardial perfusion imaging can be used to guide decisions regarding revascularisation and has potential prognostic implications. However, radiation dose remains an important concern due to the potential increase in the lifetime risk of cancer, particularly for young women.[142] Therefore it is important to develop new techniques that have the potential to reduce radiation dose in cardiovascular imaging.

Radiation dose reduction techniques that have been applied to computed tomography coronary angiography include prospective electrocardiogram gating, heart rate reduction, tube voltage reduction, tube current modulation and iterative reconstruction. In addition, tailoring the scan parameters to the individual patient's body habitus can optimise image quality and reduce radiation dose. Body mass index is widely used to select tube current and voltage but it may not adequately account for differences in body habitus and body fat distribution. Thus, methods to optimise tube current based on the scout images have been developed.

The application of iterative reconstruction and patient tailored imaging can reduce the radiation dose of computed tomography coronary angiography by 39% (Chapter 4). In this study the application of these techniques in computed tomography myocardial perfusion imaging is assessed.

Methods

Study design and participants

In this single centre retrospective cohort study participants either underwent clinically indicated computed tomography myocardial perfusion imaging using the standard imaging protocol (Group 1) or underwent computed tomography myocardial perfusion imaging using the research protocol (Group 2). The local ethics committee approved the study. The participants in Group 2 were part of a larger research study that has previously been published. [159] Exclusion criteria were documented severe allergy to iodinated contrast medium, impaired renal function (estimated glomerular filtration rate <30 mL/min), pregnancy, weight exceeding the maximum tolerance of the scanner bed (250 kg), second or third degree atrioventricular block, or asthma.

Computed tomography

All participants underwent computed tomography imaging at the Clinical Research Imaging Centre in Edinburgh using a 320-multidetector scanner (Aquilion ONE, Toshiba Medical Systems, Japan). Participants underwent electrocardiogram-gated rest computed tomography coronary angiography and adenosine stress computed tomography myocardial perfusion imaging. The differences between the computed tomography protocols for Group 1 and Group 2 are summarised in Table 5.1.

Table 5.1: Imaging protocol for Group 1 and 2 in Chapter 5.

	Group 1	**Group 2**
Reconstruction algorithm	Filtered back projection (QDS+)	Iterative reconstruction (AIDR3D)
Tube voltage	120kV for all	Tailored to BMI (100kV for BMI <30 kg/m^2, 120kV for BMI >30 kg/m^2)
Segments for reconstruction	Multi-segment if >65 /min	Half-segment reconstruction for all
Dose modulation	None	For stress imaging with 70-80% of the RR interval at full dose
Sublingual glyceryl trinitrate	None	For rest scan

Rate limiting medication

For both groups, patients with a heart rate above 60 /min received rate-limiting medication (intravenous metoprolol, up to 50 mg). Group 2 patients received sublingual glyceryl trinitrate (300 μg), unless contraindicated, prior to rest computed tomography coronary angiography.

Rest computed tomography coronary angiography

All participants underwent a prospective, electrocardiogram-gated contrast-enhanced computed tomography coronary angiography using single (half) segment reconstruction and a 0.35-ms rotation time. Detector coverage was selected based on scout images to cover from 20 mm below the carina to the base of the heart using volume sizes of 160, 140, 128, 120, 100 or 80 mm. A tri-phasic injection of intravenous contrast agent (Iomeron400, Bracco, UK) was administered based on

body mass index (<30 kg/m^2, 50 mL total volume; >30 kg/m^2, 60 mL, >40 kg/m^2, 70 mL). Half of the volume of contrast was administered at full concentration, the rest of the contrast was delivered as a 50:50 mix with saline, and the tri-phasic injection was completed with a saline flush. Imaging was triggered when a threshold of 300 Hounsfield units was reached in the descending aorta. For patients with a heart rate ≤65 /min, images were acquired with a narrow acquisition window (e.g. 70 to 80% of the interval between two consecutive QRS complexes). For patients with a heart rate >65 /min, a wider acquisition window was used (e.g. 30 to 80% of the interval between two consecutive QRS complexes).

For patients in Group 1, a tube voltage of 120 kV was used for all participants. For patients in Group 2, tube voltage was selected based on body mass index (<30 kg/m^2, 100 kV; ≥30 kg/m^2, 120 kV). For patients in Group 1, the tube current was selected based on body mass index. For participants in Group 2, individualised automated tube current selection based on scout image attenuation was applied (SUREexposure, Toshiba Medical Systems, Japan). The predetermined level of image noise was set at a standard deviation of 45 Hounsfield Units (HU; slice thickness 0.5 mm, reconstruction kernel filter FC05 (smooth kernel, Toshiba Medical Systems)).

Stress computed tomography

Pharmacological stress was induced using an infusion of adenosine (140 μg/kg/min) for 4 min prior to imaging. The infusion was stopped immediately after imaging. The same tube voltage, tube current, and contrast volume were used as for rest imaging. Detector coverage was reduced to cover only the left ventricle based on the rest

images. Imaging was triggered when a threshold of 300 Hounsfield units was reached in the descending aorta. This threshold was chosen in order to be certain that the scan did not trigger to early, which could lead to false negative assessments of myocardial perfusion. This issue is less important in CTCA where other trigger locations and attenuation values can be used.

For Group 1, a narrow window of acquisition and multi-segment reconstruction was used: 1 segment for heart rates <65 /min, 2 segments for 65-79 /min, 3 segments for 80-110 /min and 4 segments for >110 /min. For Group 2, single (half) segment reconstruction was used for all patients irrespective of heart rate with tube current modulation across one cardiac cycle. The selected tube current was applied for 70-80% of the interval between the two QRS complexes and a low tube current (100 mA) used for the rest of the QRS interval.

Image reconstruction

All images were reconstructed with a slice thickness of 0.5 mm and an increment of 0.25 mm. Images from Group 1 were reconstructed using the standard filtered back projection algorithm (Quantum Denoising Software (QDS+), Toshiba Medical Systems, Japan) and a reconstruction kernel optimised for perfusion imaging (FC03 (smooth kernel, Toshiba Medical Systems)). Images from Group 2 were reconstructed using an iterative reconstruction algorithm (Adaptive Iterative Dose Reduction (AIDR3D), Toshiba Medical Systems, Japan) with the standard level of blending and the same reconstruction kernel filter (FC03 (smooth kernel, Toshiba Medical Systems)).

Image analysis

Images were analysed on a dedicated post-processing workstation (Vitrea fX, Vital Images, Minnetonka, USA) and were assessed by two trained observers (MW, DEN).

Image noise was assessed by placing regions of interest in the ascending aorta at the level of the left main stem, the interventricular septum and in the liver. Image noise was determined as the standard deviation of the Hounsfield units within the region of interest. Contrast-to-noise ratio was calculated as the attenuation value in the aorta minus the attenuation value in the liver divided by the image noise in the aorta. Contrast-to-myocardium ratio was calculated as the attenuation value in the aorta minus the attenuation value in the interventricular septum divided by the image noise in the aorta.

For each of the 17 standard myocardial segments, subjective image quality was assessed on a four-point Likert scale: 1 excellent or 2 mild, 3 moderate and 4 severe reduction in image quality. These results were summed to give a total image quality score for the rest and stress images.

Radiation dose

The dose length product displayed on the scanner console after imaging was recorded. This was converted to millisieverts (mSv) using the commonly used conversion factor of 0.014 mSv/mGy.cm, and a scanner specific conversion factor of 0.028 mSv/mGy.cm calculated using the method described by Huda *et al*.[59]

Statistical analysis

Statistical analysis was performed using SPSS (Version 18 for Mac OS X, IBM). Normally distributed quantitative variables are presented as mean and 95% confidence intervals. Non-normally distributed data are presented as median and interquartile ranges. Statistical significance was assessed using Student's *t*-test, Pearson's Chi-squared test or Mann-Whitney U test as appropriate. A statistically significant difference was defined as a two-sided *P* value <0.05.

Results

There was no difference in age, gender, body mass index or heart rate at rest or during adenosine stress between the two groups (Table 5.2).

Table 5.2: Demographic details for Chapter 5.

		Group 1	Group 2	*P*
N		28	28	
Male		63%	75%	0.350
Age		60 (56, 63)	64 (61, 67)	0.64
Body mass index (kg/m^2)		28 (27,30)	28 (26,30)	0.667
Heart rate (beats per minute)	Rest	56 (54,59)	56 (53,59)	0.848
	Stress	73 (69,77)	71 (66,76)	0.585

(Mean (95% confidence interval))

There was a marked reduction in the number of patients imaged using a tube voltage of 120 kV in Group 2 compared to Group 1 (Table 5.3 and Figure 5.1). All rest images were acquired using single (half) segment reconstruction. For stress imaging in Group 1 images were acquired using single (half) segment reconstruction for 9%, two segment reconstruction for 74% and three segment reconstruction for 17%. However, for Group 2 all stress imaging was performed using single (half) segment reconstruction. There was no difference in the window of acquisition used for rest imaging (Table 5.3). However, for the stress imaging, all patients in Group 2 were imaged using a narrow window of acquisition and dose modulation whereas in

Group 1 stress scans were performed with either a narrow (57%) or wide (29%) window of acquisition.

Table 5.3: Scan parameters for Chapter 5.

			Group 1	Group 2	*P*
z-axis collimation (mm)		Rest	134 (128,140)	128 (123,133)	0.146
		Stress	116 (107,125)	118 (111,125)	0.737
Contrast volume (for rest and stress imaging, mL)			119 (116, 122)	122 (117, 126)	0.314
Tube current (mA)			467 (449,485)	318 (245,392)	<0.001
Tube voltage (Percentage at 120 kV)			100%	33%	<0.001
Segments	Rest	Half	100%	100%	NA
	Stress	Half	2 (9)	100%	<0.001
		2	17 (74)	0	
		3	4 (17)	0	
Window of acquisition	Rest	Narrow	22 (91)	23 (96)	0.551
		Wide	2 (8)	1 (4)	
	Stress	Narrow	16 (57)	0	<0.001
		Wide	8 (29)	0	
		Narrow with dose modulation	0	24 (100)	

(Mean (95% confidence interval)

Figure 5.1: Reduction in tube current and increased range of tube currents used with protocol improvements.

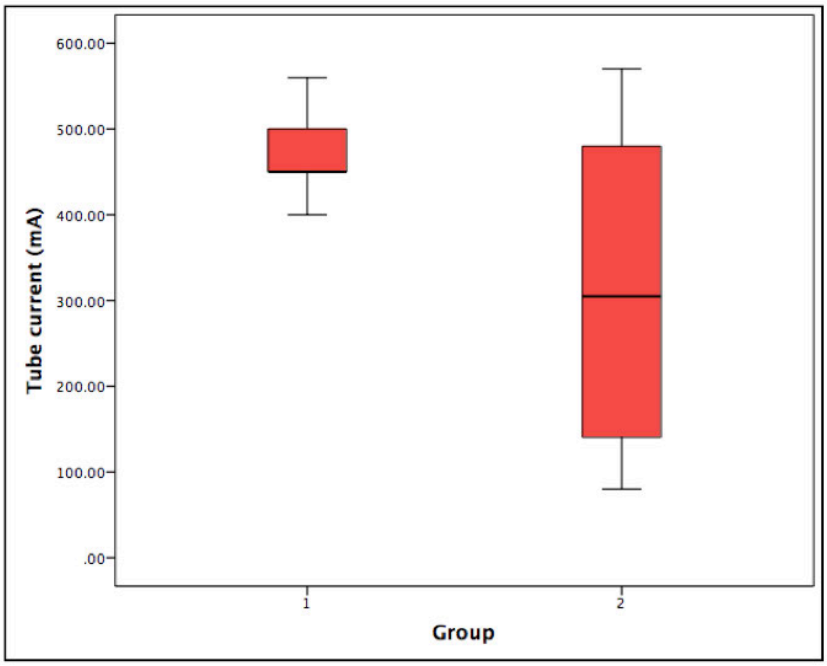

There was no difference between Group 1 and Group 2 for the attenuation in the aorta during stress imaging, septum during rest imaging or liver during rest imaging (Table 5.4). However, the contrast attenuation in Group 2 was slightly higher in the aorta during rest imaging, and septum and liver during stress imaging than in Group 1. Image noise in Group 2 was slightly higher in the aorta, septum and liver during stress imaging than in Group 1. There was also a small increase in CNR and CMR in Group 2 during rest imaging compared to Group 1, but there was no significant difference between the groups during stress imaging. There was no difference in subjective image quality for stress imaging between the two groups (17 [17,21] versus 17 [17, 19], P=0.523). An example of the images obtained in Group 1 and Group 2 are shown in Figures 5.2 and 5.3.

Table 5.4: Objective measurements of image quality in Group 1 and Group 2.

			Group 1	Group 2	P
Attenuation	Aorta	Rest	444 (417, 470)	590 (512, 668)	0.001
		Stress	381 (348, 414)	452 (368, 537)	0.114
	Septum	Rest	97 (86, 107)	101 (96, 107)	0.388
		Stress	116 (105, 127)	131 (123, 140)	0.027
	Liver	Rest	55 (48, 63)	56 (50, 61)	0.991
		Stress	68 (60, 75)	82 (75, 89)	0.008
Noise	Aorta	Rest	31 (27, 25)	33 (31, 35)	0.431
		Stress	27 (22, 32)	38 (33, 43)	0.001
	Septum	Rest	31 (28, 35)	29 (26, 31)	0.225
		Stress	116 (105, 127)	131 (123, 140)	0.027
	Liver	Rest	38 (35, 41)	32 (39, 34)	0.002
		Stress	33 (30, 37)	39 (36, 42)	0.009
CNR	Rest		13 (12, 14)	16 (14, 19)	0.030
	Stress		13 (11, 15)	10 (8, 12)	0.051
CMR	Rest		12 (10, 13)	15 (12, 17)	0.031
	Stress		11 (9, 13)	9 (7, 11)	0.082

(Mean (95% confidence interval); CNR, contrast-to-noise ratio; CMR, contrast-to-myocardium ratio)

Figure 5.2: An example of images obtained in Group 1 showing a perfusion defect identified during adenosine stress in septum on short axis images (B, yellow arrow). This was fully reversible and rest images were normal (A). This helped to confirm that the indeterminate lesion identified on CTCA in the LAD stent (C) was functionally significant.

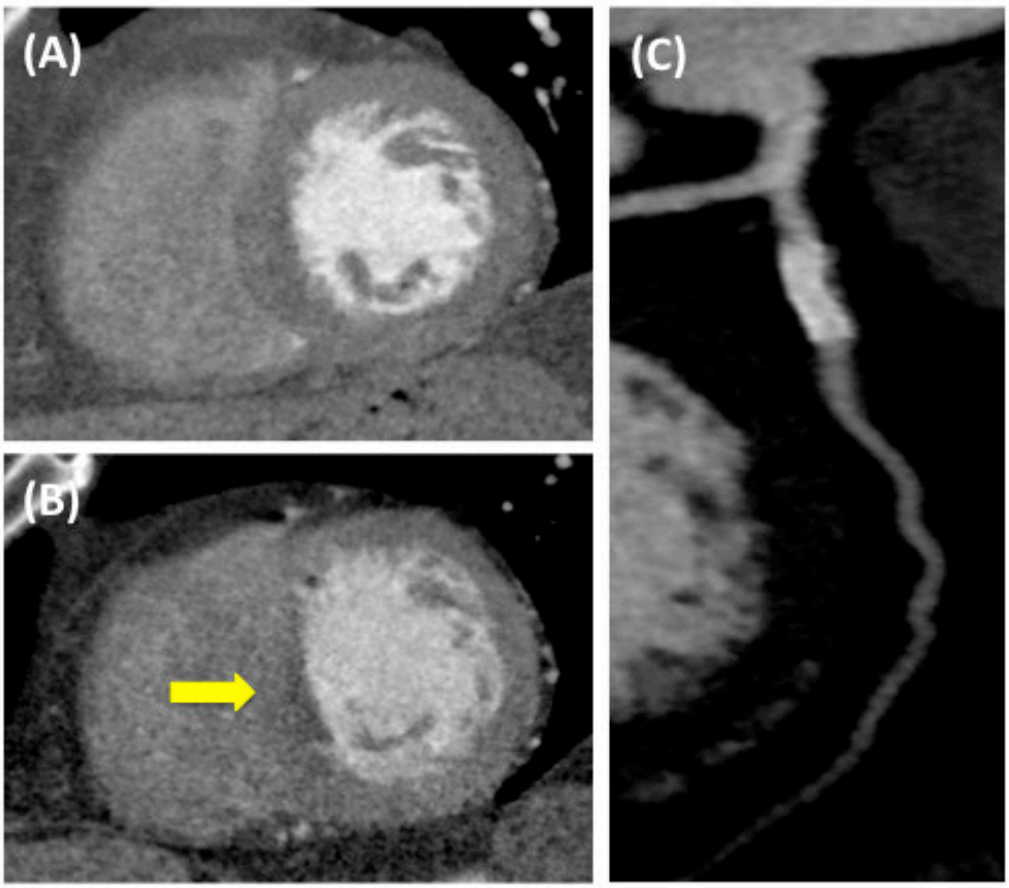

Figure 5.3: An example of the images obtained in Group 2 showing a perfusion defect identified during adenosine stress in the basal inferior and infero-septal segments on the short axis images (A, arrows) and the overlaid transmyocardial perfusion ratio plots (B, hypo-perfused area purple/pink). The CTCA image shows a significant stenosis in right coronary artery (C, arrow).

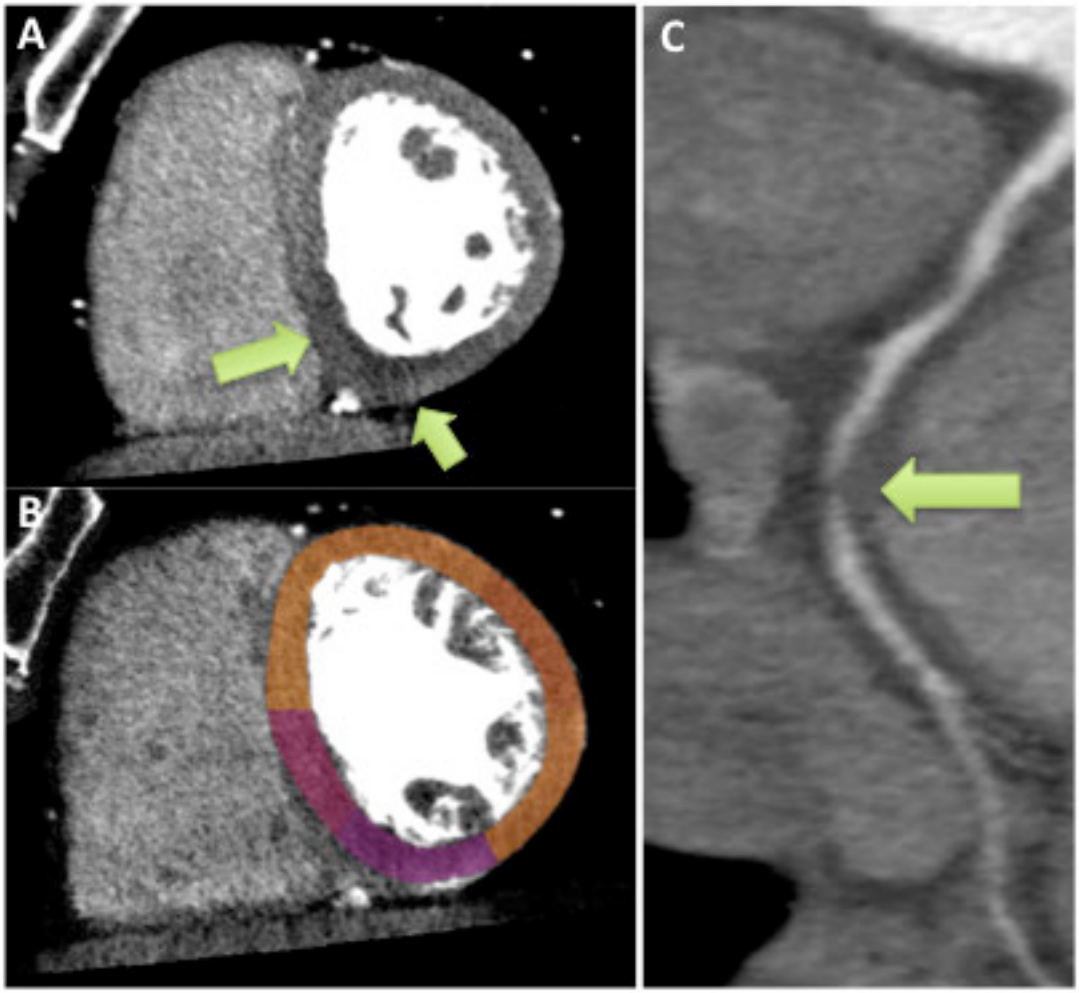

There was a reduction in radiation dose between the two groups for rest imaging, stress imaging and the total protocol radiation dose (Table 5.5, Figure 5.4). There was a 37% reduction in the radiation dose in rest imaging between Group 1 and Group 2 (224 mGy.cm (95% confidence interval 210, 238) versus 141 mGy.cm (109, 173), $P<0.001$)). The largest reduction (62%) in radiation dose was during stress imaging where the dose length product fell from 604 (486, 722) to 232 (177, 286) mGy.cm (Group 1 versus Group 2, $P<0.001$). The total protocol radiation dose reduction was 55% (828 (707, 949) versus 373 (289, 457) mGy.cm, $P<0.001$). Using the conservative conversion factor of 0.014 mSv/mGy.cm, the effective radiation dose for the total protocol fell from 11.6 to 5.22 mSv. Using a scanner specific conversion factor of 0.028 mSv/mGy.cm the radiation dose for the total protocol fell from 23.2 to 10.4 mSv.

Table 5.5: Radiation doses for the two protocols.

		Group 1	Group 2	*P*
Dose length product (mGy.cm)	Rest	224 (210, 238)	141 (109, 173)	<0.001
	Stress	604 (486, 722)	232 (177, 286)	<0.001
	Total	**828 (707, 949)**	**373 (289, 457)**	**<0.001**
Effective radiation dose (mSv, k 0.014)	Rest	3.14 (2.84, 3.33)	1.97 (1.53, 2.43)	<0.001
	Stress	8.46 (6.80, 10.11)	3.25 (2.48, 4.0)	<0.001
	Total	**11.6 (9.90, 13.3)**	**5.22 (4.05, 6.4)**	**<0.001**
Effective radiation dose (mSv, k 0.028)	Rest	6.27 (5.88, 6.66)	3.95 (3.05, 4.84)	<0.001
	Stress	16.9 (19.8, 20.2)	6.50 (4.96, 8.01)	<0.001
	Total	**23.2 (19.8, 26.6)**	**10.4 (8.09, 12.8)**	**<0.001**

(Mean (95% confidence interval))

Figure 5.4: Radiation dose reduction in computed tomography imaging for (A) rest, (B) stress, (C) the total protocol.

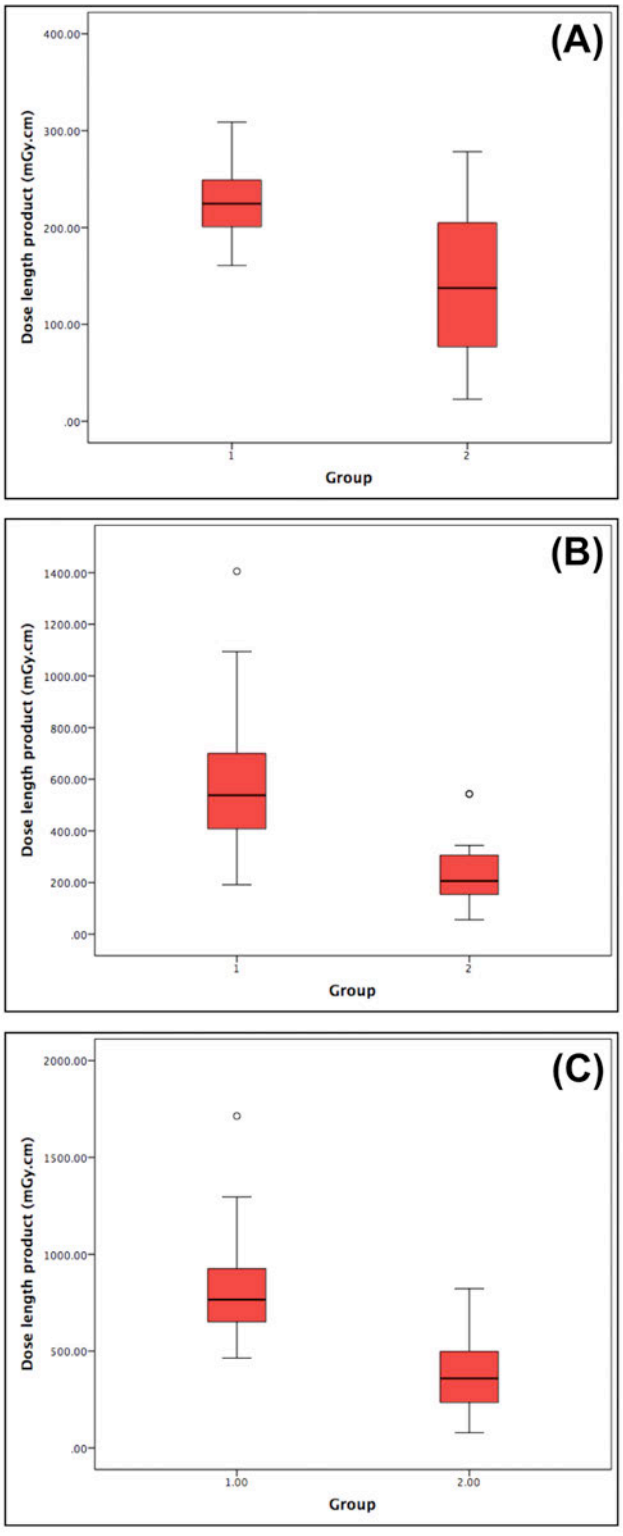

Discussion

We have shown that radiation dose reduction techniques can be successfully applied to computed tomography myocardial perfusion imaging while maintaining both subjective and objective image quality. We report a 62% reduction in the radiation dose for stress imaging and a 55% reduction for the total protocol. This major reduction in radiation dose means that combined computed tomography coronary angiography and myocardial perfusion imaging can simultaneously provide an anatomical and functional assessment of coronary artery disease at radiation exposures that are equivalent to current isolated anatomical (invasive coronary angiography) and functional (radionuclide myocardial perfusion) techniques.

Initial studies of computed tomography myocardial perfusion imaging using a wide volume scanner reported a radiation dose for rest and stress imaging of over 15 mSv.[66] This has fallen to 9-15 mSv in single centre studies [160-162] and average radiation doses of 9.32 mSv in a multicentre study.[70] In our study, we applied multiple techniques to reduce radiation dose including reducing the tube voltage, optimising the tube current based on scout image attenuation, using single (half) rather than multi-segment reconstruction and using iterative reconstruction. These techniques have previously been shown to reduce radiation dose in computed tomography coronary angiography. The application of these techniques led to a marked reduction in radiation dose with a total effective radiation dose of 5.22 mSv, without affecting image quality.

This is the first study to use automatic adjustment of the tube current based on scout image attenuation in myocardial perfusion imaging. Previous studies have either used body mass index based adjustment, or no adjustment with a single tube current. Body mass index is not always the best indicator of body habitus due to difference in the distribution of body fat. This may lead to the use of a tube current which is too high or too low, resulting in an unnecessarily high radiation dose or a poorer image quality. The increase in the range of the tube currents used in Group 2 shows that more appropriate tube currents were used for each patient, tailoring the radiation exposures to their individual requirements. This has the potential to provide a more consistent image quality, and potentially improve diagnostic accuracy.

One previous study applied iterative reconstruction algorithms to the assessment of myocardial perfusion imaging. Bhave *et al* showed an improved image quality and diagnostic accuracy when using iDose (Philips Medical Systems) as compared to standard filtered back projection.[55] Our study confirms that iterative reconstruction can be used in clinical practice to reduce radiation dose and maintain image quality in computed tomography myocardial perfusion imaging. We used the "standard" level of blending for AIDR3D but a stronger level of blending is available. Further work is required to assess whether higher levels of blending could be used to further reduce radiation dose in computed tomography myocardial perfusion imaging.

Changing the tube voltage, tube current and using iterative reconstruction alters myocardial attenuation values. In this study, there was a small but statistically significant difference in myocardial septum attenuation and noise during stress

imaging in Group 2. However, there was no difference in contrast-to-noise or contrast-to-myocardium ratios. Although this small difference would not affect visual assessment, it has the potential to affect quantitative assessment of myocardial perfusion. Further work is required to assess the effect of these radiation dose reduction techniques on the quantification of computed tomography myocardial perfusion.

The protocol described in this paper provides a single computed tomography image "snapshot" of myocardial perfusion. Recently, protocols for dynamic computed tomography myocardial perfusion have been described.[163,164] These protocols may result in higher radiation doses due to the acquisition of multiple images required over a period of about thirty seconds. In addition to the cumulative radiation dose, repeat exposure of the same area may also provide additional risks. The average radiation dose for dynamic rest and stress myocardial perfusion imaging is between 10 and 20 mSv.[164-168] One study has assessed the use of iterative reconstruction in an animal model of dynamic myocardial perfusion and identified improved image quality.[169] Further work on techniques to reduce radiation dose are particularly important for the future of dynamic myocardial perfusion imaging as a clinical technique.

This was a small single centre observational cohort study and the nature of the software changes between the two reconstruction algorithms precluded a randomised study. It is not possible to blind fully observers to the reconstruction algorithm used, as there are subtle differences between the images that an experienced observer is

aware of. In addition diagnostic accuracy was not assessed in this study, although subjective image quality was maintained.

In conclusion, computed tomography myocardial perfusion imaging is now possible at a low radiation dose with the application of patient tailored imaging, single segment image acquisition and iterative reconstruction. We believe that these approaches can now be used as part of routine clinical practice in the assessment of the functional significance of coronary artery disease.

Chapter Six: Observer variability in computed tomography coronary angiography

Extracts of this chapter are published in:

Williams MC, Golay SK, Hunter A, et al. Observer variability in the assessment of computed tomography coronary angiography and coronary artery calcium score: Sub-study of the Scottish Computed Tomography of the HEART (SCOT-HEART) trial. Open Heart 2015: 2(1): e000234.

Abstract

Introduction

Observer variability can influence the assessment of computed tomography coronary angiography (CTCA) and the subsequent diagnosis of angina pectoris due to coronary heart disease.

Methods

Reporting of CTCA images of 210 participants of the Scottish COmputed Tomography of the HEART (SCOT-HEART) trial were assessed for intra- and inter-observer variability. Calcium score, coronary angiography and image quality were assessed. Coronary artery disease was defined as none (<10%), mild (10-49%), moderate (50-70%) and severe (>70%) luminal stenosis and classified as no (<10%), non-obstructive (10-70%) or obstructive (>70%) coronary artery disease. Post CTCA diagnosis of angina pectoris due to coronary heart disease was classified as yes, probable, unlikely or no.

Results

Patients had a mean body mass index of 29 (28, 30) kg/m^2, heart rate of 58 (57, 60) /min and 62% were male. Intra- and inter-observer agreement for the presence or absence of coronary artery disease were excellent (95% agreement, Kappa 0.884 (0.817, 0.951) and good (91%, 0.791 (0.703, 0.879)). Intra and inter-observer agreement for the presence or absence of angina pectoris due to coronary heart disease were excellent (93%, 0.842 (0.918, 0.755) and good (86%, 0.701 (0.799,

0.603)) respectively. Observer variability of calcium score was excellent for calcium scores below 1000. More segments were categorized as uninterpretable with 64 compared to 320-multidetector CTCA (10.1% versus 2.6%, P <0.001) but there was no difference in observer variability.

Conclusion

Multicentre multidetector CTCA has excellent agreement in patients under investigation for suspected angina due to coronary heart disease.

Introduction

Computed tomography coronary angiography can identify the presence of coronary artery disease with excellent diagnostic accuracy as compared to invasive coronary angiography.[35] The results of computed tomography imaging are combined with clinical assessment in order to formulate an overall diagnosis on which to base management decisions. The impact of observer variability on the assessment of computed tomography images and the subsequent diagnosis of angina pectoris due to coronary heart disease has potential important implications for patient management.

The Scottish COmputed Tomography of the HEART (SCOT-HEART) trial is a randomised multicentre study that is assessing the role of computed tomography coronary angiography in the assessment of patients with suspected coronary artery disease. [170] Over 4,000 participants assessed at the Rapid Access Chest Pain Clinic will be randomised to 64 or 320-multidetector computed tomography coronary angiography plus standard care or standard care alone. This study will establish the additive diagnostic value of computed tomography imaging in the management of these patients.

Good observer variability in the anatomical assessment of coronary artery stenosis by computed tomography has previously been established.[171-173] However, the most clinically relevant question relates to the observer variability in the final diagnosis of angina pectoris due to coronary heart disease. Moreover, differing scanner specifications and vendors, generalizability across multiple different sites,

differing software applications and variations in clinic assessments are all potential sources of variability in the ultimate clinical assessment of such patients. Marked observer variability could lead to over or under diagnosis of coronary artery disease and lead to false reassurance or unnecessary further investigations or treatment.

The study aims were to assess observer variability in the assessment of stenosis severity and coronary artery calcification, to establish the observer variability of the diagnosis of angina pectoris due to coronary heart disease, and to compare observer variability between 64 and 320-multidetector computed tomography scans in the SCOT-HEART trial.

Methods

Study design

The SCOT-HEART trial is a prospective multicentre randomised study of the role of computed tomography coronary angiography in patients attending the rapid access chest pain clinic (NCT NCT01149590, [170]). It will recruit 4,138 patients randomised 1:1 to computed tomography coronary angiography plus standard care or standard care alone. The study was approved by the research ethics committee and all patients undertook written informed consent. This substudy of the SCOT-HEART trial assesses the secondary outcomes of observer variability in CTCA.

The images of 210 patients were assessed. A sample size of 200 would give a 95% confidence interval of about +/- 0.24 standard deviations, and as equal numbers were required in each group this was rounded up to the nearest possible whole number, 210 participants. [174] The first 50 scans at each site were co-reported by the peripheral and central site to ensure a comparable approach and reporting quality. These scans were excluded from this sub-study. In addition, patients with coronary artery bypass grafts or intra coronary stents were excluded from this sub-study. Images were selected randomly and were selected to include a representative sample of study participants in terms of scanner type, presence of coronary artery disease on initial assessment and image quality. This meant that one third of the 210 patients had no coronary artery disease, one third had non-obstructive coronary artery disease and one third had obstructive coronary artery disease based on the initial assessment of the computed tomography imaging.

Computed tomography imaging

Computed tomography imaging was performed using either 64 or 320-multidetector scanners (Aquilion ONE, Toshiba Medical Systems, Japan or Brilliance 64, Philips Medical Systems, the Netherlands) as described previously. [170] Patients with heart rates >65 /min received rate-limiting medication (intravenous metoprolol) and all patients received sublingual glyceryl trinitrate prior to imaging. Non-contrast imaging was performed to assess coronary artery calcification. Coronary angiography was obtained after the injection of iodinated contrast (Iomeron 400 (Bracco) or Ultravist 370 (Bayer). Computed tomography imaging using the 320-multidetector scanner was performed over a single heart-beat with wide volume

imaging using an acquisition window of 70-80% or 30-80% depending on the heart rate. Imaging using the 64-multidetector scanner was performed using prospective or retrospective gating depending on heart rate. Iterative reconstruction (Adaptive Iterative Dose Reduction or iDose4) was used to reconstruct images.

Image analysis

Images were assessed by observers blinded to the results of the other assessments. Repeat assessments were performed at least 2 weeks apart in random order to prevent recall bias. Repeat assessment was performed by the same individuals as the initial assessment to assess intra-observer variability. A second set of observers assessed the images separately to assess inter-observer variability.

Coronary artery calcium scoring was performed using dedicated software (VScore, Vital Images or Siemens console software). Agatston score was calculated using a threshold of 120 Hounsfield units (HU) for each vessel and summed to give a total score.[112]

Computed tomography coronary angiogram images were assessed for stenosis severity on a segmental basis. A 15-segment model was used. Segments that were uninterpretable or absent were excluded from the diagnosis. Luminal cross-sectional area was classified as normal (<10%) or having mild (10-49%), moderate (50-70%) or severe (≥70%) stenosis (Figure 6.1).

Figure 6.1: Computed tomography coronary angiography curved planar reformations and vessel cross sections showing lesions with different stenosis severity (none, <10%; mild, 10-49%; moderate, 50-70%; severe, >70%).

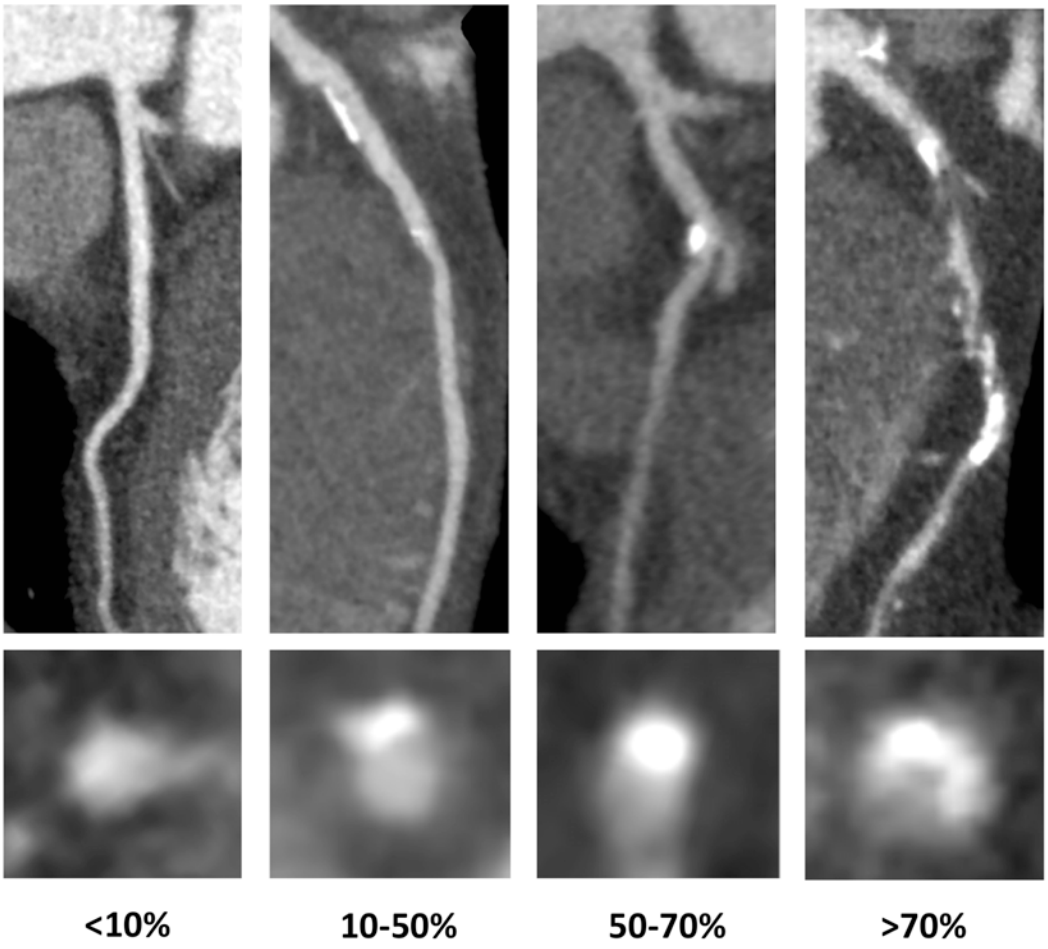

On a per-patient basis, the segmental computed tomography coronary angiogram and coronary artery calcium score were used to decide the overall computed tomography result. Obstructive coronary artery disease was defined as a stenosis ≥70% in one or more major epicardial vessels or >50% in the left main stem. Non-obstructive coronary artery disease was defined as coronary artery disease with stenosis >10% and not fulfilling the criteria for obstructive coronary artery disease.

The post computed tomography diagnosis of angina due to coronary heart disease was determined based on the computed tomography result and the chest pain clinic assessment of the likelihood of angina pectoris due to coronary heart disease including a previous history of coronary heart disease, exercise test result and type of angina chest pain. [32,170] The post computed tomography diagnosis of angina pectoris due to coronary heart disease was classified as yes, probable, unlikely and no, and were dichotomised to assess the presence or absence of angina pectoris due to coronary heart disease.

Image quality

Subjective image quality was assessed on a 4-point Likert scale (1 good scan quality, diagnostic, 2 moderate scan quality, diagnostic but sub-optimal, 3 poor scan quality, limited diagnostic and 4 non-diagnostic scan quality). Vessels were also classified as interpretable or uninterpretable on a segmental basis.

Objective assessment of image quality was assessed by measuring computed tomography attenuation and image noise, and calculating contrast-to-noise ratio. Computed tomography attenuation was measured in a region of interest in the ascending aorta at the level of the left main stem and liver of non-contrast scans and the ascending aorta at the level of the left main stem, liver and interventricular septum of contrast enhanced scans. Image noise was determined as the standard deviation of the Hounsfield units in a region of interest drawn in the ascending aorta just above the level of the left main stem. Contrast-to-noise ratio was calculated as

the attenuation in the aorta minus the attenuation in the liver and divided by the image noise in the aorta.

Statistical analysis

Statistical analysis was performed using PASWStatistics (Version 18 for Mac, IBM) and Graphpad Prism (Version 6 for Mac). Inter and intra-observer variabilities were assessed using Cohen's Kappa statistics and Bland-Altman plots. A Kappa statistic of <0.2 indicated poor agreement, 0.21 to 0.4 fair agreement, 0.41 to 0.6 moderate agreement, 0.61 to 0.8 good agreement and 0.81 to 1 excellent agreement. Normally distributed quantitative variables are presented with mean and 95% confidence interval. Non-normally distributed data are presented as median and interquartile range. Statistical significance was assessed using analysis of variance, Student's *t*-test or Pearson's chi-squared test as appropriate. A statistically significant difference was defined as a two-sided *P* value <0.05.

Results

We assessed 210 patients (62% male) who had a mean body mass index of 29 (28, 30) kg/m^2 and mean heart rate of 58 (57, 60) /min. Arrhythmia was uncommon, with 3.3% of the patients having ectopic beats and 1% atrial fibrillation. Demographic details are shown in Table 6.1.

Table 6.1: Demographic details for Chapter 6.

Parameter		
N		210
Age (years)		58 (57, 60)
Male		130 (62%)
Body mass index (kg/m^2)		29 (28, 30)
64 / 320-multidetector scanner		72 (34%) / 138 (66%)
Previous history of coronary artery disease		18 (9%)
Coronary artery calcium score (Agatston units)		373 (242, 505)
Zero coronary artery calcium score		142 (68%)
CT overall assessment	No coronary artery disease	70 (33%)
	Non obstructive coronary artery disease	70 (33%)
	Obstructive coronary artery disease	70 (33%)
CT vessels with significant coronary artery disease	One vessel disease	39 (19%)
	Two vessel disease	21 (10%)
	Three vessel disease	10 (5%)

(Mean and (95% confidence interval) or median [Interquartile range] or number (percentage); CT, computed tomography)

Coronary Artery Disease and Angina

There was excellent or good intra- and inter-observer agreement in the assessment of computed tomography imaging for the presence or absence of coronary artery disease (95% agreement, Kappa 0.884 (0.817, 0.951) and 91% agreement, Kappa 0.791 (0.703, 0.879), respectively; Table 6.2). Similar agreement was also seen for the presence or absence of angina pectoris due to coronary heart disease (93% agreement, kappa 0.842 (0.918, 0.755) and 86% agreement, kappa 0.701 (0.799, 0.603), respectively; Table 6.2).

Table 6.2: Intra and inter observer variability for (A) the presence of coronary artery disease on computed tomography imaging and (B) the diagnosis angina pectoris due to coronary heart disease after computed tomography imaging.

	Intra observer		**Inter observer**	
(A) Coronary artery disease on computed tomography		Absent	Present	
	Absent	67	3	
	Present	8	132	
		Absent	Present	
	Absent	57	13	
	Present	6	134	

	Intra observer		**Inter observer**	
(B) Angina pectoris due to coronary heart disease		Absent	Present	
	Absent	130	3	
	Present	12	65	
		Absent	Present	
	Absent	113	10	
	Present	20	67	

When the overall computed tomography result was classified as obstructive, non-obstructive or no coronary artery disease on a per-patient basis (Table 6.3), there was excellent intra-observer agreement (87% agreement, 0.807 (0.876, 0.738)) and good inter-observer agreement (81% agreement, 0.721 (0.799, 0.643)). Agreement was highest for scans with no coronary artery disease as compared to non-obstructive or obstructive coronary artery disease for both intra-observer variability (96% versus 96% and 83%, respectively) and inter-observer variability (81% versus 86% and 77%, respectively).

Table 6.3: Intra (A) and inter (B) observer variability in per-patient assessment of computed tomography coronary angiography result.

(A)

	None	Non obstructive	Obstructive
None	67	2	1
Non obstructive	7	58	5
Obstructive	1	11	58

(B)

	None	Non obstructive	Obstructive
None	57	12	1
Non obstructive	4	60	6
Obstructive	2	14	54

Using a four-point scale to assess the presence of angina pectoris secondary to coronary heart disease (yes, probable, unlikely and no, Table 6.4) there was good intra-observer variability (0.625 (0.709, 0.541)) and moderate inter-observer variability (0.497 (0.581, 0.413)). Similarly, based on a four-point scale (none, mild, moderate, severe) there was moderate intra- and inter-observer variability in the per-segment assessment of stenosis severity (0.521 (0.490, 0.552) and 0.459 (0.428, 0.490) respectively, Table 6.5).

Table 6.4: Intra (A) and inter (B) observer variability in per-patient diagnosis of angina pectoris due to coronary artery disease after computed tomography assessment.

(A)

	Yes	**Probable**	**Unlikely**	**No**
Yes	42	5	2	5
Probable	10	8	1	4
Unlikely	0	0	15	17
No	1	2	3	95

(B)

	Yes	**Probable**	**Unlikely**	**No**
Yes	34	16	3	1
Probable	9	8	5	1
Unlikely	1	9	17	5
No	4	6	14	77

Table 6.5: Intra (A) and inter (B) observer variability in per-segment computed tomography assessment of stenosis severity.

(A)

	<10%	**10-49%**	**50-70%**	**>70%**
<10%	2054	142	15	13
10-49%	112	171	35	13
50-70%	43	55	43	16
>70%	24	35	26	89

(B)

	<10%	**10-49%**	**50-70%**	**>70%**
<10%	17778	234	19	23
10-49%	91	182	33	17
50-70%	24	70	32	22
>70%	19	44	30	75

Coronary Artery Calcium Score

There were no differences in Agatston calcium score on intra- or inter-observer assessment (373 (224, 505) Agatston units versus 278 (202, 354) Agatston units, *P*=0.138 and 290 (210, 370) Agatston units, *P*=0.191). Bland-Altman plots showed that the level of calcification systematically affected intra- and inter-observer variability of the Agatston score (Figure 6.2) with both intra- and inter-observer variability increasing as the calcium score increased. However, for patients with calcium score of < 1000, the intra- and inter-observer was excellent (Figure 6.3).

Figure 6.2: Bland-Altman plots for intra and inter observer variability for the assessment of total Agatston score (dotted lines represent the limits of agreement).

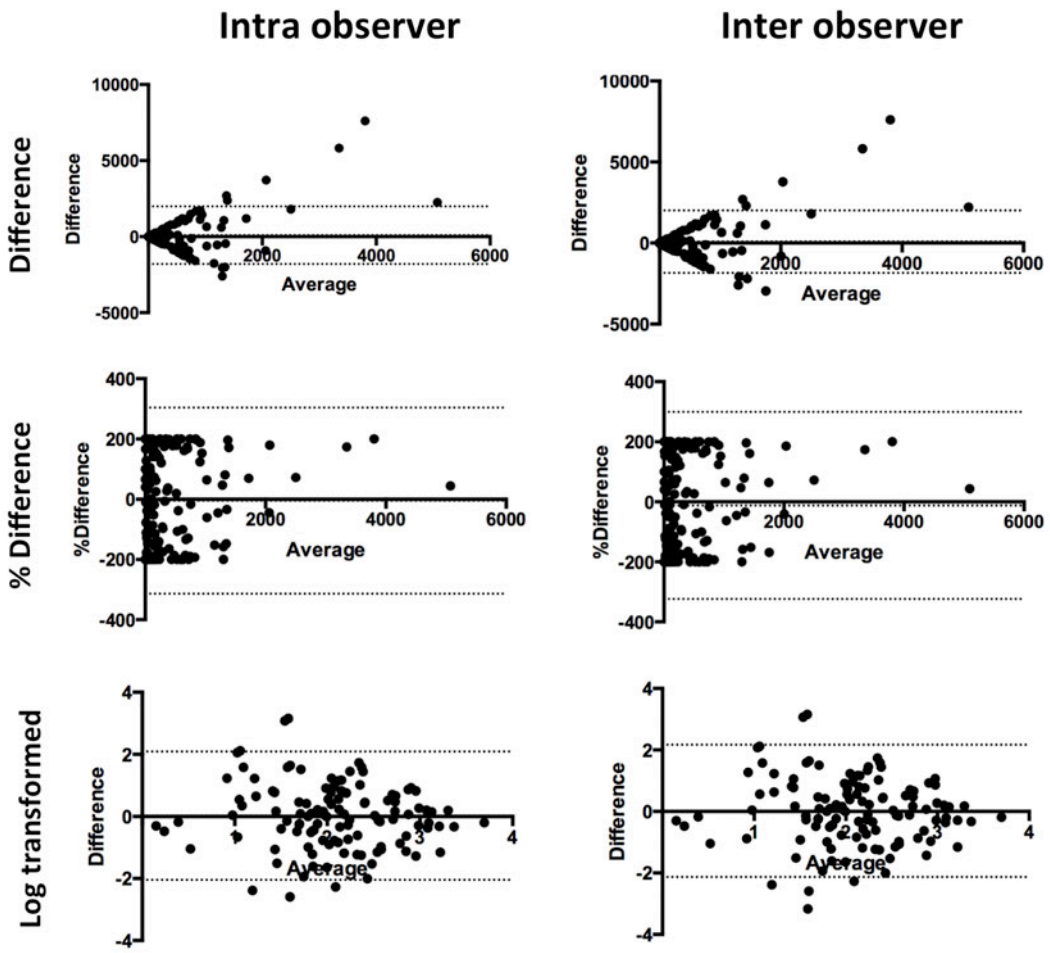

Figure 6.3: Bland-Altman plots for intra and inter observer variability for the assessment of total Agatston score for patients with a calcium score < 1000 (one outlier was excluded from the inter observer variability assessment, dotted lines represent the limits of agreement.).

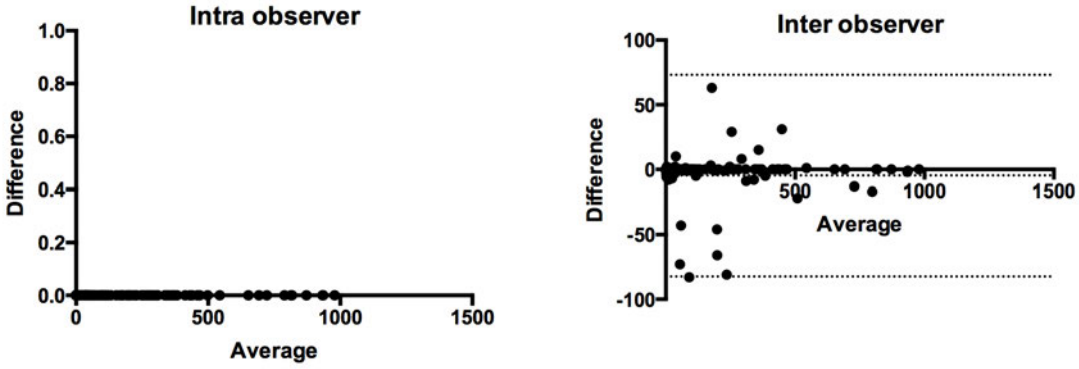

Image Quality

The number of segments that were categorized as uninterpretable was 5-fold higher using 64 as compared to 320-multidetector scanners (10.1% versus 2.6%, P <0.001). There was no difference in mean aorta contrast attenuation between 64 and 320-multidetector scanners, but there was a small but significant reduction in image noise in contrast-enhanced 320-multidetector computed tomography (Table 6.6). Inter-observer variability for 64 and 320-multidetector computed tomography were similar, with a large overlap of confidence intervals, for the assessment of coronary artery disease (0.729 (0.596, 0.862) versus 0.717 (0.619, 0.815) respectively) and the post computed tomography diagnosis of angina due to coronary heart disease (0.518 (0.416, 0.620) and 0.459 (0.314, 0.604) respectively).

Table 6.6: Quantitative assessment of image quality with 64 and 320-multidetector computed tomography.

			320 MDCT	64 MDCT	*P*
Attenuation	Non contrast	Aorta	60	38	**<0.001**
		Liver	52	49	0.085
	CTCA	Aorta	500	495	0.801
		Septum	85	138	**<0.001**
		Liver	62	66	0.466
Noise	Non contrast	Aorta	19	20	0.564
		Liver	34	31	**0.013**
	CTCA	Aorta	37	40	**0.014**
		Septum	34	41	**<0.001**
		Liver	40	41	0.558
CNR	Non contrast	Aorta	19	20	0.564
		Liver	34	31	**0.013**
	CTCA	Aorta	37	40	**0.014**
		Septum	34	41	**<0.001**
		Liver	40	41	0.558

(MDCT multidetector computed tomography; CTCA computed tomography coronary angiography; CNR contrast to noise ratio)

Discussion

This study confirms the excellent inter and intra-observer agreement for the assessment of the presence or absence of coronary artery disease by computed tomography coronary angiography. In addition, for the first time, we establish the excellent inter and intra-observer agreement for the post computed tomography diagnosis of the presence or absence of angina pectoris due to coronary heart disease. This study provides a basis for the clinical use of computed tomography coronary angiography to guide the diagnosis, management and treatment of patients being assessed for suspected angina due to coronary heart disease.

In keeping with previous studies, we have shown the excellent agreement for the per-patient assessment of computed tomography coronary angiography.[171-173] Observer variability and diagnostic accuracy in computed tomography coronary angiography may be influenced by patient factors such as the presence of heavily calcified coronary artery disease or a rapid heart rate. Calcified atherosclerotic plaque may be overestimated on computed tomography imaging due to a combination of "beam hardening" and "blooming" artifacts. The assessment of calcified plaque is associated with higher observer variability than non-calcified plaque.[175,176] In particular, eccentric calcification is associated with the highest observer variability in the assessment of stenosis severity.[171] However, Ovrehus *et al* found that for patients with an Agatston score below 400 Agatston units, the calcium score was not a predictor of observer variability in the assessment of stenosis severity.[177]

In keeping with previous studies,[178] we showed that observer variability in calcium scoring increases as the Agatston score increase. However, for patients with a calcium score below 1000 Agatston units, the observer agreement was excellent. In addition to good intra- and inter-observer variability in calcium scoring, good inter-scan variability has also been established.[179] However, differences in calcium scores have been established in phantom studies between different scanners.[180] Therefor, it is important that studies assessing the progression of calcium scoring take scanner variations into account. The excellent observer agreement identified in this study for calcium scoring supports its application in the assessment of cardiovascular risk.

The prevalence of coronary artery disease in a population can influence the results of studies of non-invasive imaging techniques. Nicol *et al* showed that there was the best observer agreement for patients with a low to intermediate pre-test probability of coronary artery disease as compared to patients with a higher pre-test probability. Previous studies of observer variability in populations with a high prevalence of coronary artery disease showed slightly poorer observer agreement as compared to studies with a lower prevalence of coronary artery disease [171,173,177,181] (Table 6.7). This is likely to be due to the higher prevalence of heavily calcified vessels in patient populations with a higher risk of cardiovascular disease. In our study we identified slightly higher observer agreement for patients with no coronary artery disease as compared to non-obstructive or obstructive coronary artery disease. Unlike other studies we did not exclude patients based on heart rate, the presence of arrhythmias, body mass index or weight. Our study assessed patients with a

representative prevalence of coronary artery disease in those presenting to the clinic for assessment of suspected angina due to coronary heart disease. Therefore our results regarding observer variability can be directly transferred to the assessment of such patient populations.

There was excellent agreement for the overall diagnosis of the presence or absence of angina pectoris due to coronary heart disease in this study. However, when more categories are included in an assessment, the level of agreement understandably decreases. On a per-segment basis, differences in anatomical classification are an important source of observer variability. For example, Figure 6.4 shows an atherosclerotic plaque in the left anterior descending artery at the branch of the first diagonal. This could be classed as either in the proximal or mid left anterior descending artery segments. In addition, lesions of borderline significance may be up or down graded depending on the observer as shown in Figure 6.5. The choice of cut-off value for the definition of stenosis severity may also affect observer variability. Most previous studies have assessed observer variability for the identification of any atherosclerotic plaque or the assessment of stenoses >50%. Previous studies identified inter-observer agreement for the presence of stenosis >50% of between 81% and 96%, with Kappa scores between 0.66 and 0.91. (Table 6.7) [171,173,177,181] Similar to our study, when using a cut off of >70%, Nicol *et al* identified inter-observer agreement of 87% on a per-patient basis, 97% on a per-vessel basis and 99% on a per-segment basis.[171] The use of the 70% cut off for the diagnosis of obstructive coronary artery disease in our study was felt to be the most clinically relevant parameter for the assessment of computed tomography imaging.

Figure 6.4: Computed tomography coronary angiography curved planar reconstruction of the left anterior descending artery showing calcified and non-calcified plaque. The location of this plaque, which spans the origin of the first diagonal vessel, can cause differences in segmental classification between observers.

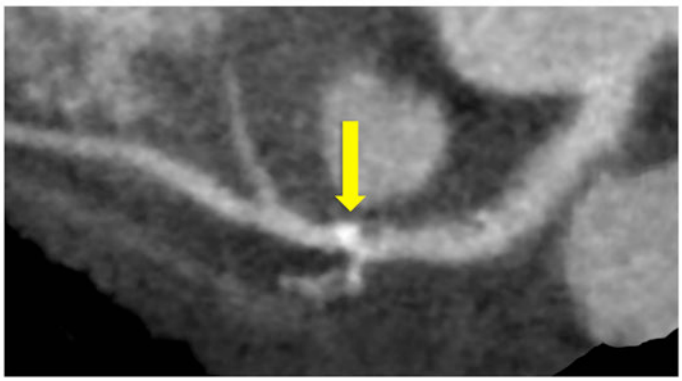

Figure 6.5: Computed tomography coronary angiography images of a heavily calcified left anterior descending artery. The "blooming" artefact from such heavily calcified plaque can lead to differences in observer classification of stenosis severity.

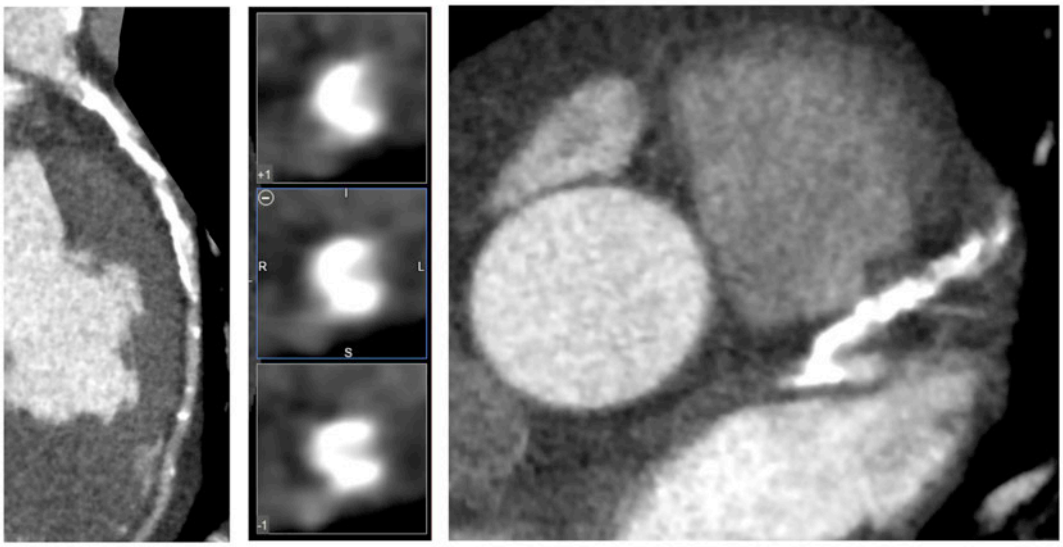

Different scanner types and computed tomography coronary angiography protocols may affect observer variability. In a study of patients undergoing 64-multidetector computed tomography coronary angiography, there was good inter-observer agreement for prospectively gated scans and excellent inter-observer agreement for retrospectively gated scans (Kappa 0.724 and 0.823 respectively). [182] In a study of 320-multidetector computed tomography, the per-patient inter-observer variation for the detection of significant coronary artery disease (≥50% stenosis) was good (Kappa 0.72 (95% confidence interval 0.62, 0.81). A study of the diagnostic accuracy of dual source computed tomography identified good inter-observer variability with a Kappa score of 0.79. [183] In our study there were more non-diagnostic segments with 64 as compared to 320-multidetector computed tomography. Khan *et al* showed that there were 0.1% non diagnostic segments with 320-multidetector as compared to 3.3%

with 64-multidetector computed tomography coronary angiography.[153] However, we have shown that despite this difference, intra- and inter-observer variability was similar between the two scanner types. The SCOT-HEART study is the largest randomized multicentre study of computed tomography coronary angiography to date. The excellent observer variability identified in this study is therefore important for the large-scale adoption of this technique for patients with suspected coronary artery disease.

This study includes a representative sample of image quality and severity of coronary artery disease selected randomly from a large multicentre study. However, this meant that the effect of image quality on observer variability could not be assessed due to low numbers in the poor image quality group. In addition, we included a representative proportion of scans from each scanner, so there are not equal numbers in both groups. This study could not assess diagnostic accuracy, as not all patients went on to have invasive coronary angiography. However, we did have broad inclusion criteria and included a representative population of patients attending the clinic that included patients with arrhythmia and nearly a half of patients had a body mass index >30 kg/m^2.

In conclusion, in this study we establish the excellent observer agreement for the assessment of coronary artery calcium score, computed tomography coronary angiography assessment of stenosis severity and the post computed tomography diagnosis of angina pectoris due to coronary heart disease. This supports the use of

computed tomography coronary angiography in the assessment of patients with suspected angina due to coronary heart disease.

Table 6.7: Studies of observer variability using a cut off of >50% stenosis.

Ref	N	Scanner	Age	Male	Population risk	Identified CAD	Inter-observer (% agreement, Kappa)			Intra-observer (% agreement, Kappa)		
							Per patient	Per vessel	Per segment	Per patient	Per vessel	Per segment
Nicol	133	64	61 ± 13	30	39% low to intermediate, 39% intermediate to high, 22% very low risk	41% normal, 26% minor, 32% moderate, 15% severe	81%	94%	97%	87%	94%	96%
Overhus	209	64 or DSCT	61 ± 6.9	56	13.4% low, 87.2% intermediate or high	35% of patients had any disease	82% 0.65	*	*	*	*	*
Stolzman	100	DSCT	56 ± 13	61	*	55% of segments had >50% stenosis	0.77	*	*	*	*	*
Meijboom	360	64	60 ± 6	68	Intermediate to high	68% had obstructive CAD	0.66	*	*	*	*	*

*(CAD, coronary artery disease; *, not given)*

Chapter Seven: Diagnostic accuracy of computed tomography myocardial perfusion imaging

Extracts of this chapter are published in:

Williams MC, Cruden NL, Uren NG, Newby DE. A low-dose comprehensive cardiac CT protocol assessing anatomy, function, perfusion, and viability. Journal of Cardiovascular Computed Tomography 2013: 7(1); 69-72.

Abstract

Introduction

Computed tomography can perform rapid comprehensive cardiac imaging. This chapter assesses the diagnostic accuracy of computed tomography coronary angiography (CTCA) with CT myocardial perfusion (CTP) imaging compared with invasive coronary angiography (ICA) with fractional flow reserve (FFR).

Methods

With research ethics committee approval and informed consent, 51 patients (63 (61, 65) years, 80% male) with suspected coronary artery disease underwent contrast enhanced, electrocardiogram-gated wide volume CTCA with a 320-multidetector scanner, followed by CTP during adenosine stress (140 μg/kg/min). ICA/FFR was performed in 47 patients. Obstructive coronary artery disease on computed tomography was defined as CTCA stenosis >50% with corresponding CTP hypoperfusion. Obstructive coronary artery disease on invasive coronary angiography imaging was defined as ICA stenosis >70% or FFR <0.80. Twenty computed tomography myocardial perfusion images were also assessed for intra and inter observer variability.

Results

On a per-patient basis, there was excellent accuracy (92%) as well as sensitivity (96%), specificity (85%), negative predictive value (90%) and positive predictive value (94%) for CTCA/CTP compared with ICA/FFR. Intra- and interobserver

variabilities for per-segment visual assessment of computed tomography myocardial perfusion were good (Kappa 0.772, and 0.721 respectively). The average radiation dose for coronary artery calcium score, rest CTCA, stress CTP and late enhancement was 8.89 mSv.

Conclusion

CTCA/CTP can accurately identify patients with obstructive coronary artery disease as identified on ICA/FFR.

Introduction

Computed tomography coronary angiography can be performed at low radiation dose with excellent diagnostic accuracy. [35] However, areas of high density, such as coronary calcification or coronary stents, can reduce the accuracy of computed tomography coronary angiography. [184] The concomitant assessment of myocardial perfusion has the potential to address this issue by providing additive functional information to guide the assessment of coronary artery disease. Computed tomography myocardial perfusion imaging can therefor improve the diagnostic accuracy of computed tomography coronary angiography and can be performed during the same examination. [70]

The selection of symptomatic patients for coronary revascularisation is based on the functional significance of coronary stenoses. This can be characterised by fractional flow reserve, which is the current "gold-standard" method of defining obstructive coronary artery disease. Management decisions based on fractional flow reserve can lead to improved clinical outcomes. [21] However, fractional flow reserve assessment requires invasive coronary angiography and is a derived ratio of pressure rather than a direct measurement of blood flow. [13] Other methods, such as magnetic resonance imaging or single photon emission computed tomography (SPECT), non-invasively assess myocardial perfusion but can be limited by poor spatial resolution, imaging artefacts, long imaging times, lack of coincidental anatomical information, and false-negatives due to balanced ischemia in three-vessel disease because they assess relative rather than absolute perfusion. [67,68]

Computed tomography myocardial perfusion imaging in this study was performed using the “snap shot” technique, which obtains a small number of images at maximal contrast enhancement. This chapter assess the diagnostic accuracy of this “snap shot” computed tomography myocardial perfusion imaging technique as compared to the "gold standard" clinical measure of coronary stenosis severity, namely fractional flow reserve measured during invasive coronary angiography.

Methods

Study design and sample size calculation

This was a single centre prospective cohort study. We estimated that a sample of 67 patients would be needed to detect at least a 10% difference in the diagnostic accuracy (measured as the area under the receiver operating characteristic curve) of at least 0.90 with a 95% confidence interval, assuming a 50% disease prevalence and an intra and inter-observer variability of 0.005 and 0.01 respectively between observers. The study recruited 51 patients in total. The primary outcome was diagnostic accuracy of CTCA/CTP as compared to ICA/FFR. Secondary outcomes were radiation dose and observer variability.

Study Population

Participants had known or suspected coronary artery disease and were due to undergo invasive coronary angiography. Exclusion criteria were renal failure (serum creatinine >250 μmol/L or estimated glomerular filtration rate <30 mL/min), allergy

to iodinated contrast, pregnancy or contraindication to adenosine. Cardiovascular risk was assessed using the Framingham 10-year cardiovascular risk score.

Computed tomography

Participants underwent rest and adenosine stress computed tomography using a 320-multidetector scanner (Aquilion ONE, Toshiba Medical Systems, Japan) as described in Chapter 2. After acquisition of scout images, patients underwent non-contrast computed tomography using tube voltage 120 kV, tube current based on body mass index and scan range from 2 cm below the carina to the base of the heart. Images were reconstructed with 3 mm non-overlapping slices and a filtered back projection reconstruction algorithm (Quantum Denoising Software, QDS+; kernel FC02 (smooth kernel, Toshiba Medical Systems)). Participants underwent resting prospective wide-volume computed tomography. Tube voltage and current were based on body mass index or scout image attenuation. A triphasic injection of iodinated intravenous contrast (iomeprol, 400 mg iodine/mL; Iomeron 400, Bracco, UK) was administered based on body mass index (<30 kg/m^2, 50 mL; 30-39 kg/m^2, 60 mL; >40 kg/m^2, 70 mL). Bolus triggering started the scan when descending aorta enhancement reached 300 Hounsfield units (HU). Stress imaging was performed 10 min after rest imaging and after 4 min of adenosine infusion (140 μg/kg/min). The same tube voltage, tube current and contrast were used as for rest imaging. However, scan range was reduced to cover only the left ventricle and tube current modulation obtained data over a single heartbeat. A further low dose CT (100 kV, targeted 75% acquisition) was performed at 3-4 min to assess myocardial late enhancement. This time interval was based on unpublished work that showed that the contrast dynamics

of iodinated contrast is different to gadolinium and earlier imaging is therefor required to identify late enhancement. Images were reconstructed using iterative reconstruction (Adaptive Iterative Dose Reduction 3D, Toshiba Medical Systems, Japan) with standard blending. Computed tomography coronary angiography images were reconstructed using the FC05 kernel and computed tomography myocardial perfusion with the FC03 kernel (smooth kernels, Toshiba Medical Systems). [78] Radiation dose was calculated using the conversion factor method and a conversion factor of 0.014 mSv/mGy.cm.

Invasive coronary angiography and fractional flow reserve

Invasive coronary angiography and fractional flow reserve were performed as described in Chapter 2. Fractional flow reserve was assessed for major coronary epicardial vessels with stenosis >50%, where technically possible. Pharmacological stress was induced using intravenous adenosine (140 μg/kg/min). Obstructive coronary artery disease was defined as luminal stenosis >70% on invasive coronary angiography or fractional flow reserve <0.80.

Image analysis

Assessment of imaging was performed blinded to results of other modalities. Computed tomography was analysed using a post-processing workstation (Vitrea fX, Vital Images, USA). Two trained observers (MCW, DEN) assessed images separately, and differences were agreed by consensus. Twenty of the scans had a repeat assessment to assess observer variability. Computed tomography myocardial perfusion was assessed as per standard guidelines with adjustment of viewing

parameters as required. [116] Visual analysis of computed tomography coronary angiography was based on the 15 segment model and computed tomography myocardial perfusion was assessed based on the 17 segment model. [115] Segmental data were consolidated into 3 territories for per-vessel perfusion analysis. [115] Obstructive coronary artery disease was defined as >50% stenosis on computed tomography coronary angiography with corresponding hypo-perfusion on computed tomography myocardial perfusion imaging.

Statistical analysis

Statistical analysis was performed using SPSS (Version 18 for Mac, IBM). Normally distributed quantitative variables are presented with mean and 95% confidence interval. Non-normally distributed data are presented with median and interquartile range. Statistical significance was assessed using analysis of variance, Student t, or Mann-Whitney U tests as appropriate. Sensitivity, specificity, positive predictive value (PPV), negative predictive value (NPV) and diagnostic accuracy were calculated on a per-vessel and per-patient basis. Receiver operator characteristic curves were constructed to assess diagnostic accuracy. A statistically significant difference was defined as a two-sided P value <0.05.

Results

Demographic details

Computed tomography was performed in 51 patients and demographic details are showing in Table 7.1. Invasive coronary angiography was performed in 47 patients. Twenty-three participants (45%) had a previous history of coronary artery disease. All but two patients presented with chest pain, with 32 (63%) having typical angina, 10 (20%) atypical angina and 7 (14%) non-anginal chest pain. According to the Framingham 10-year cardiovascular risk score, 23 (45%) were high-risk, 20 (39%) intermediate-risk and 8 (16%) low-risk. The mean coronary artery calcium score was 870 (580, 1161) Agatston units. Invasive coronary angiography and fractional flow reserve identified obstructive coronary artery disease in 27/47 (57%) patients and 51/141 (36%) of vessels.

Table 7.1: Demographic details for Chapter 7.

Baseline characteristics			
N		51	
Age (years)		63	(61, 65)
Male/Female		41/10	(80/20%)
Weight (kg)		85.0	(80.0, 90.0)
Body mass index (kg/m^2)		28.6	(27.3, 29.9)
Hypertension		36	(71)
Hypercholesterolemia		48	(94)
Diabetes mellitus		5	(10)
Cerebrovascular disease		4	(8)
Peripheral vascular disease		2	(4)
Current smoker		9	(18)
Ex-smoker (>1 month)		23	(45)
Family history		24	(47)
Previous history of coronary heart disease		23	(45)
Previous acute coronary syndrome		13	(25)
Previous revascularisation		13	(25)
Stent		12	(24)
Coronary artery bypass graft		1	(2)
Chronic beta blocker use		42	(82)
NICE chest pain history	Typical angina	32	(63)
	Atypical angina	10	(20)
	Non-anginal chest pain	7	(14)
	No chest pain	2	(3.9)
Exercise-stress electrocardiogram	Positive	13	(26)
	Equivocal	7	(14)
	Negative	7	(14)
Invasive coronary angiography defined significant coronary artery disease			
One vessel disease		14	(30)
Two vessel disease		8	(17)
Three vessel disease		7	(15)
Total cholesterol (mg/dL)		179	(163, 194)
HDL cholesterol (mg/dL)		46	(38, 49)
Resting systolic blood pressure (mmHg)		136	(129, 144)
Resting diastolic blood pressure (mmHg)		77	(72, 81)
Framingham 10-year cardiovascular risk score			
High		23	(45)
Intermediate		20	(39)
Low		8	(16)

(Mean (95% confidence interval) or number (%))

Radiation exposure

The mean total dose length product (DLP) for the computed tomography protocol was 641.44 (558.50-724.24) mGy.cm (Table 7.2). Using the 0.014 mSv/mGy.cm conversion factor, the dose of rest computed tomography was 2.73 mSv, stress computed tomography was 3.71 mSv and the total computed tomography protocol was 8.98 mSv.

Table 7.2: Radiation dose of comprehensive computed tomography cardiac imaging.

	Dose length product (mGy.cm)	Milisieverts (mSv) (k=0.014)
Coronary artery calcium score	113.63 (104.86, 122.39)	1.59 (1.47, 1.71)
Rest computed tomography	195.14 (147.64, 242.63)	2.73 (2.07, 3.4)
Stress computed tomography	265.30 (225.81, 304.79)	3.71 (3.16, 4.27)
Late enhancement imaging	67.36 (57.84, 76.90)	0.94 (0.81, 1.08)
Total	641.44 (558.5, 724.24)	8.98 (7.82, 10.14)

(Mean (95% confidence interval) or number (%))

Observer variability of computed tomography myocardial perfusion assessment

Intra and inter-observer variabilities for the visual assessment of the presence or absence of computed tomography myocardial perfusion defects on a per-segment basis were good (Kappa value 0.772, P <0.001 and 0.721, P <0.001 respectively).

Diagnostic accuracy of computed tomography myocardial perfusion imaging

When compared to the invasive gold standard of invasive coronary angiography and fractional flow reserve, the diagnostic accuracy for computed tomography coronary angiography and computed tomography myocardial perfusion imaging had sensitivity, specificity, positive predictive and negative predictive values of 96%, 85%, 90% and 94% respectively on a per-patient basis and 88%, 83%, 75% and 93% respectively on a per-vessel basis (Table 7.3). Late enhancement was identified on one computed tomography scan in a patient with a history of a previous myocardial infarction, and this was confirmed on subsequent magnetic resonance imaging.

Table 7.3: Diagnostic accuracy of computed tomography coronary angiography and myocardial perfusion compared to the gold standard of invasive coronary angiography and fractional flow reserve

	N	*TP*	*TN*	*FP*	*FN*	*Sensitivity*	*Specificity*	*PPV*	*NPV*	*Accuracy*
Per-vessel	141	45	75	15	6	88	83	75	93	85
Per-patient	47	26	17	3	1	96	85	90	94	92

(N number, TP true positive, TN true negative, FP false positive, FN false negative, PPV positive predictive value, NPV negative predictive value)

Figure 7.1 shows an example of the comprehensive cardiac computed tomography protocol with corresponding invasive coronary angiography from a 69-year old female patient (BMI 15 kg/m^2, heart rate 45 /min during rest and 67 /min during adenosine stress). The comprehensive cardiac protocol included coronary calcium score (140 mm z-axis, 120 kV, 160 mA), rest CT coronary angiography (120 mm z-

axis, 100 kV, automated tube current selection of 80 mA, 50 mL contrast, half-segment reconstruction, 70-80% acquisition), adenosine stress CTCA (80 mm z-axis to cover only the left ventricle, 100 kV, tube current 110 mA, 50 mL contrast, half-segment reconstruction, images acquired across one cardiac cycle) and delayed enhancement (5 min, 80 mm z-axis, 80 kV, 110 mA). The combined effective radiation dose (k=0.014) for CTCA (0.32 mSv), CT perfusion and function (0.79 mSv), and delayed enhancement (0.08 mSv) was 1.19 mSv compared to the non contrast scan for coronary artery calcium scoring which had a radiation dose of 1.05 mSv. The total protocol dose for this patient was 2.24 mSv.

Figure 7.1: Images from a 69-year old female patient who underwent comprehensive cardiac computed tomography imaging and invasive coronary angiography. Images (A) and (B) show short axis views of the left ventricle during adenosine stress showing hypo-enhancement in the territory of the left anterior descending artery (LAD, yellow arrows) and left circumflex artery (LCX, grey arrows). Stenoses were identified in LAD, first diagonal and LCX arteries and confirmed by invasive coronary angiography (C, D, E). Transmyocardial perfusion ratio during rest (F) and adenosine stress (G) are shown in "bull's-eye plots" with normal areas shown in yellow/orange and abnormal areas are highlighted in purple/blue. The transmyocardial perfusion ratio during adenosine stress is superimposed on short axis views of the left ventricle in image (B). Stress imaging identified reversible defects in LAD and LCX territories (A, B). Functional assessment identified a mild antero-septal wall motion abnormality. Delayed enhancement was not identified on CT or subsequent MRI imaging.

Figure 7.1

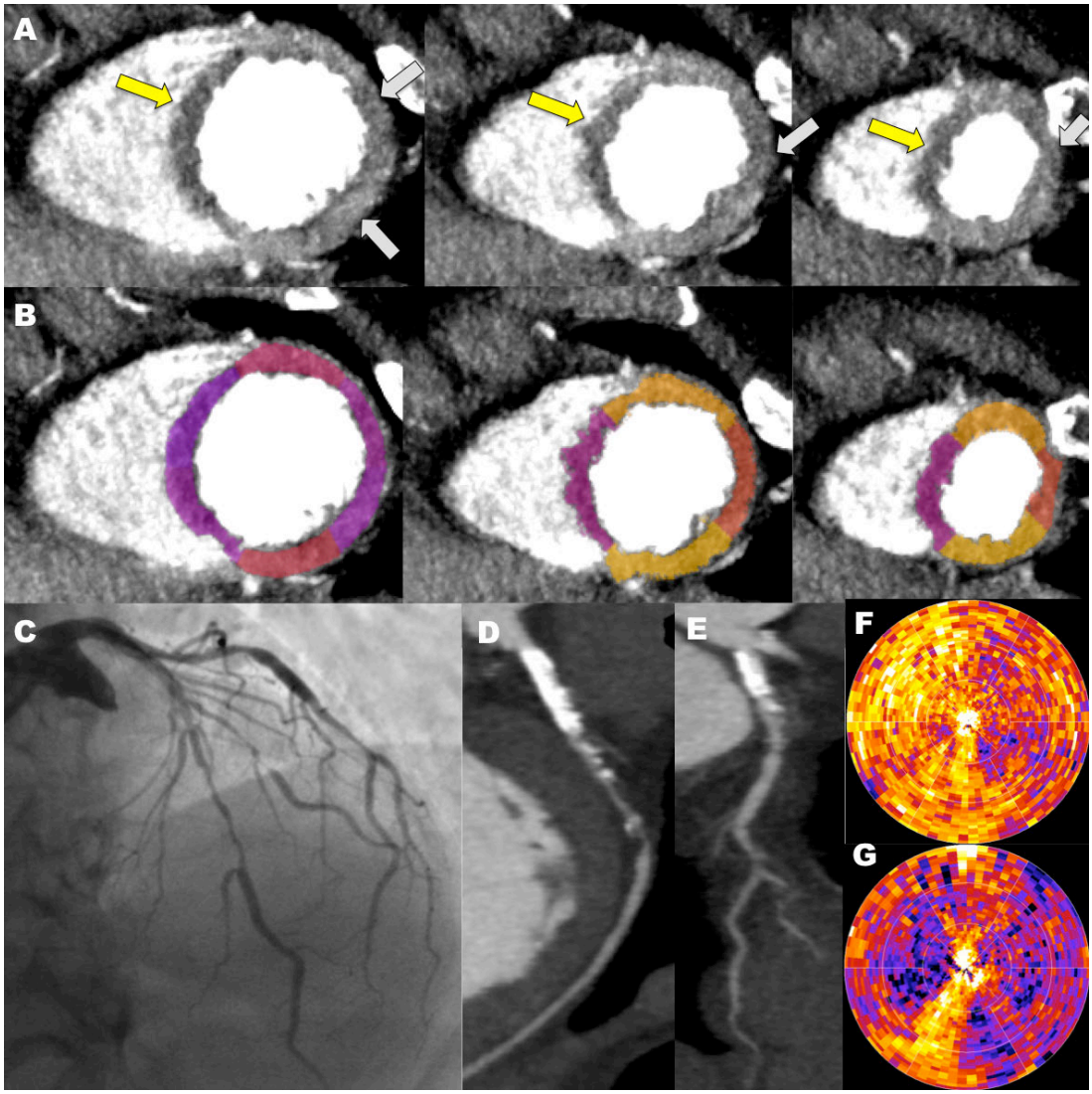

Discussion

This study has confirmed the excellent diagnostic accuracy of computed tomography myocardial perfusion imaging as compared to the clinically used invasive "gold standard" assessment, namely invasive coronary angiography and fractional flow reserve.

Computed tomography coronary angiography is now established as a non-invasive diagnostic technique for the assessment of coronary artery disease. However, computed tomography coronary angiography alone fails to identify a significant proportion of functionally significant lesions as compared to invasive coronary angiography and fractional flow reserve. [185] This is where perfusion imaging has an important discriminatory role and is additive to computed tomography coronary angiography when diagnostic comparisons are made with other techniques. The additional information provided by perfusion imaging has been shown to be additive to computed tomography coronary angiography as compared to quantitative invasive coronary angiography [186,187] invasive coronary angiography and fractional flow reserve [161], SPECT [160] and magnetic resonance imaging [188]. Computed tomography myocardial perfusion has also been shown to improve diagnostic accuracy compared to invasive coronary angiography for patients with coronary stents [184,189] and highly calcified lesions. [186,187]

The CORE320 multicentre study of computed tomography myocardial perfusion imaging showed a sensitivity, specificity, positive predictive value and negative

predictive value for detecting a >50% invasive coronary angiography stenosis associated with a perfusion defect on SPECT of 80%, 74%, 65% and 86% respectively on a per-patient basis. [70] However, although SPECT is widely used as the first line myocardial perfusion imaging technique by many clinicians, it has limitations. [186,187] Comparisons with SPECT may underrepresent the true value of computed tomography myocardial perfusion imaging. We therefore used ICA and FFR as the gold standard clinical reference comparator in this study, and have confirmed the diagnostic accuracy of CTCA/CTP.

The average radiation dose of rest and stress computed tomography imaging in the CORE320 study was 9.32 mSv. [70] Our study used the radiation dose reduction techniques described in Chapter 6, which were not applied in the CORE320 study. This included single rather than multi segment reconstruction, iterative reconstruction and patient tailored imaging. The average radiation dose for rest and stress computed tomography imaging in our study was 6.44 mSv. The total radiation dose for comprehensive imaging including calcium score, rest and stress computed tomography and late enhancement imaging using this protocol was 8.98 mSv. This is comparable to the radiation dose of low-dose nuclear medicine studies, but can provide additional information regarding anatomy, function, perfusion and viability.

Our study supports the clinical use of computed tomography myocardial perfusion imaging in the investigation of patients with suspected coronary artery disease. Computed tomography myocardial perfusion imaging can be used as an optional "add-on" investigation immediately after computed tomography coronary

angiography when heavily calcified vessels are identified or functional severity of a stenosis is uncertain. Alternatively, it can be prospectively planned for patients with known coronary artery disease who are being considered for coronary revascularisation. It can provide additional perfusion information on a per-segment basis to improve the diagnostic accuracy of computed tomography imaging. In addition to identifying major epicardial coronary artery disease, it can also identify microvascular dysfunction. In our study, some of the false positives for the identification of epicardial vessel stenosis by CTCA/CTP as compared to ICA/FFR were due to the presence of microvascular dysfunction, highlighted as "slow flow" during invasive coronary angiography with a normal FFR. FFR is primarily focused on identifying a pressure gradient across a functional stenosis but cannot assess microvascular resistance or flow directly. [190] Thus computed tomography myocardial perfusion imaging, with its excellent spatial resolution has the potential to identify small perfusion defects and microvascular dysfunction that ICA/FFR cannot identify.

This study recruited only patients referred for invasive coronary angiography leading to the potential for verification bias. The use of fractional flow reserve as a "gold standard" is limited by its invasive nature, technical problems with complicated lesions, the catheter itself causing a gradient increase in lesions with small luminal area and the fact that fractional flow reserve was validated against SPECT. [104] In addition invasive coronary angiography with fractional flow reserve assessment may underestimate the presence of microvascular disease. [16] The use of medications such as GTN or beta-blockers prior to perfusion imaging has the potential to alter the

presence or severity of perfusion imaging. [191] However, the diagnostic accuracy of computed tomography coronary angiography and computed tomography myocardial perfusion imaging identified in this study was similar to previous studies where medications such as beta-blockers and nitrates were withheld. Beam hardening artefacts are an important limitation of computed tomography coronary angiography imaging and in computed tomography myocardial perfusion imaging beam hardening can particularly affect the basal infero-lateral wall leading to potential false positive results. [68]

This study has confirmed the favourable diagnostic accuracy of computed tomography coronary angiography and computed tomography myocardial perfusion imaging as compared to invasive coronary angiography and fractional flow reserve.

Chapter Eight: Quantification of computed tomography myocardial perfusion imaging

Abstract

Introduction

Oxygen-15 water positron emission tomography (PET) is the physiological "gold standard" for the assessment of myocardial blood flow. This chapter assess oxygen-15 water positron emission tomography derived myocardial blood flow in 22 of the patients described in Chapter 7. These patients had previously undergone computed tomography (CT) coronary angiography (CTCA), computed tomography myocardial perfusion imaging (CTP), invasive coronary angiography (ICA) and measurement of fractional flow reserve (FFR).

Methods

Rest/stress oxygen-15 water PET was performed in 22 patients. Myocardial blood flow assessed by oxygen-15 water PET was compared to CTCA/CTP and to ICA/FFR. Obstructive coronary artery disease on CT was defined as a stenosis >50% with corresponding CT myocardial hypoperfusion. Obstructive coronary artery disease on ICA was defined as a stenosis >70% or fractional flow reserve <0.80.

Results

Hyperaemic myocardial blood flow measured by oxygen-15 water PET was lower in obstructive than non-obstructive territories as defined by ICA/FFR (1.76 (1.32, 2.20) versus 3.11 (2.44, 3.79) mL/g/min, P <0.001) and CTCA/CTP (1.78 (1.51, 2.05) versus 3.04 (2.70, 3.39) mL/g/min, P <0.001). Baseline and hyperaemic CT myocardial enhancement was lower in obstructive than non-obstructive vessel

territories (73 (71, 76) versus 86 (84, 88) HU, P <0.001 and (101 (96, 106) versus 111 (107, 114) HU, P <0.001 respectively). When corrected for rate pressure product, myocardial blood flow correlated with CT myocardial enhancement during hyperaemia (r=0.579, P <0.001).

Conclusion

Quantitative assessment of myocardial blood flow by oxygen-15 positron emission tomography correlates well with computed tomography myocardial perfusion imaging.

Introduction

Positron emission tomography (PET) imaging using oxygen-15 labelled water is the "gold-standard" for the assessment of myocardial blood flow as it is a freely diffusible, metabolically inert tracer with a high extraction fraction that is independent of flow rate. [90-92] This tracer enables the quantitative assessment of absolute, rather than relative, myocardial blood flow at rest and during adenosine stress.

Oxygen-15 water positron emission tomography myocardial blood flow measurements have been validated with radio-labelled microspheres in animal models [93-99] and in humans it has been compared to invasive coronary angiography, fractional flow reserve, SPECT, magnetic resonance imaging and computed tomography coronary angiography. [100-107] In addition, the assessment of absolute myocardial blood flow by oxygen-15 water positron emission tomography has good intra observer and inter observer variability as well as a low inter-scan variability. [108,109,192] Thus this is an excellent physiological "gold-standard" for the assessment of computed tomography myocardial perfusion imaging.

In Chapter 7, computed tomography coronary angiography (CTCA) and computed tomography myocardial perfusion imaging (CTP) was compared to the current clinical "gold standard" assessment of stenosis severity, namely invasive coronary angiography (ICA) and fractional flow reserve (FFR). In this chapter, CTCA/CTP

and ICA/FFR are compared to the physiological "gold standard" of absolute myocardial blood flow measured by oxygen-15 labelled water positron emission tomography. Computed tomography myocardial perfusion imaging in this study was again performed using the “snap shot” technique, which obtains a small number of images at maximal contrast enhancement.

Methods

Study design

This was a single centre prospective pilot study of oxygen-15 labelled PET imaging as compared to CTCA/CTP and ICA/FFR. No power calculation was performed.

Study Population

The study population consisted of a sub-group of 22 of the participants described in Chapter 7.

Oxygen-15 labelled water positron emission tomography

Rest and stress oxygen-15 labelled water imaging was preformed using a hybrid scanner (128-multidetector Biograph mCT, Siemens Medical Systems, Germany) as described in Chapter 2. Rest imaging was performed using a target of 500 MBq oxygen-15 labelled water (bolus over 15 s, followed by 2 min saline flush). Dynamic acquisition was performed over 5 min. After suitable decay (approximately 10 min), stress imaging was performed, 2 min after commencing adenosine, with a further 500 MBq oxygen-15 labelled water. Dynamic acquisition was performed, as for rest

imaging, during adenosine infusion. Dynamic emission images were reconstructed using the UltraHD (Siemens Medical Systems, Germany) algorithm (zoom 2, matrix 128x128, voxel size 3.18x3.18x3 mm).

Image analysis

Positron emission tomography imaging was analysed using dedicated software (Carimas 2.4, Finland) using a single tissue compartment model with correction for perfusable tissue fraction and spillover. [192] Images were reoriented into the short-axis and myocardial contours were defined on digital subtraction images automatically, with manual adjustment. Myocardial blood flow was analysed for the entire left ventricle. Segmental data was consolidated into 3 territories for per-vessel analysis. [115] Coronary vasodilator reserve was defined as the ratio of peak hyperaemic to resting myocardial blood flow. [119] Total coronary resistance was calculated as mean arterial pressure divided by myocardial blood flow at baseline and hyperaemia. [119] Myocardial blood flow and computed tomography attenuation density were corrected for rate pressure product, calculated from heart rate and blood pressure during imaging.

Quantitative assessment of CTP images was performed by assessing CT myocardial attenuation density at rest and during maximal hyperaemia. CT images were assessed in the short-axis orientation of the left ventricle and the apex was excluded because accurate contour definition is difficult on this thin region of myocardium. Automatically applied myocardial contours were edited manually as required. Attenuation density was measured in each myocardial segment for the endocardium,

mid-wall, epicardium and full thickness. The transmyocardial perfusion ratio was calculated as the ratio of segmental subendocardial attenuation divided by mean subepicardial attenuation of the short-axis slice. [66]

Statistical analysis

Statistical analysis was performed using SPSS (Version 18 for Mac, IBM). Normally distributed quantitative variables are presented with mean and 95% confidence interval. Non-normally distributed data are presented with median and interquartile range. Statistical significance was assessed using analysis of variance, Student t, or Mann-Whitney U tests as appropriate. Correlations were assessed using Pearson's correlations. Inter- and intra-observer variability was assessed using Kappa statistics and Bland-Altman plots. A statistically significant difference was defined as a two-sided P value <0.05.

Results

Demographic details

Study participants consisted of 22 of the patients imaged in Chapter 7. Demographic details are presented in Table 8.1. One third of the patients had significant coronary artery disease as defined by invasive coronary angiography. There were no other significant differences compared to the whole population studied in Chapter 7.

Table 8.1: Baseline characteristics for Chapter 8.

Baseline characteristics				***P ****
N		22		
Age (years)		62	(58, 65)	0.121
Male/Female		41/10	(80/20%)	
Weight (kg)		82	(76, 88)	0.216
Body mass index (kg/m^2)		29.4	(27.3, 31.6)	0.291
Hypertension		19	(86)	0.061
Hypercholesterolemia		20	(91)	0.571
Diabetes mellitus		3	(14)	0.641
Cerebrovascular disease		2	(9)	0.486
Peripheral vascular disease		0	(0)	0.5
Current smoker		2	(11)	0.394
Ex-smoker (>1 month)		9	(47)	0.394
Family history		10	(53)	0.5
Previous history of coronary heart disease		13	(59)	0.071
Previous acute coronary syndrome		5	(23)	0.755
Previous revascularisation		6	(27)	1.0
Stent		6	(27)	0.741
Coronary artery bypass graft		0	(0)	1.0
Chronic beta blocker use		17	(77)	0.728
NICE chest pain history	Typical angina	13	(59)	0.066
	Atypical angina	2	(9.1)	
	Non-anginal chest pain	5	(23)	
	No chest pain	2	(9.1)	
Exercise-stress electrocardiogram	Positive	4	(20)	0.19
	Equivocal	4	(20)	
	Negative	5	(25)	
Invasive coronary angiography defined significant coronary artery disease				
One vessel disease		2	(9)	0.005
Two vessel disease		4	(18)	
Three vessel disease		1	(5)	
Total cholesterol (mg/dL)		171	(151, 192)	0.099
HDL cholesterol (mg/dL)		45	(33, 58)	0.940
Resting systolic blood pressure (mmHg)		131	(120, 143)	0.086
Resting diastolic blood pressure (mmHg)		72	(64, 80)	0.027
Framingham 10-year cardiovascular risk score				
High		9	(41)	0.135
Intermediate		7	(32)	
Low		6	(27)	

*(Mean (95% confidence interval) or number (%), * compared to the whole population studied in Chapter 7)*

Radiation exposure

The mean administered activity of oxygen-15 labelled water was 474 MBq (461, 488) for rest and 465 MBq (448, 482) for stress imaging. The mean dose length product of attenuation correction competed tomography was 73 mGy.cm. Using the conversion factors of 0.014 mSv/mGy.cm and 1.1 for μSv/MBq, [193] this equates to an effective dose of 2.05 mSv for positron emission tomography.

Observer variability in the measurement of absolute myocardial blood flow

Observer agreement for the assessment of myocardial blood flow by oxygen-15 labelled water positron emission tomography was excellent (Figure 8.1), with Kappa values of 0.817 for inter-observer variability and 0.942 for intra-observer variability.

Figure 8.1: Bland-Altman plots of intra- and inter-observer variability in the assessment of global myocardial blood flow by oxygen-15 water positron emission tomography at baseline and during hyperaemia. (Dotted lines show limits of agreement)

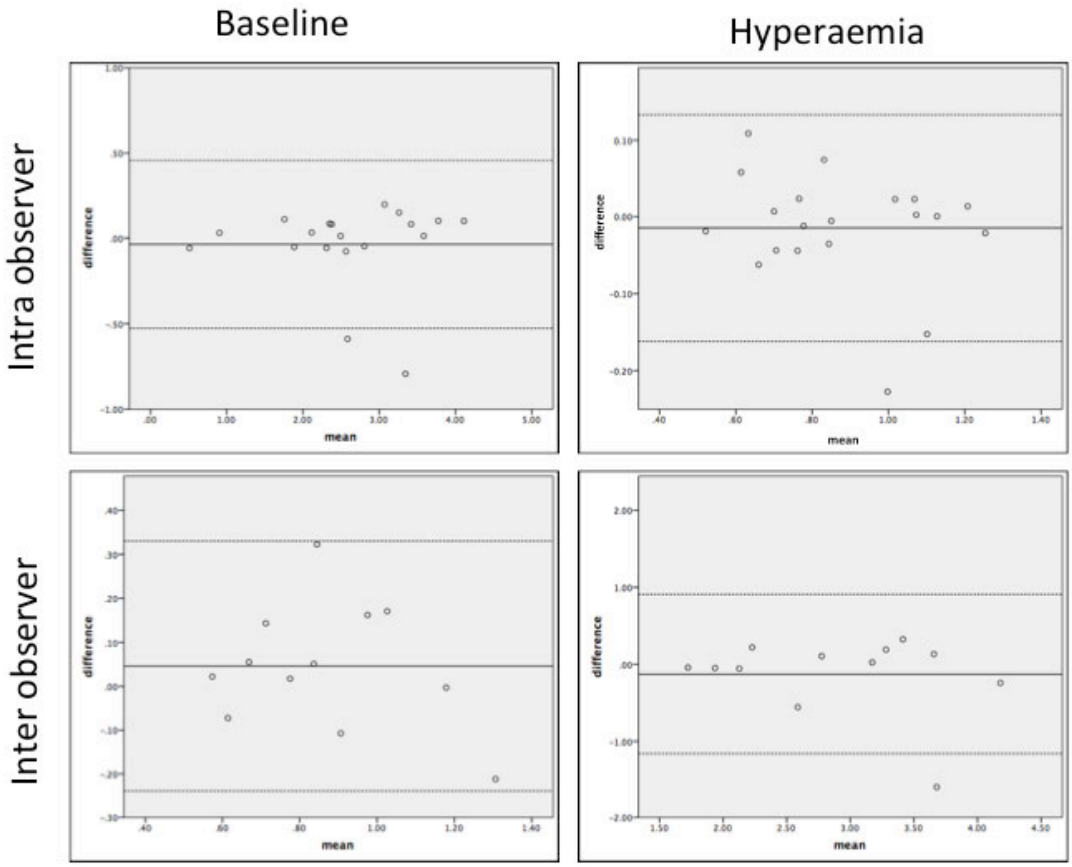

Assessment of myocardial perfusion imaging

Oxygen-15 labelled water positron emission tomography demonstrated that the mean myocardial blood flow and myocardial blood flow corrected for rate pressure product for all segments was higher during hyperemia (2.52 (2.40, 2.64) and 2.65 (2.53, 2.77) mL/g/min respectively) than rest (0.80 (0.76, 0.81) and 0.82 (0.79, 0.85) mL/g/min respectively; P <0.001 for both). (Figure 8.2)

Figure 8.2: Myocardial blood flow in all segments at rest and during adenosine stress.

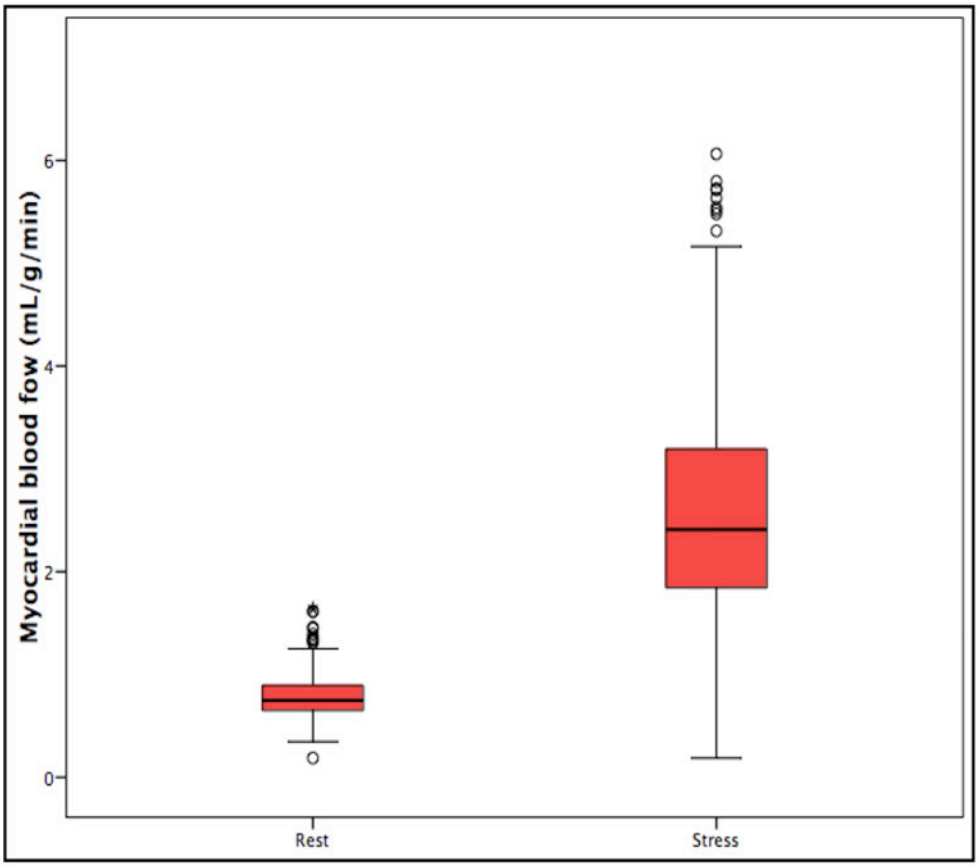

There were no differences in baseline ^{15}O-Water PET myocardial blood flow between obstructive and non-obstructive lesions as determined using ICA/FFR. However, during hyperemia, ^{15}O-Water PET myocardial blood flow was lower for obstructive lesions defined by ICA/FFR on both per-patient and per-vessel assessment. (Table 8.2, Figure 8.3)

There was also no difference in baseline ^{15}O-Water PET myocardial blood flow in territories supplied by coronary arteries with obstructive or non-obstructive lesions as

defined by CTCA/CTP on per-patient or per-vessel analysis (Table 8.2, Figure 8.3). However, on per-segment analysis, baseline ^{15}O-Water PET myocardial blood flow was lower in territories supplied by coronary arteries with obstructive lesions (0.65 versus 0.79 mL/g/min, P <0.001). Hyperaemic ^{15}O-Water PET myocardial blood flow was lower in territories supplied by coronary arteries with obstructive lesions defined by CTCA/CTP on per-patient, per-vessel and per-segment analysis (Table 8.2, Figure 8.3).

Figure 8.3: The quantitative assessment of myocardial blood flow (MBF) by oxygen-15 labelled water positron emission tomography as compared to computed tomography coronary angiography (CTCA) and myocardial perfusion (CTP) and invasive coronary angiography (ICA) with fractional flow reserve (FFR). (A) and (B) show baseline and hyperaemic myocardial blood flow in obstructive and non-obstructive vessels as defined by ICA/FFR. (C) and (D) show baseline and hyperaemic myocardial blood flow in obstructive and non-obstructive vessels as defined by CTCA/CTP. (E) and (F) show the correlation between myocardial blood flow corrected for rate pressure product and CT contrast enhancement at rest and during hyperaemia respectively.

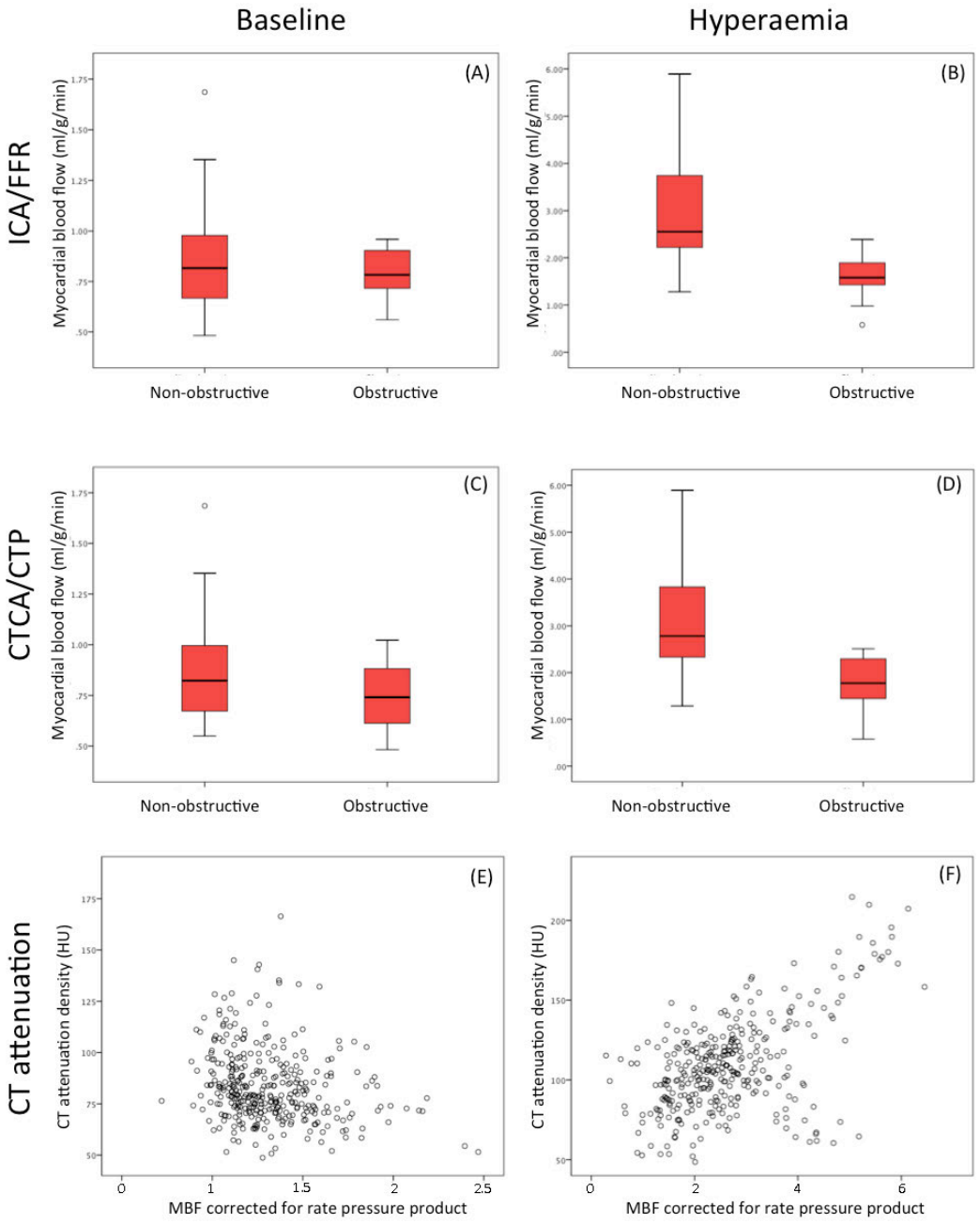
Baseline
Hyperaemia
ICA/FFR
CTCA/CTP
CT attenuation
(A)
(B)
(C)
(D)
(E)
(F)
Myocardial blood flow (ml/g/min)
CT attenuation density (HU)
Non-obstructive
Obstructive
MBF corrected for rate pressure product

Table 8.2: ^{15}O-Water PET myocardial blood flow for obstructive and non-obstructive regions as defined by (a) invasive coronary angiography with fractional flow reserve, and (b) computed tomography coronary angiography and myocardial perfusion.

(a)

		ICA / FFR				
		Non-obstructive		Obstructive		P
Per-patient	Rest Flow (mL/g/mL)	0.88	(0.74, 1.03)	0.63	(0.35, 0.89)	0.074
	Stress Flow (mL/g/min)	3.11	(2.44, 3.79)	1.76	(1.32, 2.20)	0.001
Per-vessel	Rest Flow (mL/g/mL)	0.84	(0.77, 0.91)	0.78	(0.69, 0.88)	0.3
	Stress Flow (mL/g/min)	2.92	(2.61, 3.23)	1.60	(1.28, 1.91)	<0.001

(b)

		CTCA / CTP				
		Non-obstructive		Obstructive		P
Per-patient	Rest Flow (mL/g/mL)	0.88	(0.74, 1.03)	0.63	(0.35, 0.90)	0.74
	Stress Flow (mL/g/min)	3.12	(2.44, 3.79)	1.76	(1.32, 2.20)	0.001
Per-vessel	Rest Flow (mL/g/mL)	0.86	(0.79, 0.94)	0.75	(0.67, 0.84)	0.45
	Stress Flow (mL/g/min)	3.04	(2.70, 3.39)	1.78	(1.51, 2.05)	<0.001
Per-segment	Rest Flow (mL/g/mL)	0.79	(0.76, 0.82)	0.65	(0.61, 0.70)	<0.001
	Stress Flow (mL/g/min)	2.77	(2.63, 2.91)	2.09	(1.93, 2.24)	<0.001

(Mean (95% confidence interval))

CTCA/CTP was also used to identify normal vessels as compared to vessels containing non-obstructive and obstructive lesions (Figure 8.4). Vessel territories defined as normal by CTCA/CTP had a higher baseline and hyperaemic ^{15}O-Water PET myocardial blood flow than those with non-obstructive or obstructive coronary artery lesions, but this difference was not statistically significant.

Figure 8.4: Baseline (A) and hyperaemic (B) myocardial blood flow assessed by oxygen-15 labelled water positron emission tomography in normal, non-obstructive and obstructive vessels as defined by computed tomography coronary angiography and myocardial perfusion.

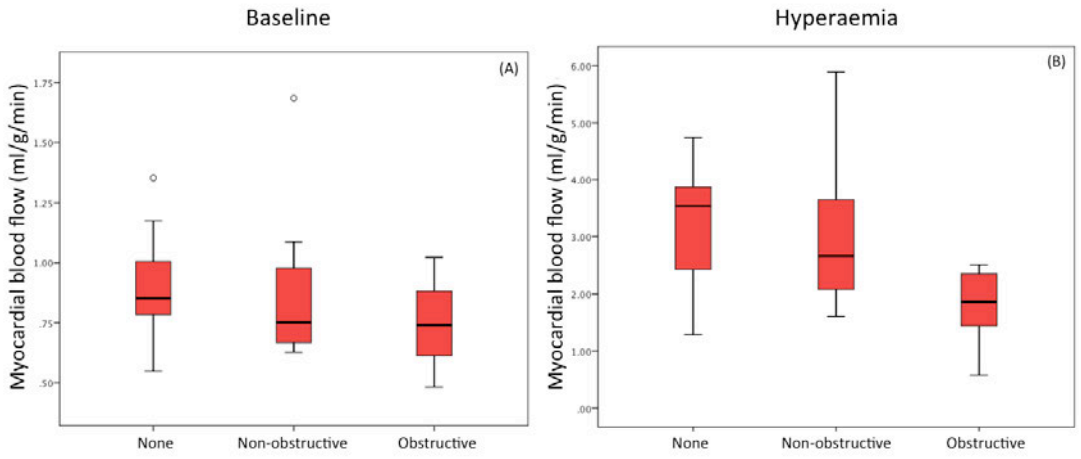

On a per-vessel basis, the optimal cut-off for ^{15}O-Water PET myocardial blood flow for assessing the presence of obstructive stenosis as defined by both ICA/FFR and CTCA/CTP imaging was 0.52 mL/g/min at baseline and 0.78 mL/g/min during hyperemia. The area under the curve was higher for hyperaemic than baseline myocardial blood flow for both ICA/FFR and CTCA/CTP comparisons (Table 8.3).

Table 8.3: Optimal cut-off value for baseline or hyperaemic myocardial blood flow (MBF) on per-vessel assessment to identify obstructive stenosis as defined by ICA/FFR or CTCA/CTP.

		Cut-off value (mL/min/g)	Area under the curve		Sensitivity (%)	Specificity (%)
			(95% CI)	*P*		
ICA/FFR	Baseline MBF	0.52	0.545 (0.368, 0.723)	0.656	98	100
	Hyperaemic MBF	0.78	0.897 (0.815, 0.979)	<0.001	100	92
	CFR	1.02	0.880 (0.773, 0.986)	<0.001	100	100
CTCA/CTP	Baseline MBF	0.52	0.637 (0.476, 0.797)	0.116	100	94
	Hyperaemic MBF	0.78	0.856 (0.761, 0.951)	<0.001	100	95
	CFR	1.02	0.880 (0.773, 0.986)	0.02	100	94

The mean CT myocardial attenuation density for all segments on CTP was 85 (83, 87) HU at baseline and 111 (107, 114) HU during hyperaemia (P <0.01). The CT transmyocardial perfusion ratio (TPR) was higher at baseline than during hyperaemia (1.68 (1.61, 1.76) versus 1.17 (1.13, 1.21), P <0.001). CT attenuation density in the endocardium was higher than the epicardium at baseline (94 (92, 96) versus 81 (78, 83), P <0.001) and during hyperaemia (114 (111, 117) versus 109 (106, 112), P <0.001). (Figure 8.5)

Figure 8.5: Computed tomography myocardial contrast enhancement at rest and during adenosine stress computed tomography imaging.

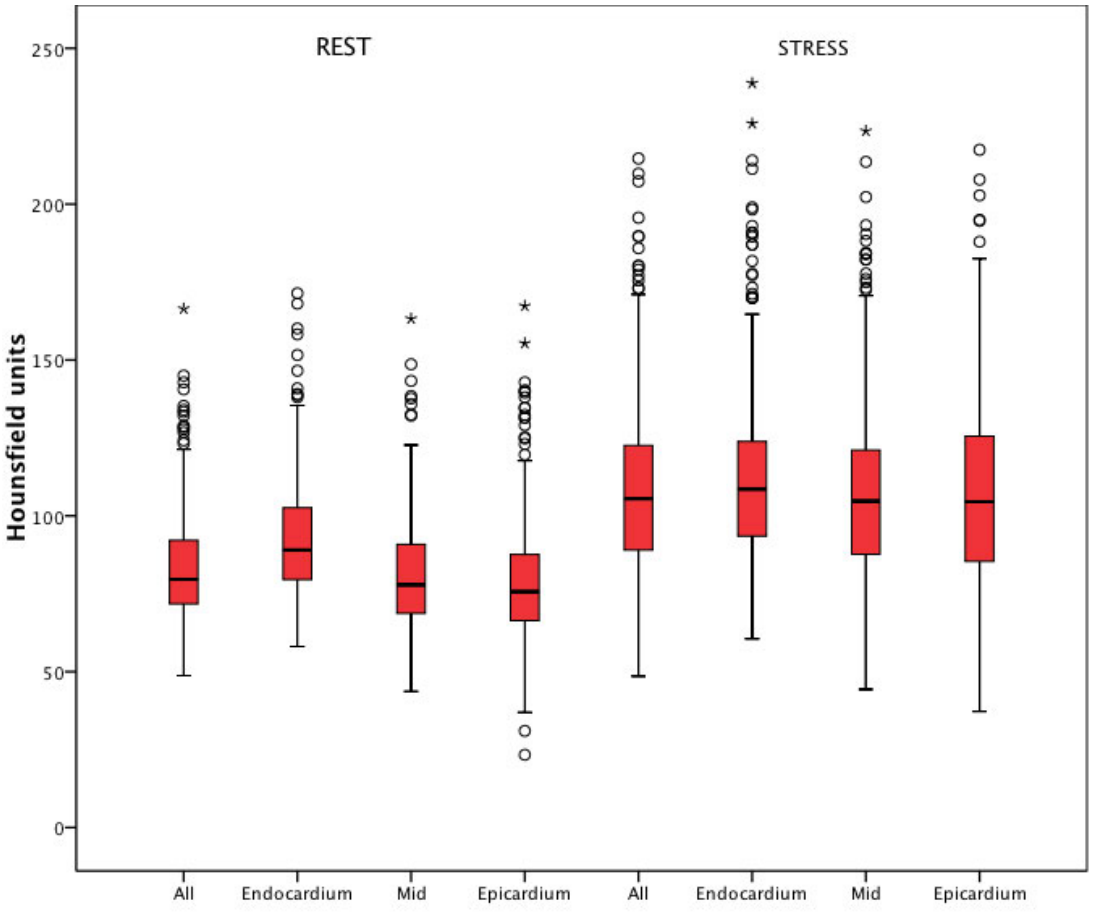

Computed tomography myocardial attenuation density was lower in territories supplied by coronary arteries with obstructive as compared to non-obstructive lesions as defined by ICA/FFR (Table 8.4). Oxygen-15 labelled water positron emission tomography measurements of myocardial blood flow correlated with CT attenuation density (Table 8.5). The correlation was greater for the endocardium and when myocardial blood flow and CT myocardial contrast enhancement were corrected for rate-pressure product or left ventricular enhancement. ^{15}O-Water PET myocardial

blood flow corrected for rate-pressure product correlated weakly with CT myocardial attenuation density at rest (r=0.19, P<0.001) but correlated well during hyperemia (r=0.579, P<0.001, Figure 8.3). CT transmyocardial perfusion ratio correlated only weakly with ^{15}O-Water PET myocardial blood flow. However, ^{15}O-Water PET defined coronary vasodilator reserve and total coronary resistance correlated more strongly with CT attenuation density. Figure 8.6 shows an example of a patient who underwent computed tomography, positron emission tomography and invasive coronary angiography.

Figure 8.6: This 74-year old non-smoker with hypertension, hypercholesterolemia and atypical chest pain underwent multimodality assessment of his cardiac anatomy and physiology. (A) shows short axis basal, mid and apical images of the left ventricle at rest and during hyperaemia along with three dimensional representations of the transmyocardial perfusion ratio and coronary anatomy. Hypoattenutation is seen in right coronary artery (RCA) and left anterior descending (LAD) artery during hyperaemia. There is also mild hypoattenuation in the RCA territory on rest imaging. (B) shows the corresponding oxygen-15 labelled water PET images which identified the same perfusion abnormalities in terms of the absolute myocardial blood flow (mL/g/min). (C) shows the corresponding images from ICA which identified an occluded LAD and severe stenosis of the RCA with FFR <0.80.

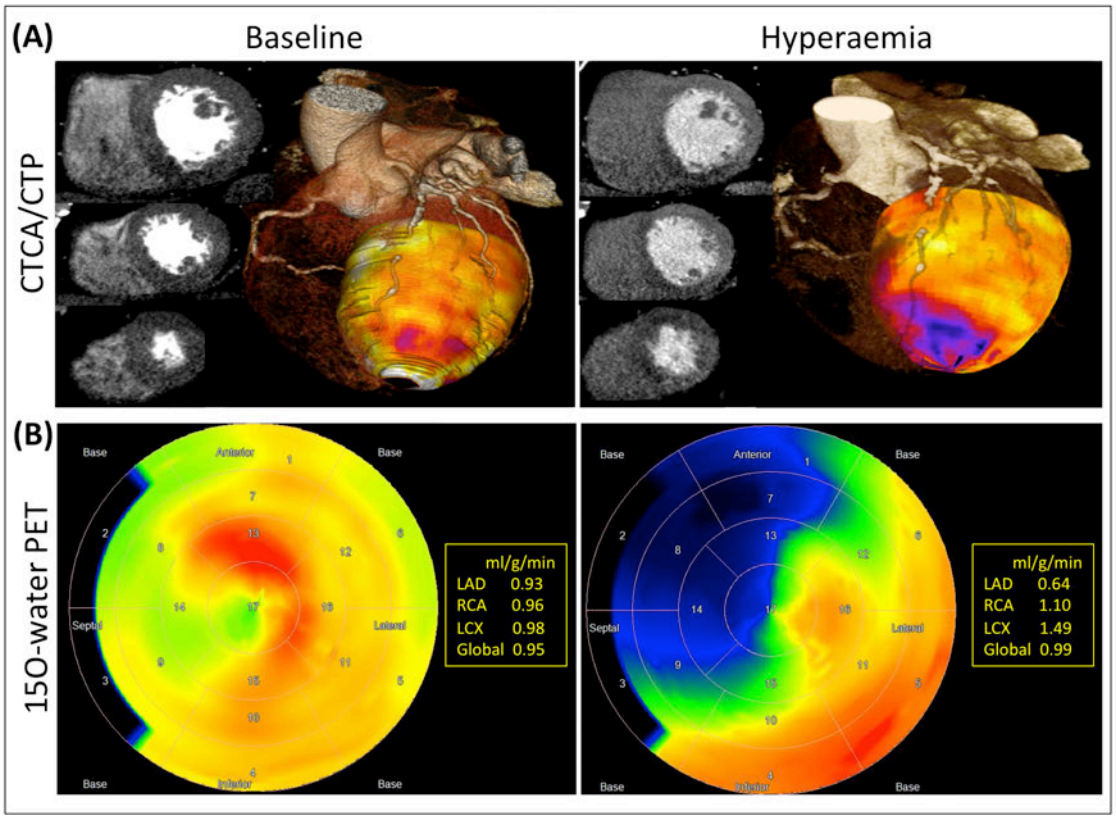
(A)
Baseline
Hyperaemia
CTCA/CTP
(B)
15O-water PET
Base
Anterior
Septal
Lateral
Inferior
ml/g/min
LAD 0.93
RCA 0.96
LCX 0.98
Global 0.95
ml/g/min
LAD 0.64
RCA 1.10
LCX 1.49
Global 0.99

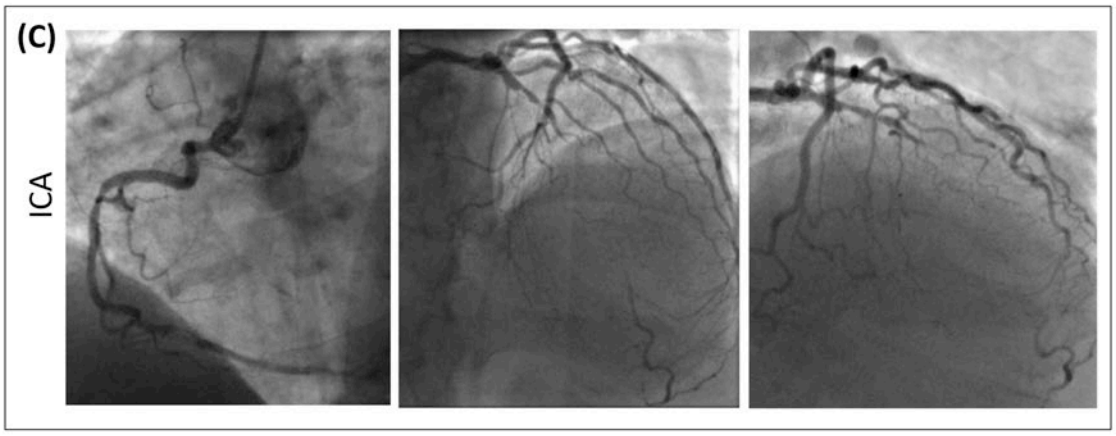
(C)
ICA

Table 8.4: Myocardial contrast enhancement for obstructive and non-obstructive segments as defined by invasive coronary angiography and fractional flow reserve.

		Non-obstructive		Obstructive		*P*
CT myocardial contrast enhancement (HU)	Rest	86	(84, 88)	73	(71, 76)	<0.001
	Stress	111	(107, 114)	101	(96, 106)	0.001
Endocardium contrast enhancement (HU)	Rest	95	(93, 97)	84	(80, 87)	<0.001
	Stress	115	(111, 118)	102	(98, 107)	<0.001
CT contrast corrected for left ventricular enhancement (HU)	Rest	0.178	(0.17, 0.18)	0.15	(0.14, 0.16)	<0.001
	Stress	0.37	(0.36, 0.39)	0.30	(0.28, 0.32)	<0.001
CT myocardial contrast enhancement corrected for rate pressure product (HU)	Rest	90	(86, 93)	81	(76, 86)	0.004
	Stress	124	(114, 134)	118	(108, 127)	0.330
TPR	Rest	1.62	(1.54, 1..71)	1.91	(1.69, 2.13)	<0.001
	Stress	1.23	(1.19, 1.28)	0.98	(0.93, 1.04)	<0.001

(*Mean (95% confidence interval))*

Table 8.5: Correlation between quantitative assessments of myocardial blood flow by oxygen-15 labelled water positron emission tomography and computed tomography myocardial perfusion imaging at rest and during adenosine stress: (a) for PET parameters as compared to CT myocardial contrast enhancement; and (b) for CT parameters as compared to PET derived myocardial blood flow corrected for rate pressure product.

(a).

PET parameter	Baseline	Hyperaemia
Myocardial blood flow	-0.227, <0.001	0.230, <0.001
Total coronary resistance	0.278, <0.001	0.274, <0.001
Change in myocardial blood flow	0.307, <0.001	0.278, <0.001
Coronary vasodilator reserve	0.411, <0.001	0.460, <0.001
Myocardial blood flow corrected for rate pressure product	-0.235, <0.001	0.553, <0.001

(b)

CT parameter	Baseline	Hyperaemia
CT contrast enhancement	-0.235, <0.001	0.553, <0.001
Endocardium CT contrast enhancement	0.328, <0.001	0.601, <0.001
CT contrast enhancement corrected for left ventricular enhancement	-0.136, 0.01	0.269, <0.001
CT contrast enhancement corrected for rate pressure product	0.19, <0.001	0.579, <0.001
Transmyocardial perfusion ratio	0.172, 0.0002	0.214, <0.001

(r value, P value)

Discussion

This chapter assessed combined computed tomography coronary angiography and “snap shot” computed tomography myocardial perfusion imaging as compared to the "gold standard" measure of absolute myocardial blood flow, namely oxygen-15 labelled water positron emission tomography. We have demonstrated that CT attenuation density correlates with ^{15}O-Water PET defined myocardial blood flow. Thus we provide physiological evidence to support the use of myocardial perfusion imaging by computed tomography.

We have shown that computed tomography estimates of myocardial perfusion correspond well with absolute myocardial blood flow obtained by oxygen-15 labelled water positron emission tomography. Moreover, the good correlation with myocardial attenuation density suggests that computed tomography myocardial perfusion is indicative of, and proportionate to, absolute rather than relative myocardial perfusion. This suggests that computed tomography myocardial perfusion assessment will be less susceptible to false-negatives due to balanced ischaemia in multi-vessel disease, and should perform well across a broad range of patients. In addition, our findings have internal validity. Consistent with previous studies [104,105,107], we have demonstrated that fractional flow reserve corresponds with absolute myocardial blood flow assessed by oxygen-15 labelled water positron emission tomography: reinforcing the validity of fractional flow reserve as a robust clinical tool to assess the hemodynamic severity of coronary stenoses.

Impaired hyperaemic myocardial blood flow has been identified using positron emission tomography in patients with coronary artery disease identified by invasive coronary angiography, fractional flow reserve, SPECT, magnetic resonance imaging and computed tomography coronary angiography. [100-107] Uren *et al* showed that hyperaemic myocardial blood flow was associated with the degree of invasive coronary angiography stenosis. [100] Impaired hyperaemic myocardial blood flow has also been identified in patients with risk factors for coronary artery disease including smoking, hypercholesterolaemia, hypertension, diabetes, age, male gender, obesity and increased intima-media thickness. [109,194-199] However, there is also significant heterogenicity in resting myocardial blood flow between individuals [100,109,110] and a genetic contribution to this has been identified in twin studies. [200]

In our study, the optimal cut-off value to identify a hemodynamically significant stenosis was 0.78 mL/g/min. Previous studies have reported the optimal cut-off values between 1.86 and 2.5 mL/g/min. [104,105,110,201,202] Nesterov *et al* showed that a cut off of 2.0 mL/g/min indicated an invasive coronary artery stenosis of 50% or greater with a diagnostic accuracy of 90% [192] and Kajander *et al* showed that this cut off and a 98% accuracy for the identification of significant stenoses as defined by ICA/FFR. [104] However, unlike these previous studies, we did not include healthy volunteers and had instead a high proportion of patients with coronary artery disease and microvascular disease. Myocardial blood flow is also known to be lower in normal vessels remote from a vessel with an obstructive

stenosis. [119] Together, these factors help explain the lower resting myocardial blood flow thresholds that we have identified. However, in keeping with the study by Kajander *et al* practically all regions with myocardial blood flow <2.0 mL/g/min identified in our study were in territories supplied by major epicardial or branch vessels with obstructive stenoses. [104]

The use of medications such as glyceryl trinitrate or beta-blockers prior to perfusion imaging has the potential to alter the presence or severity of perfusion defects on imaging. [191] However, previous studies have shown no difference in hyperaemic myocardial blood flow measured with 13N-ammonia in patients taking beta-blockers. [203] In addition the diagnostic accuracy of CTCA/CTP identified in our study was similar to previous studies where medications such as beta-blockers and nitrates were withheld. In addition, there is also significant heterogeneity in resting myocardial blood flow between individuals. [100,109,110].

Previous studies of computed tomography myocardial perfusion have suggested that the analysis of rest images alone is sufficient to identify obstructive coronary artery disease. [204] However, our data would not support this approach as the correlation between computed tomography attenuation and myocardial blood flow was much lower at baseline than during hyperaemia. In addition, rest imaging alone is not sufficient to discriminate between ischaemia and infarction.

Finally, as previously described [105], we found that hyperaemic myocardial blood flow was the best discriminator of significant coronary artery disease, rather than

derived ratios such as coronary flow reserve. This potentially simplifies the assessment of computed tomography myocardial perfusion assessment. However, the use of ratios, such as the transmyocardial perfusion ratio, may be useful in patients with small perfusion defects or microvascular disease which could be otherwise easily overlooked.

In addition to the limitations discussed in Chapter 7, this study included only a small number of patients (n = 22) due to the technical complexity of oxygen-15 labelled water positron emission tomography. Although oxygen-15 labelled water positron emission tomography is the "gold standard" for the assessment of absolute myocardial blood flow it is unlikely that this will be used outside of centres with a large research set up. Oxygen-15 is a cyclotron-derived radiotracer with a short half-life and thus this requires the presence of an on site cyclotron. Other radiotracers such as 13N-ammonia and rubidium-82 with longer half-lives can be used for positron emission tomography myocardial perfusion imaging, but their lower extraction factions reduce the diagnostic accuracy. Newer radio-tracers with high extraction fractions such as F18 labelled flupiridaz [205] hold promise for the wider utility of positron emission tomography myocardial perfusion imaging. However, at present computed tomography imaging, which is less technically complex and does not require an on site cyclotron, is an attractive alternative for assessing myocardial perfusion imaging. Motion and misregistration artefacts have been shown to be a problem for other myocardial perfusion tracers in positron emission tomography imaging. [206] However, this may be less of an issue for oxygen-15 labelled water

positron emission tomography because the method used to calculate myocardial blood flow does not rely on accumulation rate. [108,207]

In conclusion, this study assessed computed tomography myocardial perfusion imaging in comparison to absolute myocardial blood flow measurement by oxygen-15 labelled water positron emission tomography. We have shown that CTCA/CTP provides a robust physiological and clinical assessment of patients with suspected coronary artery disease with excellent correlation with absolute myocardial blood flow.

Chapter Nine: Conclusion

Extracts of this chapter are published in:

Williams MC, Newby DE. Computed tomography myocardial perfusion, a step towards quantification. Heart, 2012; 98:521-2.

Summary

Computed tomography is now an established diagnostic technique for the assessment of patients with suspected coronary artery disease. This thesis described the optimisation of computed tomography coronary angiography radiation dose and image quality. In addition, computed tomography myocardial perfusion imaging is established as compared to the current clinical "gold standard" for the assessment of stenosis severity (invasive coronary angiography and fractional flow reserve) and also compared to the physiological "gold standard" of absolute myocardial blood flow assessed by oxygen-15 labelled water positron emission tomography. Computed tomography imaging of the heart now has the potential to assess anatomy, function, perfusion and viability in a rapid diagnostic technique, at a low radiation dose.

Computed tomography coronary angiography

The assessment of coronary artery disease has advanced beyond the mere quantification of luminal stenosis to include multi-modality imaging that is capable of assessing the functional significance of a stenosis and the possible vulnerability of a coronary artery lesion. Computed tomography coronary angiography is now an established technique for the investigation of coronary artery disease and the potential of computed tomography myocardial perfusion imaging has been established in this thesis.

Computed tomography imaging involves a balance between image quality and radiation dose. Adequate image quality is important in order to provide good diagnostic accuracy and limit observer variability. However, the assessment of image quality is subjective. Measurements of image noise and signal to noise ratios are one component of computed tomography image quality. Ordinal scales of observer rated image quality can provide an overall summary of the complex interplay of determinants of image quality such as noise, contrast, edge determination and artefacts such as motion. In wide-volume 320-multidetector computed tomography coronary angiography, diagnostic image quality was obtained in 99% of unselected patients (Chapter 6). Heart rate and body mass index were the main determinants of radiation dose. However, only heart rate and the use of glyceryl trinitrate had independent (albeit small) effects on image quality.

Establishing the observer variability of the techniques applied in this thesis is important for their future clinical application. Computed tomography coronary angiography and computed tomography myocardial perfusion had excellent or good intra- and inter- observer variability (Chapter 6 and 7). In addition, the "gold standard" assessment of absolute myocardial blood flow by oxygen-15 labelled water positron emission tomography had excellent intra- and inter- observer variability (Chapter 8). The observer variability of the overall diagnosis of angina pectoris due to coronary artery disease has not previously been assessed. The excellent intra- and inter- observer variability for this establishes computed tomography coronary angiography as the non-invasive method of choice for the assessment of patients with suspected coronary artery disease attending the Rapid Access Chest Pain Clinic.

Computed tomography myocardial perfusion imaging

Computed tomography coronary angiography with modern imaging techniques has a sensitivity approaching 100%. [208] However, the specificity of this technique is reduced by its propensity to overestimate heavily calcified stenoses. [209] For such patients, additional imaging procedures may be required to adequately assess the significance of coronary artery disease. In addition, computed tomography coronary angiography alone fails to identify a significant proportion of functionally significant lesions as compared to invasive coronary angiography and fractional flow reserve. [185] The additional information provided by perfusion imaging is additive to computed tomography coronary angiography. [187] It has been established that the selection of patients for coronary revascularization is best performed by identifying inducible myocardial ischaemia. [20] Computed tomography myocardial perfusion imaging would therefore be particularly useful as a follow on test for patients with heavily calcified coronary arteries, coronary artery stents or lesions of indeterminate severity on computed tomography imaging.

This thesis established for the first time the validity of computed tomography myocardial perfusion assessment as compared to both the clinical "gold standard" for the assessment of stenosis severity, namely invasive coronary angiography and fractional flow reserve, and the physiological "gold standard" of absolute myocardial blood flow assessed by oxygen-15 labelled water positron emission tomography. The diagnostic accuracy of computed tomography coronary angiography and computed tomography myocardial perfusion imaging was excellent with per-patient accuracy,

sensitivity, specificity, negative predictive value and positive predictive value compared to invasive coronary angiography and fractional flow reserve of 92%, 96%, 85%, 90% and 94% (Chapter 7). Hyperaemic myocardial blood flow correlated with computed tomography myocardial attenuation density, supporting the use of the visual assessment of perfusion defects (Chapter 8). In addition, I highlighted the importance of stress imaging in the assessment of the functional significance of coronary artery disease, as resting computed tomography myocardial attenuation density correlated poorly with myocardial blood flow.

Pharmacological "stress" induced by vasodilators, such as adenosine, are not equivalent to the effect of exercise on myocardial perfusion. The presence of atherosclerosis limits the vasodilatory effect of adenosine and thus produces differences in coronary blood flow in normal and abnormal coronary artery territories. In addition, in the presence of a severe stenosis with collateralisation, adenosine-induced vasodilatation in the collateral circulation may produce a coronary steal phenomenon, further decreasing the presence of iodinated contrast in the affected territory. Thus measures of myocardial blood flow based on iodinated contrast measurements under pharmacological stress may not reflect "true" myocardial blood flow. Despite this limitation we showed good correlation between computed tomography myocardial perfusion imaging and measurement of absolute myocardial blood flow.

Several methods have been proposed to quantify myocardial perfusion based on computed tomography images including transmyocardial perfusion ratio [66],

transmyocardial perfusion gradient, [210] and semi-quantitative assessments such as using summed rest and stress scores. [68,211] In addition 'iodine maps' from dual energy computed tomography imaging have been used to assess myocardial perfusion with good sensitivity and specificity as compared to magnetic resonance imaging and invasive coronary angiography. However, we found that computed tomography myocardial attenuation corrected for rate pressure product was the best quantitative computed tomography assessment of myocardial perfusion as compared to oxygen-15 labelled water positron emission tomography.

Radiation dose

Radiation exposure is a major health care concern due to the increased lifetime risk of cancer. [58] The average estimated cancer induction risk in sensitive organs in a population undergoing computed tomography coronary angiography is 0.13%. [212] In order to be a useful diagnostic test computed tomography must provide good image quality at a low radiation dose. The application of new techniques to minimise radiation dose, including iterative reconstruction and patient tailored imaging, led to a 39% reduction in radiation dose of computed tomography coronary angiography. (Chapter 3) The average radiation dose for computed tomography coronary angiography with the low radiation technique was 2.35 (2.18, 2.52) mSv using a conversion factor of 0.014 mSv/mGy.cm. In addition, sub-millisievert computed tomography coronary angiography is possible using this protocol for all patients with a heart rate ≤65 /min after beta-blocker administration and a body mass index ≤25

kg/m^2. It is likely that further reductions in radiation dose would be possible using lower tube voltage (eg 80kV) or narrower acquisition windows at faster heart rates (eg 30 to 40%). However, this was not possible with the scanner technology available when these research studies were performed. The radiation doses presented in this thesis represent a snapshot of cardiac CT activity over a defined time period with a single scanner. Further improvements in CT software and hardware mean the radiation dose of cardiac CT will continue to fall.

These radiation dose reduction techniques can also be applied to computed tomography myocardial perfusion imaging. This led to a 55% reduction in the radiation dose of the rest/stress computed tomography protocol (Chapter 5). Computed tomography coronary angiography and adenosine stress computed tomography myocardial perfusion imaging can be performed at an average radiation dose 5.22 (4.05, 6.4) mSv using a conversion factor of 0.014 mSv/mGy.cm. This is a lower radiation dose than contemporary SPECT myocardial perfusion imaging. Techniques such as magnetic resonance imaging or dynamic stress echocardiography can provide similar information without the use of ionising radiation. However, these techniques cannot at present provide coincidental assessment of coronary artery anatomy as can be done with computed tomography. The comprehensive cardiac computed tomography protocol which includes coronary artery calcium score, rest computed tomography coronary angiography, computed tomography myocardial perfusion imaging and late enhancement imaging can be performed with an average radiation dose of 8.98 mSv (Chapter 8).

Interestingly, the radiation dose of the non-contrast computed tomography images used to calculate coronary artery calcium score have changed little with the advancement of computed tomography radiation dose reduction techniques. This is because of the requirement to perform coronary artery calcium scoring using a standard tube voltage (120 kV) and standardised levels of image noise in order to maintain consistency of quantification. [213] Reducing tube current, using non-gated scans or using iterative reconstruction leads to consisted overestimation of the coronary artery calcium score. Thus as the radiation dose of computed tomography coronary angiography has fallen, coronary artery calcium scoring has become an increasing proportion of the total radiation exposure. Figure 7.1 provides an important example of this as the coronary artery calcium score was responsible for 47% of the total protocol radiation dose of 2.24 mSv. Computed tomography coronary angiography can provide superior assessment of coronary artery disease as compared to the coronary artery calcium score and it is also now possible to perform "calcium scoring" on contrast enhanced computed tomography images. We do not use non-contrast computed tomography images in the clinical assessment of patients with suspected coronary artery disease, but coronary artery calcium scoring remains a major component of the current NICE guidelines. [32]

The method used to calculate radiation dose itself is also an interesting factor that can lead to differences in the presented results of research studies. The dose length product recorded from the scanner console provides a measure of the total amount of radiation used to perform the scan. Effective dose, measured in millisieverts, reflects the relative risk from exposure to ionising radiation and accounts for the

characteristics of exposed tissues. The simplest and most commonly used method to calculate effective dose involves the multiplication of the dose length product by a conversion factor (k factor). These conversion factors are based on tissue weighting factors produced by the International Commission on Radiological Protection (ICRP). ICRP tissue-weighting factors reflect the sensitivity to radiation-induced carcinogenesis of individual tissues. In 2007 the tissue-weighting factor for breast tissue was increased fro 0.05 to 0.12. [193] The 0.014 mSv/mGy.cm conversion factor which is commonly used in cardiac imaging is based on the old ICRP tissue weighting factor and does not take into account the reduced scan range used in cardiac imaging which contains an increased proportion of breast tissue as compared to lung tissue. Other factors that can affect the appropriateness of a conversion factor include scanner protocol, scanner type and individual patient factors. Thus the true conversion factor for cardiac computed tomography imaging may be up to 0.034 mSv/mGy.cm. [214] Nevertheless, 0.014 mSv/mGy.cm remains the conversion factor recommended by international societies for the calculation of radiation dose in cardiac imaging. [215] For computed tomography coronary angiography performed using the 320-multidetector scanner a more appropriate conversion factor calculated using the method described by Huda *et al* [59] is 0.028 mSv/mGy.cm. However, we do not know the additional effect of repeated imaging of the same region, so the appropriate conversion factor for dynamic computed tomography myocardial perfusion imaging is likely to be higher. Thus the accurate assessment of radiation dose is complex, and presented values can vary widely depending on the chosen conversion factor.

Defining severe coronary artery disease

CTCA and invasive coronary angiography produce fundamentally different images. invasive coronary angiography produces two-dimensional images of iodinated contrast in the coronary artery lumen at a high spatial resolution (0.2mm). CTCA provides a volumetric dataset of the coronary artery lumen, coronary artery wall including atherosclerotic plaque, and surrounding structures at a lower spatial resolution (0.5mm). invasive coronary angiography assesses diameter stenosis where as CTCA can assess area or diameter stenosis. These differences mean that there are fundamental issues using invasive coronary angiography as a "gold standard" comparator in studies of CTCA.

Animal studies show that flow in a vessel remains relatively constant until a stenosis of about 75% is reached, after which flow decreases rapidly. [12,216,217] For CTCA the optimum cut off to predict a flow-limiting stenosis as compared to fractional flow reserve is 48% for diameter stenosis and 73% for area stenosis. [218] Using a threshold of 70% also provides better agreement with SPECT detection of functionally significant coronary artery disease as compared to a threshold of 50%. [219] A referral system for invasive coronary angiography based on a 70% CTCA threshold improves the likelihood of identifying significant disease as compared to using a 50% threshold, although there is a small reduction in sensitivity. [220]

The choice of threshold has an important implication for the assessment of diagnostic accuracy. In this thesis significant coronary artery disease on CTCA was defined as a

stenosis greater than 50% with an associated perfusion defect on CT myocardial perfusion imaging. This aimed to improve the sensitivity for the detection of coronary artery disease by CT and limit the inclusion of potential artifacts as perfusion defects. This was compared to an invasive coronary angiography threshold of greater than 70% stenosis or any stenosis with a reduced fractional flow reserve. This threshold was chosen in order to make the "gold standard" as robust as possible, as it is unfortunately not possible to perform fractional flow reserve assessment in every patient due to anatomical limitations. Changing any of these thresholds will affect the results of diagnostic accuracy studies.

The definition of "severe" coronary artery disease by CTCA also has important implications on the rate of downstream testing. If a low threshold is set for the referral of patients for invasive coronary angiography then there will be a larger number of patients with normal coronary arteries who undergo invasive investigations. However, if a high threshold is set there is the potential that patients who would benefit from revascularisation will not receive the appropriate treatment. The choice of cut-off will therefor also impact on cost effectiveness assessment.

However, concentrating on luminal stenosis alone underutilises the advantages of CTCA. CTCA can provide additional information on the presence and characteristics of atherosclerotic plaque. This includes the assessment of potentially vulnerable plaques with positive remodelling, low attenuation plaque and spotty calcification [221] The assessment of positive remodelling by CT can also improve the accuracy of stenosis assessment. CT can also provide the opportunity to obtain other

functional information on stenosis severity using techniques such as CT perfusion or CT FFR.

Dynamic computed tomography coronary angiography

Recent advances in computed tomography imaging have led to the development of dynamic computed tomography myocardial perfusion protocols. [65,164-167,222-227] Dynamic computed tomography protocols (CTP) image the myocardium at multiple time points, similar to magnetic resonance myocardial perfusion imaging. This contrasts to the "snap shot" protocol described in this thesis that obtains images at one, or a small number, of time points at the peak of myocardial contrast enhancement. Dynamic computed tomography myocardial perfusion imaging enables the assessment of myocardial blood flow calculated from the first-pass of myocardial contrast. However, this is at the expense of an increased radiation dose, a prolonged breath-hold and a limited scan range. [167]

The optimal method to assess dynamic computed tomography myocardial perfusion imaging has not yet been established. A variety of methods have previously been used to assess dynamic computed tomography myocardial perfusion including deconvolution, upslope and Patlak plot analysis. [65,164,165] These mathematical models are widely used in other imaging techniques including magnetic resonance imaging and nuclear medicine. The upslope method uses a single compartment model and perfusion is calculated as the maximum slope of the tissue enhancement

curve divided by the maximum arterial enhancement. The Patlak plot method is based on a two-compartment model and plots the change in myocardial attenuation against the area under the arterial-time attenuation curve. Unlike the upslope and Patlak plot methods, deconvolution analysis requires imaging of the full first pass of contrast from which the tissue output and arterial input functions are calculated. The continuous arterial input function can be thought of as a series of idealized bolus injections, and the corresponding tissue output curve can be considered as the sum of the tissue response to each bolus, the so-called impulse residue function. Deconvolution of input and output curves gives the perfusion scaled impulse residue function curve, from which total blood flow and blood volume can be calculated. The upslope and deconvolution methods correlate well with microsphere-derived measurements of myocardial blood flow in canine models of coronary stenosis. [77] Measurements of hyperaemic myocardial blood flow in humans from dynamic computed tomography myocardial perfusion range from 52 to 96 mL/100mL/min. [166] These methods calculate "absolute" rather than "relative" myocardial perfusion, but nevertheless they do not measure "true" myocardial blood flow. They are limited by the assumptions inherent in the mathematical models, along with the effects of the contrast material and adenosine.

Further work in developing dynamic computed tomography myocardial perfusion imaging will involve improvements in the method and speed of analysis. In addition, radiation dose remains a major health care concern. Software and hardware improvements will continue to reduce the radiation dose of dynamic computed tomography myocardial perfusion imaging. However, the radiation dose of “snap

shot" computed tomography myocardial perfusion imaging established in this thesis means that this technique can now be used clinically.

Beyond the coronary arteries

In the investigation of patients with coronary artery disease the assessment of the coronary artery lumen alone may not be adequate for diagnosis, risk stratification or the selection of patients for revascularisation. The ability of computed tomography to provide additional diagnostically useful information in one rapid test is of benefit to patients. Other techniques can perform selected components of a comprehensive assessment such as the assessment of myocardial viability and function with magnetic resonance imaging, or myocardial perfusion and function with nuclear medicine techniques. However, computed tomography is the only technique to date that can perform a comprehensive "one-stop" assessment. Fractional flow reserve is the current clinical "gold standard" for the assessment of stenosis severity, but this is an invasive technique with inherent risk. Thus, the development of non-invasive imaging techniques capable of providing such information is important.

Of the non-invasive imaging techniques used in cardiac imaging, magnetic resonance imaging and echocardiography are the only techniques associated with no radiation dose. However, neither can routinely be used to assess the coronary arteries. Nuclear medicine techniques such as SPECT are associated with a comparatively high radiation dose when compared with current low dose computed tomography coronary angiography techniques. Despite being the "gold standard" for the

assessment of myocardial blood flow, oxygen-15 positron emission tomography is unlikely to be used widely on a clinical basis because of the requirement of an on site cyclotron. Thus at present, computed tomography is the only non-invasive imaging modality capable of comprehensive imaging at a low radiation dose.

Conclusion

This is an evolving and exciting time for cardiac computed tomography imaging. Techniques to reduce radiation dose and improve image quality can be used to optimise computed tomography coronary angiography. Radiation dose reduction techniques mean that it is now possible to perform comprehensive assessment of the heart at a low radiation dose. Computed tomography can be used to assess coronary and cardiac anatomy, function, perfusion and viability in a rapid non-invasive technique, at a low radiation dose. This thesis has validated computed tomography myocardial perfusion imaging as compared to both physiological and clinical "gold standards". Computed tomography myocardial perfusion imaging has an excellent diagnostic accuracy as compared to invasive coronary angiography and fractional flow reserve, the current clinical "gold standard" for the assessment of stenosis severity. In addition, computed tomography myocardial attenuation correlates with absolute myocardial blood flow measured with oxygen-15 labelled water positron emission tomography. Thus, the comprehensive cardiac computed tomography protocol can provide a robust physiological and clinical assessment of patients with suspected coronary artery disease.

References

1 WHO. *Global status report on noncommunicable diseases 2010*. Geneva: : World Health Organisation 2011.

2 Scarborough P, Wickramasinghe K, Bhatnagar P, *et al. Trends in coronary heart disease, 1961-2011*. London: : British Heart Foundation 2014.

3 Nichols M, Townsend N, Scarborough P, *et al.* Cardiovascular disease in Europe: epidemiological update. *European Heart Journal* 2013;**34**:3028–34. doi:10.1093/eurheartj/eht356

4 NICE. *Chest pain of recent onset. Costing report. Implementing NICE guidance. NICE clinical guideline 95*. London: : NICE 2011.

5 Ruigomez A. Chest pain in general practice: incidence, comorbidity and mortality. *Family Practice* 2006;**23**:167–74. doi:10.1093/fampra/cmi124

6 Braunwald E. The rise of cardiovascular medicine. *European Heart Journal* 2012;**33**:838–45–845a. doi:10.1093/eurheartj/ehr452

7 Riley RF, Don CW, Powell W, *et al.* Trends in Coronary Revascularization in the United States From 2001 to 2009: Recent Declines in Percutaneous Coronary Intervention Volumes. *Circulation: Cardiovascular Quality and Outcomes* 2011;**4**:193–7. doi:10.1161/CIRCOUTCOMES.110.958744

8 Scanlon PJ, Faxon DP, Audet AM, *et al.* ACC/AHA guidelines for coronary angiography. A report of the American College of Cardiology/American Heart Association Task Force on practice guidelines (Committee on Coronary Angiography). Developed in collaboration with the Society for Cardiac Angiography and Interventions. JACC. 1999;**33**:1756–824.

9 Patel MR, Peterson ED, Dai D, *et al.* Low diagnostic yield of elective coronary angiography. *N Engl J Med* 2010;**362**:886–95. doi:10.1056/NEJMoa0907272

10 Phibbs B, Fleming T, Ewy GA, *et al.* Frequency of normal coronary arteriograms in three academic medical centers and one community hospital. *AJC* 1988;**62**:472–4.

11 Joshi NV, Vesey AT, Williams MC, *et al.* 18F-fluoride positron emission tomography for identification of ruptured and high-risk coronary atherosclerotic plaques: a prospective clinical trial. *Lancet* 2014;**383**:705–13. doi:10.1016/S0140-6736(13)61754-7

12 Topol EJ, Nissen SE. Our preoccupation with coronary luminology. The dissociation between clinical and angiographic findings in ischemic heart disease. *Circulation* 1995;**92**:2333–42.

13 Gould KL, Johnson NP, Bateman TM, *et al.* Anatomic versus physiologic assessment of coronary artery disease. Role of coronary flow reserve, fractional flow reserve, and positron emission tomography imaging in revascularization decision-making. *Journal of the American College of Cardiology* 2013;**62**:1639–53. doi:10.1016/j.jacc.2013.07.076

14 Kern MJ, Samady H. Current Concepts of Integrated Coronary Physiology in the Catheterization Laboratory. *Journal of the American College of Cardiology* 2010;**55**:173–85. doi:10.1016/j.jacc.2009.06.062

15 Pijls NH, Van Gelder B, Van der Voort P, *et al.* Fractional flow reserve. A useful index to evaluate the influence of an epicardial coronary stenosis on myocardial blood flow. *Circulation* 1995;**92**:3183–93. doi:10.1056/NEJMoa1205361

16 van de Hoef TP, van de Hoef TP, Meuwissen M, *et al.* Fractional flow reserve and beyond. *Heart* 2013;**99**:1699–705. doi:10.1136/heartjnl-2012-302325

17 Muller O, Mangiacapra F, Ntalianis A, *et al.* Long-term follow-up after fractional flow reserve-guided treatment strategy in patients with an isolated proximal left anterior descending coronary artery stenosis. *JACC: Cardiovascular Interventions* 2011;**4**:1175–82. doi:10.1016/j.jcin.2011.09.007

18 Tonino PAL, De Bruyne B, Pijls NHJ, *et al.* Fractional flow reserve versus angiography for guiding percutaneous coronary intervention. *N Engl J Med* 2009;**360**:213–24. doi:10.1056/NEJMoa0807611

19 Hamilos M, Muller O, Cuisset T, *et al.* Long-term clinical outcome after fractional flow reserve-guided treatment in patients with angiographically equivocal left main coronary artery stenosis. *Circulation* 2009;**120**:1505–12. doi:10.1161/CIRCULATIONAHA.109.850073

20 Pijls NHJ, Fearon WF, Tonino PAL, *et al.* Fractional flow reserve versus angiography for guiding percutaneous coronary intervention in patients with multivessel coronary artery disease: 2-year follow-up of the FAME (Fractional Flow Reserve Versus Angiography for Multivessel Evaluation) study. *Journal of the American College of Cardiology* 2010;**56**:177–84. doi:10.1016/j.jacc.2010.04.012

21 Tonino PAL, Fearon WF, De Bruyne B, *et al.* Angiographic Versus Functional Severity of Coronary Artery Stenoses in the FAME Study. *Journal of the American College of Cardiology* 2010;**55**:2816–21. doi:10.1016/j.jacc.2009.11.096

22 Fearon WF, Yeung AC, Lee DP, *et al.* Cost-effectiveness of measuring fractional flow reserve to guide coronary interventions. *American Heart Journal* 2003;**145**:882–7. doi:10.1016/S0002-8703(03)00072-3

23 Fearon WF, Bornschein B, Tonino PAL, *et al.* Economic evaluation of fractional flow reserve-guided percutaneous coronary intervention in patients with multivessel disease. *Circulation* 2010;**122**:2545–50. doi:10.1161/CIRCULATIONAHA.109.925396

24 Fearon WF, Shilane D, Pijls NHJ, *et al.* Cost-effectiveness of percutaneous coronary intervention in patients with stable coronary artery disease and abnormal fractional flow reserve. *Circulation* 2013;**128**:1335–40. doi:10.1161/CIRCULATIONAHA.113.003059

25 De Bruyne B, Sarma J. Fractional flow reserve: a review. *Heart* 2008;**94**:949–59. doi:10.1136/hrt.2007.122838

26 Pijls NHJ, Tanaka N, Fearon WF. Functional assessment of coronary stenoses: can we live without it? *European Heart Journal* 2013;**34**:1335–44. doi:10.1093/eurheartj/ehs436

27 Hounsfield GN. *Nobel Award address. Computed medical imaging.* 1980.

28 Berrington de Gonzalez A, Mahesh M, Kim K-P, *et al.* Projected cancer risks from computed tomographic scans performed in the United States in 2007. *ARchives of Internal Medicine* 2009;**169**:2071–7. doi:10.1001/archinternmed.2009.440

29 DOH. Imaging and radiodiagnostic examinations and tests, Strategic Health Authorities in England 2009-10. *Department of Health*

30 ISDScotland. Radiology services. *ISD Scotland* 2010.

31 Hurlock GS, Higashino H, Mochizuki T. History of cardiac computed tomography: single to 320-detector row multislice computed tomography. *Int J Cardiovasc Imaging* 2009;**25**:31–42. doi:10.1007/s10554-008-9408-z

32 NICE. *Chest pain of recent onset*. NICE 2010.

33 Fayad ZA, Fuster V, Fallon JT, *et al.* Noninvasive in vivo human coronary artery lumen and wall imaging using black-blood magnetic resonance imaging. *Circulation* 2000;**102**:506–10.

34 Schroeder S, Achenbach S, Bengel F, *et al.* Cardiac computed tomography: indications, applications, limitations, and training requirements: Report of a Writing Group deployed by the Working Group Nuclear Cardiology and Cardiac CT of the European Society of Cardiology and the European Council of Nuclear Cardiology. *European Heart Journal* 2008;**29**:531–56. doi:10.1093/eurheartj/ehm544

35 Miller JM, Rochitte CE, Dewey M, *et al.* Diagnostic performance of coronary angiography by 64-row CT. *N Engl J Med* 2008;**359**:2324–36. doi:10.1056/NEJMoa0806576

36 Leber AW, Knez A, Becker A, *et al.* Accuracy of multidetector spiral computed tomography in identifying and differentiating the composition of coronary atherosclerotic plaques. *Journal of the American College of Cardiology* 2004;**43**:1241–7. doi:10.1016/j.jacc.2003.10.059

37 Pflederer T, Marwan M, Schepis T, *et al.* Characterization of culprit lesions in acute coronary syndromes using coronary dual-source CT angiography. *Atherosclerosis* 2010;**211**:437–44. doi:10.1016/j.atherosclerosis.2010.02.001

38 Motoyama S, Kondo T, Sarai M, *et al.* Multislice Computed Tomographic Characteristics of Coronary Lesions in Acute Coronary Syndromes. *Journal of the American College of Cardiology* 2007;**50**:319–26. doi:10.1016/j.jacc.2007.03.044

39 Pohle K, Achenbach S, MacNeill B, *et al.* Characterization of non-calcified coronary atherosclerotic plaque by multi-detector row CT: Comparison to IVUS. *Atherosclerosis* 2007;**190**:174–80. doi:10.1016/j.atherosclerosis.2006.01.013

40 Kim SY, Kim K-S, Seung MJ, *et al.* The culprit lesion score on multi-detector computed tomography can detect vulnerable coronary artery plaque. *Int J Cardiovasc Imaging* 2010;**26**:245–52. doi:10.1007/s10554-010-9712-2

41 George RT. Computed tomography myocardial perfusion imaging: developmental points of emphasis. *Expert Rev Cardiovasc Ther* 2009;**7**:99–101. doi:10.1586/14779072.7.2.99

42 Sarwar A, Rieber J, Mooyaart EAQ, *et al.* Calcified Plaque: Measurement of Area at Thin-Section Flat-Panel CT and 64-Section Multidetector CT and Comparison with Histopathologic Findings1. *Radiology* 2008;**249**:301–6. doi:10.1148/radiol.2483072003

43 Alvarez RE, Macovski A. Energy-selective reconstructions in X-ray computerized tomography. *Phys Med Biol* 1976;**21**:733–44.

44 Rutherford RA, Pullan BR, Isherwood I. X-ray energies for effective atomic number determination. *Neuroradiology* 1976;**11**:23–8.

45 Donnino R, Jacobs JE, Doshi JV, *et al.* Dual-Source Versus Single-Source Cardiac CT Angiography: Comparison of Diagnostic Image Quality. *American Journal of Roentgenology* 2009;**192**:1051–6. doi:10.2214/AJR.08.1198

46 Feuerlein S, Roessl E, Proksa R, *et al.* Multienergy Photon-counting K-edge Imaging: Potential for Improved Luminal Depiction in Vascular Imaging. *Radiology* 2008;**249**:1010–6. doi:10.1148/radiol.2492080560

47 Cormode DP, Roessl E, Thran A, *et al.* Atherosclerotic plaque composition: Analysis with multicolor CT and targeted gold nanoparticles1. *Radiology* 2010;**256**:774–82. doi:10.1148/radiol.10092473/-/DC1

48 Dewey M, Vavere AL, Arbab-Zadeh A, *et al.* Patient characteristics as predictors of image quality and diagnostic accuracy of MDCT compared with conventional coronary angiography for detecting coronary artery stenoses: CORE-64 Multicenter International Trial. *American Journal of Roentgenology* 2010;**194**:93–102. doi:10.2214/AJR.09.2833

49 Brodoefel H, Reimann A, Burgstahler C, *et al.* Noninvasive coronary angiography using 64-slice spiral computed tomography in an unselected patient collective: effect of heart rate, heart rate variability and coronary calcifications on image quality and diagnostic accuracy. *European Journal of Radiology* 2008;**66**:134–41. doi:10.1016/j.ejrad.2007.05.013

50 Leschka S, Wildermuth S, Boehm T, *et al.* Noninvasive coronary angiography with 64-section CT: effect of average heart rate and heart rate variability on image quality. *Radiology* 2006;**241**:378–85. doi:10.1148/radiol.2412051384

51 Park K-H, Lee HY, Lim C, *et al.* Clinical impact of computerised tomographic angiography performed for preoperative evaluation before coronary artery bypass grafting. *European Journal of Cardio-Thoracic Surgery* 2010;**37**:1346–52. doi:10.1016/j.ejcts.2009.12.040

52 Beister M, Kolditz D, Kalender WA. Iterative reconstruction methods in X-ray CT. *Phys Med* 2012;**28**:94–108. doi:10.1016/j.ejmp.2012.01.003

53 Nelson RC, Feuerlein S, Boll DT. New iterative reconstruction techniques for cardiovascular computed tomography: how do they work, and what are the advantages and disadvantages? *J Cardiovasc Comput Tomogr* 2011;**5**:286–92. doi:10.1016/j.jcct.2011.07.001

54 Willemink MJ, Takx RAP, de Jong PA, *et al.* The impact of CT radiation dose reduction and iterative reconstruction algorithms from four different vendors on coronary calcium scoring. *Eur Radiol* 2014;**24**:2201–12. doi:10.1007/s00330-014-3217-7

55 Bhave NM, Mor-Avi V, Kachenoura N, *et al.* Analysis of myocardial perfusion from vasodilator stress computed tomography: Does improvement in image quality by iterative reconstruction lead to improved diagnostic accuracy? *J Cardiovasc Comput Tomogr* 2014;**8**:238–45. doi:10.1016/j.jcct.2014.04.008

56 Harder Den AM, Willemink MJ, De Ruiter QMB, *et al.* Dose reduction with iterative reconstruction for coronary CT angiography: a systematic review and meta-analysis. *British Journal of Radiology* 2015;**89**:20150068–9. doi:10.1259/bjr.20150068

57 Hausleiter J. Estimated Radiation Dose Associated With Cardiac CT Angiography. *JAMA* 2009;**301**:500. doi:10.1001/jama.2009.54

58 Christner JA, Kofler JM, McCollough CH. Estimating Effective Dose for CT Using Dose-Length Product Compared With Using Organ Doses: Consequences of Adopting International Commission on Radiological Protection Publication 103 or Dual-Energy Scanning. *American Journal of Roentgenology* 2010;**194**:881–9. doi:10.2214/AJR.09.3462

59 Huda W, Tipnis S, Sterzik A, *et al.* Computing effective dose in cardiac CT. *Phys Med Biol* 2010;**55**:3675–84. doi:10.1088/0031-9155/55/13/007

60 Chen MY, Shanbhag SM, Arai AE. Submillisievert Median Radiation Dose for Coronary Angiography with a Second-Generation 320-Detector Row CT Scanner in 107 Consecutive Patients. *Radiology* Published Online First: 22 January 2013. doi:10.1148/radiol.13122621

61 Bourque JM, Beller GA. Stress myocardial perfusion imaging for assessing prognosis: an update. *JACC: Cardiovascular Imaging* 2011;**4**:1305–19. doi:10.1016/j.jcmg.2011.10.003

62 Hachamovitch R, Berman DS, Shaw LJ, *et al.* Incremental prognostic value of myocardial perfusion single photon emission computed tomography for the prediction of cardiac death: differential stratification for risk of cardiac death and myocardial infarction. *Circulation* 1998;**97**:535–43. doi:10.1161/01.CIR.97.6.535

63 Dorbala S, Hachamovitch R, Curillova Z, *et al.* Incremental prognostic value of gated Rb-82 positron emission tomography myocardial perfusion imaging over clinical variables and rest LVEF. *JACC: Cardiovascular Imaging* 2009;**2**:846–54. doi:10.1016/j.jcmg.2009.04.009

64 Achenbach S. Computed tomography coronary angiography. *Journal of the American College of Cardiology* 2006;**48**:1919–28. doi:10.1016/j.jacc.2006.08.012

65 Kido T, Kurata A, Higashino H, *et al.* Quantification of regional myocardial blood flow using first-pass multidetector-row computed tomography and adenosine triphosphate in coronary artery disease. *Circ J* 2008;**72**:1086–91.

66 George RT, Arbab-Zadeh A, Miller JM, *et al.* Adenosine stress 64- and 256-row detector computed tomography angiography and perfusion imaging: a pilot study evaluating the transmural extent of perfusion abnormalities to predict atherosclerosis causing myocardial ischemia. *Circulation: Cardiovascular Imaging* 2009;**2**:174–82. doi:10.1161/CIRCIMAGING.108.813766

67 Blankstein R, Shturman LD, Rogers IS, *et al.* Adenosine-Induced Stress Myocardial Perfusion Imaging Using Dual-Source Cardiac Computed Tomography. *Journal of the American College of Cardiology* 2009;**54**:1072–84. doi:10.1016/j.jacc.2009.06.014

68 Direct comparison of rest and adenosine stress myocardial perfusion CT with rest and stress SPECT. *J Nucl Cardiol* 2009;**17**:27–37. doi:10.1007/s12350-009-9156-z

69 Vavere AL, Simon GG, George RT, *et al.* Diagnostic performance of combined noninvasive coronary angiography and myocardial perfusion imaging using 320 row detector computed tomography: design and implementation of the CORE320 multicenter, multinational diagnostic study. *J Cardiovasc Comput Tomogr* 2011;**5**:370–81. doi:10.1016/j.jcct.2011.11.001

70 Rochitte CE, George RT, Chen MY, *et al.* Computed tomography angiography and perfusion to assess coronary artery stenosis causing perfusion defects by single photon emission computed tomography: the CORE320 study. *European Heart Journal* 2014;**35**:1120–30. doi:10.1093/eurheartj/eht488

71 Beller GA. Recent advances and future trends in multimodality cardiac imaging. *Heart, Lung and Circulation* 2010;**19**:193–209. doi:10.1016/j.hlc.2009.11.003

72 Hoffman JI. Transmural myocardial perfusion. *Prog Cardiovasc Dis* 1987;**29**:429–64.

73 Nagel E, Lima JAC, George RT, *et al.* Newer Methods for Noninvasive Assessment of Myocardial Perfusion. *JACC: Cardiovascular Imaging* 2009;**2**:656–60. doi:10.1016/j.jcmg.2009.02.007

74 George RT, Bengel FM, Lardo AC. Coronary flow reserve by CT perfusion. *J Nucl Cardiol* 2010;**17**:540–3. doi:10.1007/s12350-010-9250-2

75 Choi KM, Kim RJ, Gubernikoff G, *et al.* Transmural Extent of Acute Myocardial Infarction Predicts Long-Term Improvement in Contractile Function. *Circulation* 2001;**104**:1101–7. doi:10.1161/hc3501.096798

76 Shapiro MD, Sarwar A, Nieman K, *et al.* Cardiac computed tomography for prediction of myocardial viability after reperfused acute myocardial infarction. *J Cardiovasc Comput Tomogr* 2010;**4**:267–73. doi:10.1016/j.jcct.2010.04.004

77 George RT, Jerosch-Herold M, Silva C, *et al.* Quantification of myocardial perfusion using dynamic 64-detector computed tomography. *Invest Radiol* 2010;**42**:815–22. doi:10.1097/RLI.0b013e318124a884

78 Kitagawa K, George RT, Arbab-Zadeh A, *et al.* Characterization and correction of beam-hardening artifacts during dynamic volume CT assessment of myocardial perfusion. *Radiology* 2010;**256**:111–8. doi:10.1148/radiol.10091399

79 White HD, Norris RM, Brown MA, *et al.* Left ventricular end-systolic volume as the major determinant of survival after recovery from myocardial infarction. *Circulation* 1987;**76**:44–51.

80 Hundley WG, Bluemke DA, Finn JP, *et al.* ACCF/ACR/AHA/NASCI/SCMR 2010 Expert Consensus Document on Cardiovascular Magnetic Resonance. *Journal of the American College of Cardiology* 2010;**55**:2614–62. doi:10.1016/j.jacc.2009.11.011

81 Juergens KU, Fischbach R. Left ventricular function studied with MDCT. *Eur Radiol* 2005;**16**:342–57. doi:10.1007/s00330-005-2888-5

82 Cury RC, Nieman K, Shapiro MD, *et al.* Comprehensive assessment of myocardial perfusion defects, regional wall motion, and left ventricular function by using 64-section multidetector CT. *Radiology* 2008;**248**:466–75. doi:10.1148/radiol.2482071478

83 Mendoza DD, Joshi SB, Weissman G, *et al.* Viability imaging by cardiac computed tomography. *J Cardiovasc Comput Tomogr* 2010;**4**:83–91. doi:10.1016/j.jcct.2010.01.019

84 Brodoefel H, Klumpp B, Reimann A, *et al.* Late myocardial enhancement assessed by 64-MSCT in reperfused porcine myocardial infarction: diagnostic accuracy of low-dose CT protocols in comparison with magnetic resonance imaging. *Eur Radiol* 2006;**17**:475–83. doi:10.1007/s00330-006-0334-y

85 Lardo AC. Contrast-Enhanced Multidetector Computed Tomography Viability Imaging After Myocardial Infarction: Characterization of Myocyte Death, Microvascular Obstruction, and Chronic Scar. *Circulation* 2006;**113**:394–404. doi:10.1161/CIRCULATIONAHA.105.521450

86 Nieman K, Shapiro MD, Ferencik M, *et al.* Reperfused myocardial infarction: contrast-enhanced 64-Section CT in comparison to MR imaging. *Radiology* 2008;**247**:49–56. doi:10.1148/radiol.2471070332

87 Rodriguez-Granillo GA, Rosales MA, Baum S, *et al.* Early Assessment of Myocardial Viability by the Use of Delayed Enhancement Computed Tomography After Primary Percutaneous Coronary Intervention. *JCMG* 2009;**2**:1072–81. doi:10.1016/j.jcmg.2009.03.023

88 Paul JF, Wartski M, Caussin C, *et al.* Late Defect on Delayed Contrast-enhanced Multi-Detector Row CT Scans in the Prediction of SPECT Infarct Size after Reperfused Acute Myocardial Infarction: Initial Experience. *Radiology* 2005;**236**:485–9. doi:10.1148/radiol.2362040912

89 Rogers WJ, Kramer CM, Geskin G, *et al.* Early contrast-enhanced MRI predicts late functional recovery after reperfused myocardial infarction. *Circulation* 1999;**99**:744–50.

90 Bergmann SR, Fox KA, Rand AL, *et al.* Quantification of regional myocardial blood flow in vivo with H215O. *Circulation* 1984;**70**:724–33. doi:10.1161/01.CIR.70.4.724

91 Knuuti J, Kajander S, Mäki M, *et al.* Quantification of myocardial blood flow will reform the detection of CAD. *J Nucl Cardiol* 2009;**16**:497–506. doi:10.1007/s12350-009-9101-1

92 Knaapen P, de Haan S, Hoekstra OS, *et al.* Cardiac PET-CT: advanced hybrid imaging for the detection of coronary artery disease. *Neth Heart J* 2010;**18**:90–8.

93 Bol A, Melin JA, Vanoverschelde JL, *et al.* Direct comparison of [13N]ammonia and [15O]water estimates of perfusion with quantification of regional myocardial blood flow by microspheres. *Circulation* 1993;**87**:512–25. doi:10.1161/01.CIR.87.2.512

94 Bergmann SR, Herrero P, Markham J, *et al.* Noninvasive quantitation of myocardial blood flow in human subjects with oxygen-15-labeled water and positron emission tomography. *JACC* 1989;**14**:639–52.

95 Chareonthaitawee P, Christenson SD, Anderson JL, *et al.* Reproducibility of measurements of regional myocardial blood flow in a model of coronary artery disease: Comparison of H215O and 13NH3 PET techniques. *Journal of Nuclear Medicine* 2006;**47**:1193–201.

96 Huang SC, Schwaiger M, Carson RE, *et al.* Quantitative measurement of myocardial blood flow with oxygen-15 water and positron computed tomography: an assessment of potential and problems.[Dogs]. *Journal of Nuclear Medicine* 1985;**26**.

97 Lee JS, Lee DS, Ahn JY, *et al.* Blind separation of cardiac components and extraction of input function from H(2)(15)O dynamic myocardial PET using independent component analysis. *Journal of Nuclear Medicine* 2001;**42**:938–43.

98 Rimoldi O, Schäfers KP, Boellaard R, *et al.* Quantification of subendocardial and subepicardial blood flow using 15O-labeled water and PET: experimental validation. *Journal of Nuclear Medicine* 2006;**47**:163–72.

99 Schäfers KP, Spinks TJ, Camici PG, *et al.* Absolute quantification of myocardial blood flow with H(2)(15)O and 3-dimensional PET: an experimental validation. *Journal of Nuclear Medicine* 2002;**43**:1031–40.

100 Uren NG, De Bruyne B, Wijns W, *et al.* Relation between myocardial blood flow and the severity of coronary-artery stenosis. *N Engl J Med* 1994;**330**:1782–8. doi:10.1056/NEJM199406233302503

101 Araujo LI, Lammertsma AA, Rhodes CG, *et al.* Noninvasive quantification of regional myocardial blood flow in coronary artery disease with oxygen-15-labeled carbon dioxide inhalation and positron emission tomography. *Circulation* 1991;**83**:875–85. doi:10.1161/01.CIR.83.3.875

102 Prior JO, Allenbach G, Valenta I, *et al.* Quantification of myocardial blood flow with 82Rb positron emission tomography: clinical validation with 15O-water. *Eur J Nucl Med Mol Imaging* 2012;**39**:1037–47. doi:10.1007/s00259-012-2082-3

103 Schaefer WM, Nowak B, Kaiser H-J, *et al.* Comparison of microsphere-equivalent blood flow (15O-water PET) and relative perfusion (99mTc-tetrofosmin SPECT) in myocardium showing metabolism-perfusion mismatch. *Journal of Nuclear Medicine* 2003;**44**:33–9.

104 Kajander S, Joutsiniemi E, Saraste M, *et al.* Cardiac Positron Emission Tomography/Computed Tomography Imaging Accurately Detects Anatomically and Functionally Significant Coronary Artery Disease. *Circulation* 2010;**122**:603–13. doi:10.1161/CIRCULATIONAHA.109.915009

105 Danad I, Raijmakers PG, Appelman YE, *et al.* Hybrid Imaging Using Quantitative H215O PET and CT-Based Coronary Angiography for the Detection of Coronary Artery Disease. *Journal of Nuclear Medicine* 2013;**54**:55–63. doi:10.2967/jnumed.112.104687

106 Morton G, Chiribiri A, IShida M, *et al.* Quantification of Absolute Myocardial Perfusion in Patients With Coronary Artery Disease. *Journal of the American College of Cardiology* 2012;**60**:1546–55. doi:10.1016/j.jacc.2012.05.052

107 Marques KM, Knaapen P, Boellaard R, *et al.* Microvascular Function in Viable Myocardium After Chronic Infarction Does Not Influence Fractional Flow Reserve Measurements. *Journal of Nuclear Medicine* 2007;**48**:1987–92. doi:10.2967/jnumed.107.044370

108 Harms HJ, Nesterov SV, Nesterov SV, *et al.* Comparison of clinical non-commercial tools for automated quantification of myocardial blood flow using oxygen-15-labelled water PET/CT. *European Heart Journal - Cardiovascular Imaging* 2014;**15**:431–41. doi:10.1093/ehjci/jet177

109 Iida H, Yokoyama I, Agostini D, *et al.* Quantitative assessment of regional myocardial blood flow using oxygen-15-labelled water and positron emission tomography: a multicentre evaluation in Japan. *Eur J Nucl Med* 2000;**27**:192–201.

110 Chareonthaitawee P, Kaufmann PA, Rimoldi O, *et al.* Heterogeneity of resting and hyperemic myocardial blood flow in healthy humans. *Cardiovascular Research* 2001;**50**:151–61.

111 Klass O, Mutlu S, Hohl K, *et al.* Multidetector computed tomography coronary angiography: sublingual nitroglycerine improves image quality significantly because of peripheral coronary vasodilatation. *J Comput Assist Tomogr* 2009;**33**:199–203. doi:10.1097/RCT.0b013e31817c6b33

112 Agatston AS, Janowitz WR, Hildner FJ, *et al.* Quantification of coronary artery calcium using ultrafast computed tomography. *JACC* 1990;**15**:827–32.

113 Austen WG, Edwards JE, Frye RL, *et al.* A reporting system on patients evaluated for coronary artery disease. Report of the Ad Hoc Committee for Grading of Coronary Artery Disease, Council on Cardiovascular Surgery, American Heart Association. *Circulation* 1975;**51**:5–40.

114 EditorialImaging Systemic Inflammation in Patients With Acute Myocardial Infarction. 2014;:1–3. doi:10.1161/CIRCIMAGING.114.002410

115 Cerqueira MD, Weissman NJ, Dilsizian V, *et al.* Standardized myocardial segmentation and nomenclature for tomographic imaging of the heart. A statement for healthcare professionals from the Cardiac Imaging Committee of the Council on Clinical Cardiology of the American Heart Association. 2002. 539–42.

116 Mehra VC, Valdiviezo C, Arbab-Zadeh A, *et al.* A stepwise approach to the visual interpretation of CT-based myocardial perfusion. *J Cardiovasc Comput Tomogr* 2011;**5**:357–69. doi:10.1016/j.jcct.2011.10.010

117 Kudomi N, Sipilä H, Autio A, *et al.* Cross-validation of Input Functions Obtained by H2 15O PET Imaging of Rat Heart and a Blood Flow-through Detector. *Mol Imaging Biol* 2011;**14**:509–16. doi:10.1007/s11307-011-0511-5

118 Al-Mallah MH, Dorbala S. Assessment of myocardial perfusion and function with PET and PET/CT. *J Nucl Cardiol* 2010;**17**:498–513. doi:10.1007/s12350-010-9223-5

119 Uren NG. Reduced coronary vasodilator function in infarcted and normal myocardium after myocardial infarction. *N Engl J Med* 1994;**331**:222–7. doi:10.1056/NEJM199407283310402

120 Raff GL, Chinnaiyan KM, Share DA, *et al.* Radiation dose from cardiac computed tomography before and after implementation of radiation dose-reduction techniques. *JAMA* 2009;**301**:2340–8. doi:10.1001/jama.2009.814

121 Labounty TM, Earls JP, Leipsic J, *et al.* Effect of a standardized quality-improvement protocol on radiation dose in coronary computed tomographic angiography. *The American Journal of Cardiology* 2010;**106**:1663–7. doi:10.1016/j.amjcard.2010.07.023

122 Alkadhi H, Stolzmann P, Scheffel H, *et al.* Radiation dose of cardiac dual-source CT: the effect of tailoring the protocol to patient-specific parameters. *European Journal of Radiology* 2008;**68**:385–91. doi:10.1016/j.ejrad.2008.08.015

123 Hosch W, Stiller W, Mueller D, *et al.* Reduction of radiation exposure and improvement of image quality with BMI-adapted prospective cardiac computed tomography and iterative reconstruction. *European Journal of Radiology* 2012;**81**:3568–76. doi:10.1016/j.ejrad.2011.06.055

124 Rogalla P, Blobel J, Kandel S, *et al.* Radiation dose optimisation in dynamic volume CT of the heart: tube current adaptation based on anterior–posterior chest diameter. *Int J Cardiovasc Imaging* 2010;**26**:933–40. doi:10.1007/s10554-010-9630-3

125 Paul NS, Kashani H, Odedra D, *et al.* The influence of chest wall tissue composition in determining image noise during cardiac CT. *American Journal of Roentgenology* 2011;**197**:1328–34. doi:10.2214/AJR.11.6816

126 Gao J, Li J, Earls J, *et al.* Individualized tube current selection for 64-row cardiac CTA based on analysis of the scout view. *European Journal of Radiology* 2011;**79**:266–71. doi:10.1016/j.ejrad.2010.04.026

127 Paul J-F. Individually adapted coronary 64-slice CT angiography based on precontrast attenuation values, using different kVp and tube current settings: evaluation of image quality. *Int J Cardiovasc Imaging* 2011;**27 Suppl 1**:53–9. doi:10.1007/s10554-011-9960-9

128 Deetjen A, Möllmann S, Conradi G, *et al.* Use of automatic exposure control in multislice computed tomography of the coronaries: comparison of 16-slice and 64-slice scanner data with conventional coronary angiography. *Heart* 2007;**93**:1040–3. doi:10.1136/hrt.2006.103838

129 Gervaise A, Osemont B, Lecocq S, *et al.* CT image quality improvement using Adaptive Iterative Dose Reduction with wide-volume acquisition on 320-detector CT. *Eur Radiol* 2012;**22**:295–301. doi:10.1007/s00330-011-2271-7

130 Gagarina NV, Irwan R, Gordina G, *et al.* Image quality in reduced-dose coronary CT angiography. *Academic Radiology* 2011;**18**:984–90. doi:10.1016/j.acra.2011.03.009

131 Tatsugami F, Matsuki M, Nakai G, *et al.* The effect of adaptive iterative dose reduction on image quality in 320-detector row CT coronary angiography. *Br J Radiol* 2012;**85**:e378–82. doi:10.1259/bjr/10084599

132 Bittencourt MS, Schmidt B, Seltmann M, *et al.* Iterative reconstruction in image space (IRIS) in cardiac computed tomography: initial experience. *Int J Cardiovasc Imaging* 2011;**27**:1081–7. doi:10.1007/s10554-010-9756-3

133 Leipsic J, Labounty TM, Heilbron B, *et al.* Adaptive statistical iterative reconstruction: assessment of image noise and image quality in coronary CT angiography. *American Journal of Roentgenology* 2010;**195**:649–54. doi:10.2214/AJR.10.4285

134 Wang R, Schoepf UJ, Wu R, *et al.* CT coronary angiography: image quality with sinogram-affirmed iterative reconstruction compared with filtered back-projection. *Clinical Radiology* 2013;**68**:272–8. doi:10.1016/j.crad.2012.08.007

135 Park E-A, Lee W, Kim KW, *et al.* Iterative reconstruction of dual-source coronary CT angiography: assessment of image quality and radiation dose. *Int J Cardiovasc Imaging* 2012;**28**:1775–86. doi:10.1007/s10554-011-0004-2

136 Leipsic J, Labounty TM, Heilbron B, *et al.* Estimated radiation dose reduction using adaptive statistical iterative reconstruction in coronary CT angiography: the ERASIR study. *American Journal of Roentgenology* 2010;**195**:655–60. doi:10.2214/AJR.10.4288

137 Oda S, Utsunomiya D, Funama Y, *et al.* A hybrid iterative reconstruction algorithm that improves the image quality of low-tube-voltage coronary CT angiography. *American Journal of Roentgenology* 2012;**198**:1126–31. doi:10.2214/AJR.11.7117

138 Renker M, Nance JW, Schoepf UJ, *et al.* Evaluation of heavily calcified vessels with coronary CT angiography: comparison of iterative and filtered back projection image reconstruction. *Radiology* 2011;**260**:390–9. doi:10.1148/radiol.11103574

139 Ebersberger U, Tricarico F, Schoepf UJ, *et al.* CT evaluation of coronary artery stents with iterative image reconstruction: improvements in image quality and potential for radiation dose reduction. *Eur Radiol* 2013;**23**:125–32. doi:10.1007/s00330-012-2580-5

140 Habets J, Symersky P, de Mol BAJM, *et al.* A novel iterative reconstruction algorithm allows reduced dose multidetector-row CT imaging of mechanical prosthetic heart valves. *Int J Cardiovasc Imaging* 2012;**28**:1567–75. doi:10.1007/s10554-011-9954-7

141 Horiguchi J, Matsuura N, Yamamoto H, *et al.* Evaluation of attenuation-based tube current control in coronary artery calcium scoring on prospective ECG-triggered 64-detector CT. *Academic Radiology* 2009;**16**:1231–40. doi:10.1016/j.acra.2009.04.008

142 Einstein AJ, Henzlova MJ, Rajagopalan S. Estimating Risk of Cancer Associated With Radiation Exposure From 64-Slice Computed Tomography Coronary Angiography. *JAMA* 2007;**298**:317–23. doi:10.1001/jama.298.3.317

143 Achenbach S, Schuhbäck A, Ropers D, *et al.* Influence of heart rate and phase of the cardiac cycle on the occurrence of motion artifact in dual-source CT angiography of the coronary arteries. *J Cardiovasc Comput Tomogr* 2012;**6**:91–8. doi:10.1016/j.jcct.2011.11.006

144 Tomizawa N, Komatsu S, Akahane M, *et al.* Relationship between beat to beat coronary artery motion and image quality in prospectively ECG-gated two heart beat 320-detector row coronary CT angiography. *Int J Cardiovasc Imaging* 2012;**28**:139–46. doi:10.1007/s10554-010-9759-0

145 Sun G, Li M, Jiang XS, *et al.* 320-detector row CT coronary angiography: effects of heart rate and heart rate variability on image quality, diagnostic accuracy and radiation exposure. *Br J Radiol* 2012;**85**:e388–94. doi:10.1259/bjr/92160185

146 Ko S-M, Kim NR, Kim DH, *et al.* Assessment of image quality and radiation dose in prospective ECG-triggered coronary CT angiography compared with retrospective ECG-gated coronary CT angiography. *Int J Cardiovasc Imaging* 2010;**26 Suppl 1**:93–101. doi:10.1007/s10554-009-9554-y

147 Hosch W, Heye T, Schulz F, *et al.* Image quality and radiation dose in 256-slice cardiac computed tomography: comparison of prospective versus retrospective image acquisition protocols. *European Journal of Radiology* 2011;**80**:127–35. doi:10.1016/j.ejrad.2010.07.011

148 Herzog BA, Husmann L, Burkhard N, *et al.* Low-dose CT Coronary Angiography Using Prospective ECG-Triggering. *Academic Radiology* 2009;**16**:15–21. doi:10.1016/j.acra.2008.06.010

149 Stolzmann P, Goetti RP, Maurovich-Horvat P, *et al.* Predictors of image quality in high-pitch coronary CT angiography. *American Journal of Roentgenology* 2011;**197**:851–8. doi:10.2214/AJR.10.6072

150 Bamberg F, Abbara S, Schlett CL, *et al.* Predictors of image quality of coronary computed tomography in the acute care setting of patients with chest pain. *European Journal of Radiology* 2010;**74**:182–8. doi:10.1016/j.ejrad.2009.03.001

151 Matt D, Scheffel H, Leschka S, *et al.* Dual-source CT coronary angiography: image quality, mean heart rate, and heart rate variability. *American Journal of Roentgenology* 2007;**189**:567–73. doi:10.2214/AJR.07.2078

152 Zheng M, Li J, Xu J, *et al.* Dual-source computed tomographic coronary angiography: image quality and stenosis diagnosis in patients with high heart rates. *Tex Heart Inst J* 2009;**36**:117–24.

153 Khan A, Khosa F, Nasir K, *et al.* Comparison of radiation dose and image quality: 320-MDCT versus 64-MDCT coronary angiography. *American Journal of Roentgenology* 2011;**197**:163–8. doi:10.2214/AJR.10.5250

154 Xu L, Yang L, Fan Z, *et al.* Diagnostic performance of 320-detector CT coronary angiography in patients with atrial fibrillation: preliminary results. *Eur Radiol* 2011;**21**:936–43. doi:10.1007/s00330-010-1987-0

155 Pasricha SS, Nandurkar D, Seneviratne SK, *et al.* Image quality of coronary 320-MDCT in patients with atrial fibrillation: initial experience. *American Journal of Roentgenology* 2009;**193**:1514–21. doi:10.2214/AJR.09.2319

156 Decramer I, Vanhoenacker PK, Sarno G, *et al.* Effects of sublingual nitroglycerin on coronary lumen diameter and number of visualized septal branches on 64-MDCT angiography. *American Journal of Roentgenology* 2008;**190**:219–25. doi:10.2214/AJR.07.2648

157 Dewey M, Hoffmann H, Hamm B. Multislice CT coronary angiography: effect of sublingual nitroglycerine on the diameter of coronary arteries. *Rofo* 2006;**178**:600–4. doi:10.1055/s-2006-926755

158 Chun EJ, Lee W, Choi YH, *et al.* Effects of nitroglycerin on the diagnostic accuracy of electrocardiogram-gated coronary computed tomography angiography. *J Comput Assist Tomogr* 2008;**32**:86–92. doi:10.1097/rct.0b013e318059befa

159 Clayton B, Morgan-Hughes G, Roobottom C. Transcatheter aortic valve insertion (TAVI): a review. *Br J Radiol* 2014;**87**:20130595. doi:10.1259/bjr.20130595

160 Nasis A, Ko BS, Leung MC, *et al.* Diagnostic accuracy of combined coronary angiography and adenosine stress myocardial perfusion imaging using 320-detector computed tomography: pilot study. *Eur Radiol* 2013;**23**:1812–21. doi:10.1007/s00330-013-2788-z

161 Ko BS, Cameron JD, Leung M, *et al.* Combined CT coronary angiography and stress myocardial perfusion imaging for hemodynamically significant stenoses in patients with suspected coronary artery disease: a comparison with fractional flow reserve. *JACC: Cardiovascular Imaging* 2012;**5**:1097–111. doi:10.1016/j.jcmg.2012.09.004

162 Qayyum AA, Kühl JT, Mathiasen AB, *et al.* Value of cardiac 320-multidetector computed tomography and cardiac magnetic resonance imaging for assessment of myocardial perfusion defects in patients with known chronic ischemic heart disease. *Int J Cardiovasc Imaging* Published Online First: 8 May 2013. doi:10.1007/s10554-013-0234-6

163 Bastarrika G, Ramos-Duran L, Schoepf UJ, *et al.* Adenosine-stress dynamic myocardial volume perfusion imaging with second generation dual-source computed tomography: Concepts and first experiences. *J Cardiovasc Comput Tomogr* 2010;**4**:127–35. doi:10.1016/j.jcct.2010.01.015

164 Ho K-T, Chua K-C, Klotz E, *et al.* Stress and rest dynamic myocardial perfusion imaging by evaluation of complete time-attenuation curves with dual-source CT. *JACC: Cardiovascular Imaging* 2010;**3**:811–20. doi:10.1016/j.jcmg.2010.05.009

165 Bastarrika G, Ramos-Duran L, Rosenblum MA, *et al.* Adenosine-stress dynamic myocardial CT perfusion imaging: initial clinical experience. *Invest Radiol* 2010;**45**:306–13. doi:10.1097/RLI.0b013e3181dfa2f2

166 Bamberg F, Becker A, Schwarz F, *et al.* Detection of hemodynamically significant coronary artery stenosis: incremental diagnostic value of dynamic CT-based myocardial perfusion imaging. *Radiology* 2011;**260**:689–98. doi:10.1148/radiol.11110638

167 Wang Y, Qin L, Shi X, *et al.* Adenosine-stress dynamic myocardial perfusion imaging with second-generation dual-source CT: comparison with conventional catheter coronary angiography and SPECT nuclear myocardial perfusion imaging. *American Journal of Roentgenology* 2012;**198**:521–9. doi:10.2214/AJR.11.7830

168 Choi JH, Chang SA, Choe YH. Detection of ischaemic myocardial lesions with coronary CT angiography and adenosine-stress dynamic perfusion imaging using a 128-slice dual-source CT: diagnostic performance in comparison with cardiac MRI. *British Journal of Radiology* 2013;**86**:20130481–1. doi:10.1259/bjr.20130481

169 Gramer BM, Muenzel D, Leber V, *et al.* Impact of iterative reconstruction on CNR and SNR in dynamic myocardial perfusion imaging in an animal model. *Eur Radiol* 2012;**22**:2654–61. doi:10.1007/s00330-012-2525-z

170 Role of multidetector computed tomography in the diagnosis and management of patients attending the rapid access chest pain clinic, The Scottish computed tomography of the heart (SCOT-HEART) trial: study protocol for randomized controlled trial. 2012;**13**:184. doi:10.1186/1745-6215-13-184

171 Nicol ED, Stirrup J, Roughton M, *et al.* 64-Channel cardiac computed tomography: intraobserver and interobserver variability (part 1): coronary angiography. *J Comput Assist Tomogr* 2009;**33**:161–8. doi:10.1097/RCT.0b013e31817c423e

172 Ferencik M, Nieman K, Achenbach S. Noncalcified and Calcified Coronary Plaque Detection by Contrast-Enhanced Multi-Detector Computed Tomography: A Study of Interobserver Agreement. *Journal of the American College of Cardiology* 2006;**47**:207–9. doi:10.1016/j.jacc.2005.10.005

173 Stolzmann P, Scheffel H, Leschka S, *et al.* Influence of Calcifications on Diagnostic Accuracy of Coronary CT Angiography Using Prospective ECG Triggering. *American Journal of Roentgenology* 2008;**191**:1684–9. doi:10.2214/AJR.07.4040

174 Bland JM. How can I decide the sample size for a study of agreement between two methods of measurement? www-users.york.ac.ukmbmeassizemeth.htm.

175 Schuhbäck A, Marwan M, Gauss S, *et al.* Interobserver agreement for the detection of atherosclerotic plaque in coronary CT angiography: comparison of two low-dose image acquisition protocols with standard retrospectively ECG-gated reconstruction. *Eur Radiol* 2012;**22**:1529–36. doi:10.1007/s00330-012-2389-2

176 Øvrehus KA, Marwan M, Bøtker HE, *et al.* Reproducibility of coronary plaque detection and characterization using low radiation dose coronary computed tomographic angiography in patients with intermediate likelihood of coronary artery disease (ReSCAN study). *Int J Cardiovasc Imaging* 2011;**28**:889–99. doi:10.1007/s10554-011-9895-1

177 Ovrehus KA, Munkholm H, Bøttcher M, *et al.* Coronary computed tomographic angiography in patients suspected of coronary artery disease: impact of observer experience on diagnostic performance and interobserver reproducibility. *J Cardiovasc Comput Tomogr* 2010;**4**:186–94. doi:10.1016/j.jcct.2010.03.010

178 Ghadri JR, Goetti R, Fiechter M, *et al.* Inter-scan variability of coronary artery calcium scoring assessed on 64-multidetector computed tomography vs. dual-source computed tomography: a head-to-head comparison. *European Heart Journal* 2011;**32**:1865–74. doi:10.1093/eurheartj/ehr157

179 Horiguchi J, Matsuura N, Yamamoto H, *et al.* Coronary artery calcium scoring on low-dose prospective electrocardiographically-triggered 64-slice CT. *Academic Radiology* 2009;**16**:187–93. doi:10.1016/j.acra.2008.05.017

180 Danad I, Raijmakers PG, Harms HJ, *et al.* Effect of cardiac hybrid 15O-water PET/CT imaging on downstream referral for invasive coronary angiography and revascularization rate. *European Heart Journal - Cardiovascular Imaging* 2014;**15**:170–9. doi:10.1093/ehjci/jet125

181 Meijboom WB, Meijs MFL, Schuijf JD, *et al.* Diagnostic Accuracy of 64-Slice Computed Tomography Coronary Angiography. *JACC* 2008;**52**:2135–44. doi:10.1016/j.jacc.2008.08.058

182 DeFrance T, Dubois E, Gebow D, *et al.* Helical prospective ECG-gating in cardiac computed tomography: radiation dose and image quality. *Int J Cardiovasc Imaging* 2009;**26**:99–107. doi:10.1007/s10554-009-9522-6

183 Armand S. Comparison of diagnostic accuracy of dual-source CT and conventional angiography in detecting congenital heart diseases. *Pol J Radiol* 2014;**79**:164–8. doi:10.12659/PJR.890732

184 Rief M, Zimmermann E, Stenzel F, *et al.* Computed tomography angiography and myocardial computed tomography perfusion in patients with coronary stents: prospective intraindividual comparison with conventional coronary angiography. *Journal of the American College of Cardiology* 2013;**62**:1476–85. doi:10.1016/j.jacc.2013.03.088

185 Meijboom WB, van Mieghem CAG, van Pelt N, *et al.* Comprehensive Assessment of Coronary Artery Stenoses. *Journal of the American College of Cardiology* 2008;**52**:636–43. doi:10.1016/j.jacc.2008.05.024

186 Bettencourt N, Rocha J, Ferreira N, *et al.* Incremental value of an integrated adenosine stress-rest MDCT perfusion protocol for detection of obstructive coronary artery disease. *J Cardiovasc Comput Tomogr* 2011;**5**:392–405. doi:10.1016/j.jcct.2011.10.002

187 Rocha-Filho JA, Blankstein R, Shturman LD, *et al.* Incremental value of adenosine-induced stress myocardial perfusion imaging with dual-source CT at cardiac CT angiography. *Radiology* 2010;**254**:410–9. doi:10.1148/radiol.09091014

188 Bettencourt N, Chiribiri A, Schuster A, *et al.* Direct Comparison of Cardiac Magnetic Resonance and Multidetector Computed Tomography Stress-Rest Perfusion Imaging for Detection of Coronary Artery Disease. *Journal of the American College of Cardiology* 2013;**61**:1099–107. doi:10.1016/j.jacc.2012.12.020

189 Magalhães TA, Cury RC, Pereira AC, *et al.* Additional value of dipyridamole stress myocardial perfusion by 64-row computed tomography in patients with coronary stents. *J Cardiovasc Comput Tomogr* 2011;**5**:449–58. doi:10.1016/j.jcct.2011.10.013

190 Plein S, Motwani M. Fractional flow reserve as the reference standard for myocardial perfusion studies: fool's gold? *European Heart Journal - Cardiovascular Imaging* 2013;**14**:1211–3. doi:10.1093/ehjci/jet110

191 Zoghbi GJ, Dorfman TA, Iskandrian AE. The Effects of Medications on Myocardial Perfusion. *Journal of the American College of Cardiology* 2008;**52**:401–16. doi:10.1016/j.jacc.2008.04.035

192 Nesterov SV, Han C, Mäki M, *et al.* Myocardial perfusion quantitation with 15O-labelled water PET: high reproducibility of the new cardiac analysis software (Carimas). *Eur J Nucl Med Mol Imaging* 2009;**36**:1594–602. doi:10.1007/s00259-009-1143-8

193 ICRP. Radiation Dose to Patients from Radiopharmaceuticals. ICRP Publication 106. *Annals of the ICRP* 2008;**38**:1. doi:10.1016/j.icrp.2008.08.002

194 Raitakari OT, Toikka JO, Laine H, *et al.* Reduced myocardial flow reserve relates to increased carotid intima-media thickness in healthy young men. *Atherosclerosis* 2001;**156**:469–75.

195 Hwang KH, Lee B-I, Kim SJ, *et al.* Evaluation of coronary endothelial dysfunction in healthy young smokers: Cold pressor test using [(15)O]H(2)O PET. *Appl Radiat Isot* 2009;**67**:1199–203. doi:10.1016/j.apradiso.2009.02.012

196 Morita K, Tsukamoto T, Naya M, *et al.* Smoking cessation normalizes coronary endothelial vasomotor response assessed with 15O-water and PET in healthy young smokers. *Journal of Nuclear Medicine* 2006;**47**:1914–20.

197 Johansson BL. C-peptide improves adenosine-induced myocardial vasodilation in type 1 diabetes patients. *AJP: Endocrinology and Metabolism* 2003;**286**:14E–19. doi:10.1152/ajpendo.00236.2003

198 Laine H, Raitakari OT, Niinikoski H, *et al.* Early impairment of coronary flow reserve in young men with borderline hypertension. *JACC* 1998;**32**:147–53.

199 Danad I, Raijmakers PG, Appelman YE, *et al.* Coronary risk factors and myocardial blood flow in patients evaluated for coronary artery disease: a quantitative [15O]H2O PET/CT study. *Eur J Nucl Med Mol Imaging* 2011;**39**:102–12. doi:10.1007/s00259-011-1956-0

200 Su S, Votaw J, Faber T, *et al.* Measurement of heritability of myocardial blood flow by positron emission tomography: the Twins Heart Study. *Heart* 2012;**98**:495–9. doi:10.1136/heartjnl-2011-301080

201 Kajander SA, Joutsiniemi E, Saraste M, *et al.* Clinical value of absolute quantification of myocardial perfusion with (15)O-water in coronary artery disease. *Circulation: Cardiovascular Imaging* 2011;**4**:678–84. doi:10.1161/CIRCIMAGING.110.960732

202 Karamitsos TD, Leccisotti L, Arnold JR, *et al.* Relationship Between Regional Myocardial Oxygenation and Perfusion in Patients With Coronary Artery Disease: Insights From Cardiovascular Magnetic Resonance and Positron Emission Tomography. *Circulation: Cardiovascular Imaging* 2010;**3**:32–40. doi:10.1161/CIRCIMAGING.109.860148

203 Hajjiri MM, Leavitt MB, Zheng H, *et al.* Comparison of Positron Emission Tomography Measurement of Adenosine-Stimulated Absolute Myocardial Blood Flow Versus Relative Myocardial Tracer Content for Physiological Assessment of Coronary Artery Stenosis Severity and Location. *JCMG* 2009;**2**:751–8. doi:10.1016/j.jcmg.2009.04.004

204 Osawa K, Miyoshi T, Koyama Y, *et al.* Additional diagnostic value of first-pass myocardial perfusion imaging without stress when combined with 64-row detector coronary CT angiography in patients with coronary artery disease. *Heart* 2014;**100**:1008–15. doi:10.1136/heartjnl-2013-305468

205 Berman DS, Maddahi J, Tamarappoo BK, *et al.* Phase II safety and clinical comparison with single-photon emission computed tomography myocardial perfusion imaging for detection of coronary artery disease: flurpiridaz F 18 positron emission tomography. *Journal of the American College of Cardiology* 2013;**61**:469–77. doi:10.1016/j.jacc.2012.11.022

206 Slomka PJ, Alexanderson E, Jacome R, *et al.* Comparison of clinical tools for measurements of regional stress and rest myocardial blood flow assessed with 13N-ammonia PET/CT. *J Nucl Med* 2012;**53**:171–81. doi:10.2967/jnumed.111.095398

207 Bakker E, HJ H, Raijmakers P, *et al.* Motion-induced PET-CT misalignment does not affect absolute myocardial blood flow as measured with 15O-water. *Eur J Nucl Med Mol Imaging* 2010;**37**:S198–S311.

208 Mowatt G, Cook JA, Hillis GS, *et al.* 64-Slice computed tomography angiography in the diagnosis and assessment of coronary artery disease: systematic review and meta-analysis. *Heart* 2008;**94**:1386–93. doi:10.1136/hrt.2008.145292

209 Park MJ, Jung JI, Choi Y-S, *et al.* Coronary CT angiography in patients with high calcium score: evaluation of plaque characteristics and diagnostic accuracy. *Int J Cardiovasc Imaging* 2011;**27 Suppl 1**:43–51. doi:10.1007/s10554-011-9970-7

210 Hosokawa K, Kurata A, Kido T, *et al.* Transmural perfusion gradient in adenosine triphosphate stress myocardial perfusion computed tomography. *Circ J* 2011;**75**:1905–12.

211 Tamarappoo BK, Dey D, Nakazato R, *et al.* Comparison of the Extent and Severity of Myocardial Perfusion Defects Measured by CT Coronary Angiography and SPECT Myocardial Perfusion Imaging. *JCMG* 2010;**3**:1010–9. doi:10.1016/j.jcmg.2010.07.011

212 Huda W, Schoepf UJ, Abro JA, *et al.* Radiation-related cancer risks in a clinical patient population undergoing cardiac CT. *American Journal of Roentgenology* 2011;**196**:W159–65. doi:10.2214/AJR.10.4981

213 McCollough CH, Ulzheimer S, Halliburton SS, *et al.* Coronary artery calcium: a multi-institutional, multimanufacturer international standard for quantification at cardiac CT. *Radiology* 2007;**243**:527–38. doi:10.1148/radiol.2432050808

214 Einstein AJ, Elliston CD, Arai AE, *et al.* Radiation Dose from Single-Heartbeat Coronary CT Angiography Performed with a 320-Detector Row Volume Scanner. *Radiology* 2010;**254**:698–706. doi:10.1148/radiol.09090779

215 Halliburton SS, Abbara S, Chen MY, *et al.* SCCT guidelines on radiation dose and dose-optimization strategies in cardiovascular CT. J Cardiovasc Comput Tomogr. 2011;**5**:198–224. doi:10.1016/j.jcct.2011.06.001

216 Gould KL, Lipscomb K, Hamilton GW. Physiologic basis for assessing critical coronary stenosis: instantaneous flow response and regional distribution during coronary hyperemia as measures of coronary …. *The American Journal of Cardiology* 1974;**33**:87–94. doi:10.1016/0002-9149(74)90743-7

217 Young DF, Cholvin NR, Roth AC. Pressure drop across artificially induced stenoses in the femoral arteries of dogs. *Circulation Research* 1975;**36**:735–43.

218 Rossi A, Papadopoulou S-L, Pugliese F, *et al.* Quantitative computed tomographic coronary angiography: does it predict functionally significant coronary stenoses? *Circulation: Cardiovascular Imaging* 2014;**7**:43–51. doi:10.1161/CIRCIMAGING.112.000277

219 Nicol ED, Stirrup J, Reyes E, *et al.* Sixty-four-slice computed tomography coronary angiography compared with myocardial perfusion scintigraphy for the diagnosis of functionally significant coronary stenoses in patients with a low to intermediate likelihood of coronary artery disease. *J Nucl Cardiol* 2008;**15**:311–8. doi:10.1016/j.nuclcard.2008.02.017

220 Nicol ED, Schultz C, Stirrup J, *et al.* Defining the appropriate CTA stenosis threshold for gatekeeping to invasive angiography: 50% or 70%? *International Journal of Cardiology* 2010;**144**:297–8. doi:10.1016/j.ijcard.2009.02.031

221 Motoyama S, Sarai M, Harigaya H, *et al.* Computed Tomographic Angiography Characteristics of Atherosclerotic Plaques Subsequently Resulting in Acute Coronary Syndrome. *JACC* 2009;**54**:49–57. doi:10.1016/j.jacc.2009.02.068

222 Williams MC. How can adherence with multi-drug therapy in leprosy be improved? *Lepr Rev* 2005;**76**:160–1.

223 Bamberg F, Klotz E, Flohr T, *et al.* Dynamic myocardial stress perfusion imaging using fast dual-source CT with alternating table positions: initial experience. *Eur Radiol* 2010;**20**:1168–73. doi:10.1007/s00330-010-1715-9

224 Kurata A, Kawaguchi N, Kido T, *et al.* Qualitative and quantitative assessment of adenosine triphosphate stress whole-heart dynamic myocardial perfusion imaging using 256-slice computed tomography. *PLoS ONE* 2013;**8**:e83950. doi:10.1371/journal.pone.0083950

225 Rossi A, Dharampal A, Wragg A, *et al.* Diagnostic performance of hyperaemic myocardial blood flow index obtained by dynamic computed tomography: does it predict functionally significant coronary lesions? *European Heart Journal - Cardiovascular Imaging* 2014;**15**:85–94. doi:10.1093/ehjci/jet133

226 Schwarz F, Hinkel R, Baloch E, *et al.* Myocardial CT Perfusion Imaging in a Large Animal Model: Comparison of Dynamic Versus Single-Phase Acquisitions. *JACC: Cardiovascular Imaging* 2013;**6**:1229–38. doi:10.1016/j.jcmg.2013.05.018

227 Nakauchi Y, Iwanaga Y, Ikuta S, *et al.* Quantitative myocardial perfusion analysis using multi-row detector CT in acute myocardial infarction. *Heart* 2012;**98**:566–72. doi:10.1136/heartjnl-2011-300915

Appendix 1: Acknowledgements

I would like to thank my supervisor Professor David E Newby for giving me the opportunity to undertake this research, and many other exciting projects. I would like to thank everyone who taught me cardiovascular imaging, in particular Dr Russell Bull (Bournemouth) who taught me how to use the Aquillion ONE scanner and Dr John H Reid (Borders General Hospital) who convinced me to become a radiologist. I would like to thank my family for their continued support.

In addition I would like to thank:

Radiologists – Dr G McKillop, Dr S Mirsadraee, Professor E van Beek

Cardiologists – Dr N Uren, Dr M Dweck, Dr P Henrikson, Dr N Cruden

CRIC radiographers, image analysis staff and axillary staff.

I am very grateful to the funders of this work. This work was supported by a British Heart Foundation Clinical Research and Training Fellowship (FS/11/14/28692) and Chest Heart and Stroke Scotland (R12/A143). Professor Newby holds the British Heart Foundation John Wheatley Chair of Cardiology. The Centre for Cardiovascular Science is the recipient of a British Heart Foundation Centre of Research Excellence Award (RE/08/001). The Clinical Research Imaging Centre is supported by NHS Research Scotland (NRS) through NHS Lothian.

Appendix 2: Bibliography

Papers – Original research

Putman RK … **Williams MC,** *et al.* Mortality and undiagnosed interstitial lung abnormalities. JAMA 2016, *In press.*

Rabinovich R … **Williams MC**, *et al.* Circulating desmosine levels do not predict emphysema progression but are associated with cardiovascular risk and mortality in COPD. European Radiology Journal 2016, *In press.*

The SCOT-HEART Investigators. Newby DE, **Williams MC**, *et al.* CT coronary angiography in patients with suspected angina due to coronary heart disease (SCOT-HEART): an open label parallel group multicentre trial. Lancet 2015: 385 (9985); 2383-2391.

Williams MC, Golay SK, Hunter A, *et al*. Observer variability in the assessment of computed tomography coronary angiography and coronary artery calcium score: Sub-study of the Scottish Computed Tomography of the HEART (SCOT-HEART) trial. Open Heart 2015: 2 (1); e000234.

Papanastasiou G, **Williams MC**, et al. Measurement of myocardial blood flow by magnetic resonance perfusion imaging. Comparison of distributed parameter and Fermi models with single and dual bolus. Journal of Cardiovascular Magnetic Resonance. 2015: 17 (17).

Pellegrini E, Robertson G, Trucco E, MacGillivray TJ, Lupascu C, van Hemert K, **Williams MC** *et al*. Blood vessel segmentation and width estimation in ultra-wide field scanning laser ophthalmoscopy. Biomedical Optics Express. 2014: 5 (12); 4329-4337.

Williams MC, Murchison JT, Edwards LD, *et al*. Coronary artery calcification is increased in patients with COPD and associated with increased morbidity and mortality. Thorax 2014: 69(8); 718-23.

Papanastasiou G, **Williams MC,** *et al*. Assessing the reliability of DP and Fermi estimates in single and dual bolus cardiac MR perfusion imaging. Journal of Cardiovascular Magnetic Resonance 2014: 16 (Suppl 1); P347.

Joshi NV, Vesey AT, **Williams MC**, *et al*. 18F-fluoride positron emission tomography identifies ruptured and high-risk coronary atherosclerotic plaques. Lancet 2014: 383 (9918); 705-713.

Williams MC, Weir NW, Mirsadraee S, *et al*. Image quality with single heart beat 320 multidetector computed tomography coronary angiography. Journal of Computer Assisted Tomography 2014: 38 (3); 444-450.

Williams MC, Weir NW, Mirsadraee S, *et al*. Iterative reconstruction and individualized automatic tube current selection reduce radiation dose while maintaining image quality in 320-multidetector computed tomography coronary angiography. Clinical Radiology 2013: 2013: 68(11); e570-7.

Williams MC, Cruden NL, Uren NG, Newby DE. A low-dose comprehensive cardiac CT protocol assessing anatomy, function, perfusion, and viability. Journal of Cardiovascular Computed Tomography 2013: 7(1); 69-72.

Dweck MR, Khaw HJ, Sng GKZ, Luo ELC, Baird A, **Williams MC,** *et al*. Aortic stenosis, atherosclerosis, and skeletal bone: is there a common link with calcification and inflammation. European Heart Journal 2013: 34 (21); 1532-3.

Romme EAPM, Murchiston TJ, Edwards LD, van Beek EJR, Murchison DM, Rutten EPA, Smeenk FWJM, **Williams MC**, Wouters EFM, MacNee W. CT measured bone attenuation in patients with chronic obstructive pulmonary disease: relation to clinical features and outcomes. Journal of Bone and Mineral Research. 2013: 28 (6); 1369-77.

Newby DE, **Williams MC**, Flapan AD, *et al*. Role of multidetector computed tomography in the diagnosis and management of patients attending the rapid access chest pain clinic: the Scottish COmputed Tomography of the HEART randomised controlled trial. Trials 2012; 13: 184.

Richards JMJ, Shaw CA, Lang NN, **Williams MC**, *et al*. In vivo mononuclear cell tracking using superparamagneic particles of iron oxide: feasibility and safety in humans. Circulation cardiovascular imaging. 2012: 5(4); 504-17.

Dweck MR, Chow MWL, Joshi NV, **Williams MC**, *et al*. Coronary Arterial 18F-NaF Uptake: a novel potential marker of plaque biology. JACC Cardiovascular Imaging 2012: 59 (17); 1593-48.

Richards JMJ, Semple SI, MacGillivray TJ, Gray C, Langrish JP, **Williams MC**, *et al*. Abdominal aortic aneurysm growth predicted by uptake of ultrasmall superparamagnetic particles of iron oxide: A pilot study. Circulation: Cardiovascular Imaging. 2011: 4; 273-81.

Papers – Reviews

Williams MC, Reid J, McKillop G, Weir N, van Beek EJR, Uren, NG, Newby DE. Cardiac and coronary CT comprehensive imaging approach in the assessment of coronary heart disease. Heart. 2012: 98(7); 512-2.

Papers – Editorials

Williams MC, Newby DE. Computed tomography myocardial perfusion, a step towards quantification. Heart, 2012; 98:521-2.

Papers – Guidelines

Maroules CD, Cheezum MK, Joshi PH, **Williams MC,** *et al.* SCCT curriculum guidelines for general (level 1) cardiovascular CT training. JCCT 2015: 9 (2); 81-88.

Book Chapters

Williams MC. Conversion factors specific to CCTA. In Radiation Dose in Adult and Paediatric Multidetector CT, Second Edition. Editors Tack D, Kalra M. Springer, 2012.

Appendix 3: Public engagement in science

I have always been keen on facilitating the engagement of the public in science and research. My PhD at the University of Edinburgh and time as a British Heart Foundation Clinical Research Fellow provided me with excellent opportunities to continue this.

The image on the front cover of this thesis was selected as a finalist in the 2012 British Heart Foundation *"Reflections in Research"* competition. The image was obtained using the 320-multidetector computed tomography scanner, and subsequent post-processing of the data produced the image of the heart within the rib cage. It highlights that although the heart is at the centre of my research, this is always within the wider context of the rest of the human body. This image was published widely in the national press, emphasising the excitement surrounding this incredible technology that can see inside the human body.

There are many ways to explain science to the general public including in images and in spoken and written word. The "Dance Your PhD" competition organised by the American Academy of Science and Gonzolabs.org seeks to widen this range even further and invites participants to explain their PhD through the medium of dance. I participated in the 2010 "Dance Your PhD" competition and my submission was featured in the Science article "Why do Scientists Dance?" (Science 2010: 330

(6005); 752). The dance tells the story of a girl who develops chest pain and undergoes a computed tomography scan, set to the classic blues song "The St James Infirmary Blues". The video is available at www.vimeo.com/14453110 or www.youtu.be/Ov1s1BYtEck and the description is reproduced below.

"Dance Your Phd Contest, 2010

Heart disease is now the primary cause of death in the developed world. Diagnosing and treating heart disease is therefore a major health care priority. Recent advances in medical imaging technology means that we can now look at the blood vessels around the heart without needing to insert tubes or wires into the body. Two such techniques are computed tomography (CT) coronary angiography, which looks at the blood vessels around the heart, and computed tomography myocardial perfusion, which look at the blood flow to the heart muscle. A CT scan uses x-rays to build-up a three dimensional picture of inside the body. For my Phd I am studying the use of these techniques in patients with heart disease.

Blues dancing is a very versatile dance with no real "steps". Everything in our video is improvised around the only central move - a simple weight shift. We have a thriving blues dancing community in Edinburgh which I have been involved in for the past two years. But on with the story …

All good stories start with "Once upon a time …". My thesis is no exception, so, Once upon a time …

… a girl and her friend enjoy a walk in the sunshine on one of the hills around Edinburgh. In the distance you can see Arthur's seat, one of two ancient volcanoes within the city. Suddenly, she develops chest pain and collapses.

She is taken to hospital (to the Royal Infirmary of Edinburgh) and a doctor asks her some questions, examines her and organises some tests. One of these tests is a CT scan (using the Toshiba Aquilion ONE scanner at the Clinical Research Imaging Centre in Edinburgh). The dancers circle around each other, just like the x-ray tube and detectors do within the donut-shaped ring of the CT scanner.

The next stage involves me sitting in a darkened room for a considerable amount of time! I analyse the thousands of pictures created by the CT scan. Modern computing power means that this is much quicker and more detailed than the original CT images that were produced by Hounsfield in 1972. However, dancing in the image analysis room certainly makes time pass a little faster!

Heart disease is caused by narrowings ("plaques") in the tiny blood vessels that surround the heart. In our story we zoom in on some red blood cells that are travelling happily down a blood vessel. However, suddenly they come across an obstacle. The yellow barrier represents the collection of fat cells (also pale yellow in real life!) that cause the narrowings in the blood vessels of the heart. The poor red and white blood cells are confused and can't find a way out. In the image analysis room I assess the extent of these narrowings and their implication on the blood flow to the heart muscle. We hope that computed tomography coronary angiography and

computed tomography perfusion scans will enable more rapid and accurate diagnosis of heart disease.

And the girl in our story? The CT scan helped diagnose her heart disease so that she could be started on the appropriate treatment. She can go back to walking in the hills, and her blood cells are happy too! Just like all good stories, this one ends with our duo walking hand-in-hand into the sunset."